THESIS ON POWER ENGINEERING,
ELECTRICAL ENGINEERING, MINING ENGINEERING D63

Low Speed Permanent Magnet Slotless Generator Development and Implementation for Windmills

ANTS KALLASTE

TUT
PRESS

TALLINN UNIVERSITY OF TECHNOLOGY
Faculty of Power Engineering
Department of Electrical Engineering

Dissertation was accepted for defence of the degree of Doctor of Philosophy in Engineering on August 26, 2013

Supervisors: Prof. Kuno Janson, Department of Electrical Engineering, Tallinn University of Technology, Estonia

Prof. Anouar Belahcen, Department of Electrical Engineering, Tallinn University of Technology, Estonia
Aalto University, Finland

Opponents: Assoc. Prof. Avo Reinap
Lund University, Sweden

Dr. Tech. Jenni Pippuri
VTT Technical Research Centre, Finland

Defence of the thesis: September 26, 2013

Author's declaration:

Hereby I declare that this Doctoral Thesis, my original investigation and achievement, submitted for the doctoral degree at Tallinn University of Technology, has not been submitted for any academic degree.

Ants Kallaste ……..

Copyright: Ants Kallaste, 2013
ISSN 1406-474X
ISBN 978-9949-23-541-4 (publication)
ISBN 978-9949-23-542-1 (PDF)

ENERGEETIKA. ELEKTROTEHNIKA. MÄENDUS D63

Aeglasekäigulise uurdevaba püsimagnetgeneraatori väljatöötamine ja rakendamine tuulikutes

ANTS KALLASTE

TTÜ
KIRJASTUS

Contents

Symbol index 7
List of abbreviations 10
1 Introduction 11
1.1 Direct drive or gearbox wind generators 12
1.2 Windmills with constant or adjustable rotational speed 14
1.3 Electric generators in windmills 16
1.4 PM generators in windmills 17
1.4.1 Constraints imposed by PM generators 18
1.4.2 PM generators classified by the orientation of field excitation 19
1.4.3 Construction of the rotor of radial PM excitation synchronous generator 20
1.4.4 Main properties of permanent magnet materials 22
1.4.5 Permanent magnets using Halbach's array 23
1.4.6 Demagnetization of permanent magnets 24
1.4.7 Eccentricity of electrical machines 26
1.5 State of arte 27
1.6 Goals and tasks of the thesis 27
2 Designing methodology 30
2.1 Background of the design 30
2.2 Design process and parameter identification 30
2.2.1 Power and rotational speed from wind 30
2.2.2 Voltage and current requirements from the inverter 37
2.2.3 Choice of generator design 38
2.2.4 Generator radius and thickness 40
2.3 Magnetic field calculation 50
2.3.1 Magnetic field calculation principles 51
2.3.2 Vector potentials 52
2.3.3 Finite element method 56
2.3.4 Electromagnetic Force 58
2.3.5 Conclusion 61
2.4 EMF calculation 61
2.4.1 Winding factor 62
2.4.2 Coil windings 65
2.4.3 EMF and harmonics 68
2.5 Loading and losses 69
2.5.1 Eddy current loss 70
2.5.2 Hysteresis loss 71
2.5.3 Copper loss 72
2.5.4 Output power and efficiency 73
2.6 Thermal design 76
2.6.1 Heat transfer 76
2.6.2 Thermal resistance network 77
2.7 Conclusion 80

3 Prototype machine and test results 81
3.1 Construction of the prototype 82
3.2 Experimental set-up 83
3.3 Magnetic field 84
3.4 Coil resistance 86
3.5 Open circuit test 86
3.6 Load test 88
3.7 Temperature measurements 89
3.8 Conclusion 91
4 Generator with different permanent magnets 93
4.1 Conclusion 95
5 Analyses of manufacturing tolerances 96
5.1 Eccentricity 96
5.1.1 Type of eccentricities 97
5.1.2 Stress and electrical parameters 99
5.1.3 Eccentricity calculation results 100
5.1.4 Analyses 104
5.2 Demagnetization 105
5.2.1 Method of analysis and case study 105
5.2.2 Demagnetization process 105
5.2.3 Method 107
5.2.4 Computation results 109
5.2.5 Testing and measurement 113
5.2.6 Validation 114
6 Conclusion and Future Works 116
References 118
Acknowledgements 125
Abstract 126
Kokkuvõte 127
Author's publications 129
Curriculum Vitae 133
Elulookirjeldus 136

Symbol index

1. Units and constants

This thesis is written on the basis of SI-units. All formulas, calculations and measurement results have been presented only using SI-units and the derived SI-units.

List of constants used in this thesis

Symbol	Description	Value
μ_0	Magnetic permeability of free space	$4 \cdot \pi \cdot 10^{-7}$ H/m
ε_0	Dielectric permittivity of free space	$8{,}85 \cdot 10^{-12}$ F/m
ς	Stefan-Boltzmanin constant	$5{,}6703 \times 10^{-8}$ W/m^{2}K^4

2. General assignments

$\bar{v}$ mean wind velocity
μ permeability
μ_0 permeability of vacum
μ_r relative permeability
A linear current density
B magnetic flux density
B_g magnetic flux density in the ar-gap
B_n magnetic flux density normal component
B_r remanence flux density
BH_{max} energy density
c productivity factor
C_p coefficient of power
E electromotive force, electric field strength
F force
f_n nominal frequency
G conductance
G_g air gap conductance
G_l leakage conductance over magnet edge
G_p leakage conductance from magnet to magnet
G_{pm} permanent magnet conductance
h heat transfer coefficient
H magnetic field strength
H_c coersitivity
h_{coil} coil height
h_{con} convection heat transfer coefficient
h_m magnet height
H_n magnetic field strength normal component
H_{tan} magnetic field strength tangential component
$h_{winding}$ winding total height
h_y total air gap height

I	current
J	current density
k_{coil}	coefficient of coil height to total air gap
k_g	coefficient of air gap height to pole with
$k_{inn/out}$	coefficient of coil inner outer width
k_p	coil pitch factor
k_d	coil distribution factor
k_{niso}	coefficient of isolation at coil surfaces
k_p	coefficient of magnet width to pole width
k_{tiso}	coefficient of isolation in coil edges
k_{wn}	winding factor
k_f	coil filling factor
L	inductance
l	length
l_c	active length of winding
l_g	air gap length
l_{laup}	end winding length
l_m	average length of winding
l_m	magnet length
n_c	number of coils
n_n	nominal rotation speed
p	number of poles
P	power
P_{con}	dissipated power due to the convection
P_{copper}	copper loss
P_{ekv}	equivalent power
P_h	hysteresis loss
P_n	nominal power
P_n^e	wind turbine nominal output power
P_n^t	wind turbine nominal power
$P_{pööris}$	eddy current loss
P_{turbin}	power from wind turbine
P_{wind}	wind power
Q	number of coils
q	number of coils per phase per pole
r	radius
R	resistance
R_c	coil resistance
r_s	inner radius
R_{th}	thermal resistance
r_v	outer radius
S	surface area
S_{coil}	coil cross-sectional area
S_w	winding cross-sectional area
T	temperature

t	time
T_{amb}	ambient temperature
T_{sur}	surface temperature
u	tip speed of blade, wave length
U	voltage
w	number of turns
v	speed
W_a	annual energy consumption
w_{cinner}	winding window width
w_{coil}	width of coil
W_h	hysteresis loss energy
w_m	magnet width
V_m	magnet volume
V_{mat}	material volume
w_p	pole width
w_s	gap between the magnets
v_w	wind speed
$w_{winding}$	winding total width
X	reactance
α	angle or temperature coefficient
α_{Br}	temperature coefficient of remanence
α_{Hr}	temperature coefficient of coercitive force
δ	penetration depth
ε_{sur}	emissivity of surface
η	efficiency
η_g	generator efficiency
η_m	converter efficiency
θ_{coil}	coil angle
λ	scale parameter
λ_i	thermal conductivity of the material
λ_{tip}	tip speed ratio
ρ	density
ρ	resistivity
ρ_{air}	air density
σ	electric conductivity, Maxwell stress tensor
σ_r	magnetic field tension
σ_{tan}	magnetic field tangential tension
ς	Stefan-Boltzman constant
σ_F	Maxwell stess tension
σ_{Ftan}	tangential component of Maxwell stess tension
τ	torque
Φ	magnetic flux
ω	angular velocity

List of abbreviations

Abbreviation	Description
PM	Permanent magnet
PMSG	Permanent magnet synchronous generator
MMF	Magnetomotive force
EMF	Electromotive force
SE	Static eccentricity
EE	Elliptic eccentricity
DE	Dynamic eccentricity
LV	Low voltage
DFIG	Doubly Fed Induction Generator
AC	Alternating current
DC	Direct current
NdFeB	Neodymium magnet
SmCo	Samarium-cobalt magnet
AlNiCo	Aluminium, Nickel, Cobalt magnets
FEM	Finite element method

1 Introduction

Due to the fear for fossil fuel exhaustion and climate warming, renewable energy sources have found ever wider use. From the various renewable sources, wind has become the most used, as also the amount of energy harvested from wind has been growing [1]. Most wind energy in the world is produced using the megawatt scale wind generators. Such wind plants are expensive, complicated and they need strong grid connections in hand with sufficient reserve power in the grid. In some cases it makes more sense to use wind generators smaller in scale with power ranging 0.2-30 kW. In situations, where power is needed in places where there is no grid connection (islands, lone-standing summer houses, distant farms) small wind generators are amongst the few usable on-the-spot supply units available for the consumers. Local electricity generation has in some cases a lot of advantages. It creates the possibility to cut the investments to distribution grids and there are no distribution losses. Furthermore, electricity generated from renewable sources minimizes local pollution due to fossil fuel burning and possible harm to global climate system.

Small wind generators have been in use for practically the whole 20th century (for example Aglo wind generator before the Second World War [2]), although their more intensive exploitation started about 25 years ago. The interest in small wind turbines in the world has been gradually growing as it is shown in Fig. 1.1. From there it can be seen that the number of small wind generator manufacturers has been rising during the last half of the century [3].

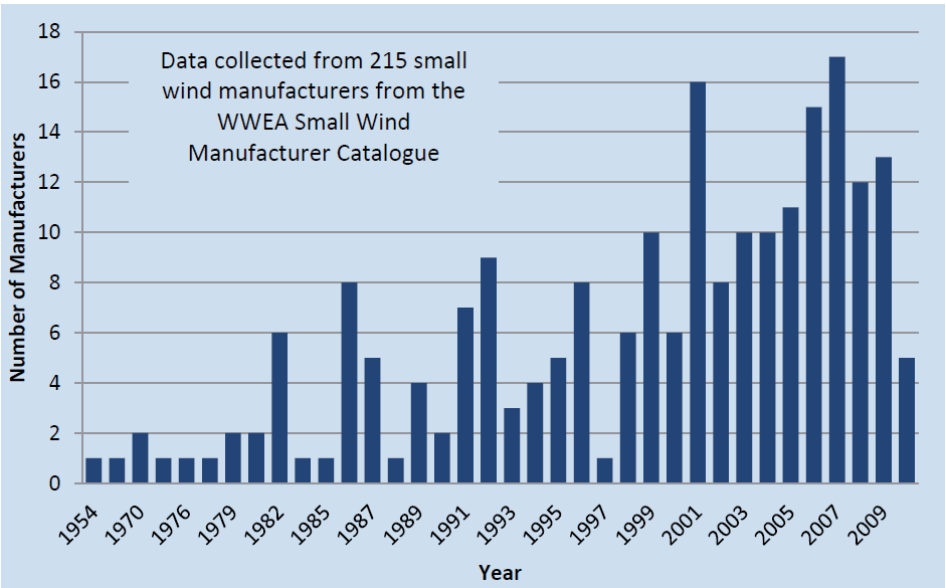

Figure 1.1. Emerged small wind generator manufacturers during the last half of the century.

There is no exact data of the small wind generators usage in Estonia. It can be estimated that there are around a few hundred small wind generators in use and a few dozens of them are connected to the grid [4]. However, according to World Wind Energy Association's report [3], 730 000 small wind generators were installed in the world by the end of 2011. In the end of 2010 the number was 656 000, a year before that 521 000 and in 2008 there were 460 000 small wind turbines installed. The total installed power of small wind generators in 2011 was around 576 MW and all the power generated from wind summed to 240 GW.

The concept of small wind generator is not exactly defined globally. At first a small wind generator was defined as a wind generator that is able to supply energy to the devices in a household. However, this definition does not make sense in a global perspective, as consumer profiles vary very largely in different regions and states. For example an average US household would need a 10 kW wind generator to meet their needs of electricity; an average European family would need a 4 kW generator to meet the same requirements. At the same time an average Chinese household could very easily use a 1 kW wind generator to produce all the electricity needed in the family [3]. Small wind generators described in this thesis are defined according to the energy consumption of an average European household.

Two main types of wind generator solutions are used in wind power plants: windmills with a horizontal shaft and a vertical shaft. Horizontal shaft solutions have been dominant for the small wind generator industry during the past 30 years. During last 5-7 years vertical shaft wind generators have been developed more actively, but their market share remains marginal [3]. The most used vertical shaft wind generators use the so called Darrieus type turbines. Those turbines have a simple and reliable construction. As the rotational speed of Darrieus turbine is slow, a gearbox is often used to raise the rotational speed to meet the requirements of the electric generator. There are also different solutions where slow speed electric generators are used and the rotation of rotor is transmitted to the generator either installed on the ground or mounted next to the wind turbine.

1.1 Direct drive or gearbox wind generators

Power and rotational speed of the electric generator used in a windmill is defined by the wind turbine. The rotational speed of a wind turbine, which is usually relatively slow, is dependent on the construction of the windmill blades and power. Rotational speed of the megawatt class windmills is around 10-40 rpm. At the same time, smaller wind turbines have a higher rotational speed, for example 30 kW windmill has a rotational speed of 80-100 rpm, 5 kW windmill can rotate with a speed of 200-220 rpm. When the power falls to 200-1000 W, the blades will rotate even faster, achieving a speed of 300-500 rpm [5, 6, 7]

Electric generators are usually high speed machines, with rotational speed varying in the range of 1000-3000 rpm. When such machine is used in a windmill, single step or multiple step gearbox must be used between the

generator and windmill shaft as shown on Fig. 1.2 a. Alternatively, solutions are used where the generator is directly connected to the windmill shaft as Fig. 1.2 b shows. Slow speed multiple pole electric generators are used in this case.

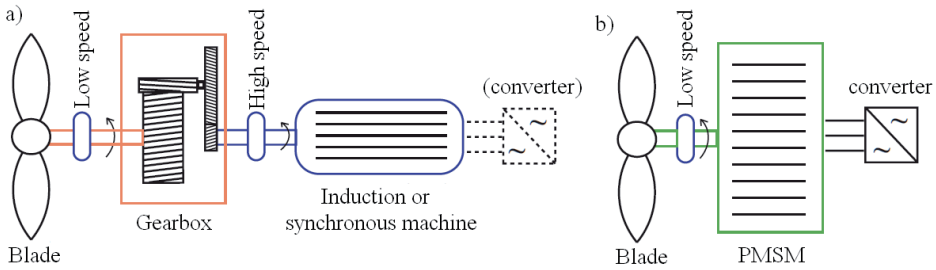

Figure 1.2. Kinematic scheme of a wind power plant using a gearbox between blades and generator (a) or a generator connected directly to the shaft of the windmill (b) [8]

Using high speed generators in wind applications gives the opportunity to use generators that have been developed for a long time and are already in a good technical level. Mainly high speed induction machines are used in the windmills, squirrel cage machines are mainly used in small windmills as in Easywind applications, and wound rotor machines that are used in large windmills such as Vestas. The advantage for using high speed generators in wind applications is the light weight of the machines. On the other hand, windmill equipped with such machine needs a gearbox, which raises significantly the weight and losses of the wind application. Due to more moving and wearing parts such applications need more maintenance and are less reliable.

When compared to high speed generators, using slow speed machines in windmills grants many benefits [8]:

- energy productivity of the generator is rising, as low wind speeds are better utilized;
- maintenance costs drop, reliability rises;
- noise level emitted to the surrounding environment drops;
- flicker in the grid is lower;
- power factor is higher.

As the rotational speed of the generator in direct drive windmills is low, the generator has to have multiple poles. This means that the diameter of the generator must be relatively large compared to the length of the machine. This phenomenon raises many problems that are particularly recognizable in large megawatt scale wind generators. Additionally, the weight of such generators is high, exceeding even the weight of high speed generator and gearbox.

Both permanent magnet (PM) and electromagnet synchronous generators are used in windmills. PM generators can be found in small windmills such as Estonian produced Konesko applications, as well as in large megawatt class windmills like Siemens SWT-3.0-101 DD. Wind generators equipped with electromagnets are only used in large applications such as Enercon.

There are a lot of scientific publications that are trying to find which solution, direct drive or the use of a gearbox, suits better for the use in windmills [9, 10, 11, 12]. Generally it can be concluded from the papers that applications using a gearbox are still more economically feasible. This is mainly deriving from the fact that in such solutions the windmill weighs is the least and standard components can be used. At the same time it is found that using the gearbox and wearing of generator brushes (usually wound rotor induction machines are used in this case) means more maintenance and risk for reliability. Slow speed wind applications, where synchronous machines with electromagnets are used, are the heaviest and the most expensive applications. Such machines are produced and developed nowadays only by Enercon. Slow speed windmills using PM machines are considered to be the most perspective in the industry. Today they are more expensive than the gearbox applications, but there are many benefits. Due to permanent magnets, the generator remains relatively lightweight and as the excitation for the generator comes from permanent magnets, there are no excitation losses. Due to this fact such applications have the highest efficiency and additionally they are the most reliable.

1.2 Windmills with constant or adjustable rotational speed

According to the rotational speed, windmills can be divided in two classes. Firstly, windmills with constant rotational speed or fixed speed windmills, where the rotational speed of the generator remains the same regardless of the wind speed. In such case the generator is connected directly to the grid as shown on Fig. 1.3 a. Secondly, windmills with adjustable rotational speed, where the rotation of the generator is adjusted according to the wind speed. This case needs a converter to be connected to the grid as Fig. 1.3 b and c are showing.

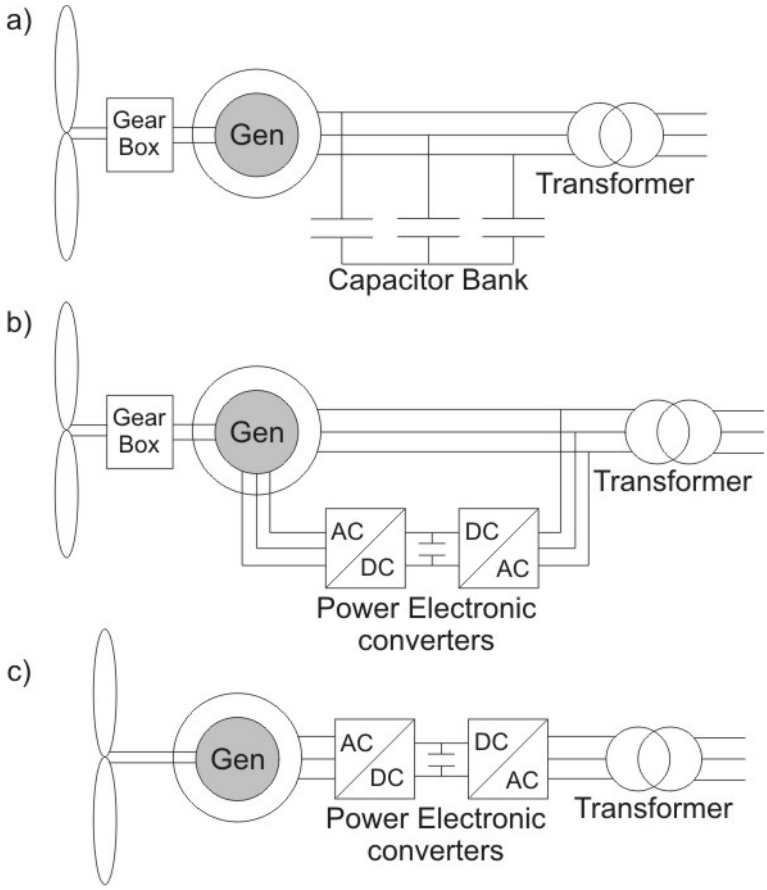

Figure 1.3. Fixed speed windmill solution (a) and the windmill with adjustable rotational speed (b, c).

Fixed speed windmills are mainly used for their simplicity and robustness. Such solution allows direct grid connection for the generator, which means that no converters are needed in the system. This also makes the system significantly cheaper than in case of adjustable speed windmills. The main problem of this solution is the voltage sag passing ability [13]. Also, using constant speed, the wind turbine is not working effectively in all span of the wind speed and does not produce energy in low wind speeds. Due to these reasons such solutions are almost not used in practice anymore.

Adjustable rotational speed in windmills mean that the rotational speed of the generator is adjusted according to wind speed. Such solution demands a converter to control the windmill, but it grants the possibility for a more effective use of the application. There are many advantages of the adjustable rotational speed when compared to fixed speed solutions [14, 15, 16]:

- larger amount of wind power is utilized (up to 6% more depending on the location and blade construction);
- voltage and power deviations as well as flicker in the grid are lower;
- noise made by turbine and generator on low rotational speed is smaller;

– mechanical stress on the wind turbine components during the changes of the torque coming from turbine rotor blades is lower.

Generally, in case of direct drive windmills where synchronous machines are used, always the adjustable rotational speed is used as well. Sometimes it is considered to be a benefit when compared to the solutions using a gearbox, but generators equipped with gearboxes can also work with varying speeds when adequate control systems are used [8].

1.3 Electric generators in windmills

Both induction generators and synchronous machines are used in wind power industry. In the windmills used today mostly induction machines are used. Wound rotor induction machines are used more in large scale windmills whereas small windmills are usually equipped with squirrel cage induction generators. For an induction machine to run in the generator mode, its rotor has to rotate faster than its synchronous speed. Additionally, induction generator needs magnetizing current to work. In case of generators directly connected to the electric grid, the needed magnetizing current is drawn from the grid. In such case the generator becomes reactive energy consumer for the grid, which is not always desired. In case of autonomous generator, the needed magnetizing current can be produced using capacitors. Until now, induction machines used in windmills have been equipped with gearboxes, so high speed machines have been used. However, it can be found in literature, that solutions have been investigated, where the induction generator is connected directly to the wind turbine shaft [17, 18]. Sadly, there are no reliable and applicable solutions known at the moment.

Fixed speed as well as induction generators with variable rotational speed are both used in windmills. Due to the torque-speed characteristics of induction generators, it is easy to connect them directly to the grid. However, as its torque-speed curve is relatively rigid, natural changes in the wind speed lead to large deviations in the power [8]. To soften the torque-speed curve, slip control is used in case of induction generators, thus mainly wound rotor induction generators can be found in large windmills, with controllable active resistance or conductor connected to the rotor circuit. Such control methodology lets one control not only the slip of the generator but also the power. Such a generator is known as Doubly Fed Induction Generator (DFIG).

During the last decade, mainly DFIGs are used in high power wind applications. Frequency converters are used to control the currents in wound rotor windings of such machines. This grants the possibility to control the working point of generator characteristic and output power up to 20-30% of rated power [8].

Synchronous generators have also been used more widely in wind applications during the last decade. This has happened mainly due to two reasons. Firstly, as synchronous machines need a converter to be connected to the grid in the case of windmills, the prices as well as the quality of the

converters have become more reasonable during the last years. Second reason is the usage of permanent magnets in the excitation field of electrical machines that raises the reliability and efficiency of the generator, thus making the usage of such machines in windmills highly prospective. It can also be noted, that the properties of the magnets have been improving, giving the opportunity to produce permanent magnet excitation generators (PM generators) that are competitive in the market.

Synchronous generators using electromagnetic excitations that are used in windmills get their needed excitations mainly from the pole windings that are situated usually on the rotor and fed with direct current. Both brushless and slip ring equipped excitation systems are used [8]. Such solutions are industrially used, but as generally such generators are the heaviest and are not too often used in windmills.

1.4 PM generators in windmills

Electric generator must fit several conditions to be implemented in wind applications. As usually the generator is mounted on the top of the windmill mast, where particularly heavy equipment is not recommended, the energy density of the generator must be as high as possible, so that its weight to power ratio would be low. Maintenance need of the windmill system plays also an important role, especially in the case of small wind generators. In case of small windmills it is hard to reach the top part of the mast, which means that usually the mast must be lowered in order to do the needed maintenance procedures. This is a difficult and costly task. The minimization of the necessity for such procedures is thus desired. Furthermore, as windmills are designed to work for 20 years or more, the reliability of the components is important as well.

When different electrical machines are confronted with these conditions, it can be seen that PM generators have many benefits over the other types. Squirrel cage induction machine offers high reliability, low maintenance need and light weight, if used with a gearbox. On the other hand, excitation may pose a problem, as capacitors are needed in the system, which in hand with the needed gearbox lowers reliability of the whole system and the need for maintenance is rising. In case of synchronous machines PM generators have advantages compared to traditional electromagnet excited generators, as they have no brushes and slip rings that would need maintenance. Additionally, high energy density magnets give the possibility to build much lighter machines than in case of electromagnets. Also, efficiency of PM machines is one of the highest amongst other electrical machines, as there are almost no losses in the rotor. Due to these facts, there has been growing interest and research in the field of PM generators development which has been described in several scientific publications [20, 21, 22] and numerous PhD dissertations have been defended on the topic [7, 8, 16, 19].

In addition to light weight, reliability and low maintenance needs, peculiarities of wind generation must be taken into account during the design process [23, 24]. Namely, wind generators do not work at the rated but

substantially lower power and rotational speed during most of its exploitation period. Thus, also exploitation peculiarities and not only nominal data of the machine should be the initial input for the generator design.

1.4.1 Constraints imposed by PM generators

The use of PM generators has some disadvantages too that must not be forgotten. One of the main drawbacks is the strength of the excitation magnetic field that cannot be controlled. Because of this, it is difficult to use wind energy in low wind speed when the rotational speed of the wind turbine is also low. Additionally, higher wind speeds than the rated speed when also the turbine exceeds its nominal rotational speed poses problems. This can lead to dangerously high levels of generator output voltage. To avoid this, additional protection means should be implemented, that will prohibit the rotational speed of the turbine to get too high. As the output voltage of PM generator varies in large scale, more complex converters must be used to connect the windmill to the consumer network or to the grid [5, 7, 15, 16, 25, 26].

There are different solutions proposed in the literature to control the excitation field of a PM machine. One possibility is to use stator windings to overcome this problem. This means that windings are reconnected according to rotational speed of the generator to smoothen the output voltage [27]. Cheaper converter can be used in the output of the generator when such solution is used. However, this control system needs an additional converter that reconnects the windings at the right spot. Systems, where permanent magnets create the base part of excitation field and the needed control is implemented through excitation windings on the same pole, are more widely in use. These systems can be easily used when the excitation system of the generator stays in one position and armature winding with the rectifier is situated on the spinning rotor. Preliminary excitation system of a high power generator could be solved in the described way, the rectified and controlled armature current of which could be the excitation current of the main generator. Using of the armature current gained from the spinning rotor directly as supplying load current for the consumers through slip rings and brushes is not practical, as additional elements such as slip rings and brushes decrease the reliability and efficiency of the generator as well as rises the maintenance needs [8].

In case of permanent magnet excitation it has to be remembered that excitation field exists permanently in the generator, even when the machine is at standing still. Such solution raises some specific technical issues. One of them is the magnetic attraction forces existing between magnetic poles and the ferromagnetic parts of the rotor. Depending on the construction of the machine, this force depends on the rotational angle of the rotor and its position with respect to the stator. The rotor always tries to take and maintain the position where the air gap for the magnetic flux has the smallest possible magnetic resistance [8]. This creates a jumping braking torque also known as cogging torque when the rotor is rotating with respect to the stator. The blades of the wind turbine have very small torque at the starting moment of the windmill, and

when cogging torque is high, rotating the turbine at low wind speeds can become impossible. In addition to that, as the cogging torque is directly linked to the generator construction, than with generator eccentricity this phenomenon may increase [33, 34].

The literature suggests numerous solutions to overcome this problem too. One of the possibilities is to use special winding connection [8]. Typically, cogging torque is minimized with the right selection of slots and additionally shifting of slots or magnets [28, 29, 30, 31]. These solutions fit relatively well with the traditional radial flux machines that have slots. On the other hand, special electrical machine types are used in windmills, the main goal of which is the minimization of cogging torque. One of such machines is the slotless machine [32, 33]. In that case the inner surface of the stator is smooth and the magnetic resistance between the stator and the rotor is the same in every position of rotation.

1.4.2 PM generators classified by the orientation of field excitation

PM generators can be divided in three different categories depending on their construction and orientation of the magnetic flux in the air gap:

- **radial magnetic flux** generators [7] where magnetic flux passes the air gap in radial direction as in case of traditional electrical machine solutions. Traditionally construction with inner rotor and outer stator is used shown on Fig. 1.4 a, more seldom *vice versa* construction can be found as it is shown on Fig. 1.4 b;
- **axial magnetic flux** generators [22] magnetic flux passes the air gap in axial direction, it is the direction of rotational axis of the generator. The rotor of the generator is situated axially opposite to the stator, e.g. next to the stator in axial direction. Usually one sided rotor and stator are used, but double sided stator or multiple rotor solutions can also be found;
- **transversal flux** generators [35] magnetic flux passes the air gap in transversal direction. This construction is relatively new and under investigation. The layout is achieved using permanent magnet joints situated next to each other. An important downside of this solution is that it is considered to be the noticeable decline in magnetic flux and output voltage due to the demagnetizing effect of PM generator load current magnetic field.

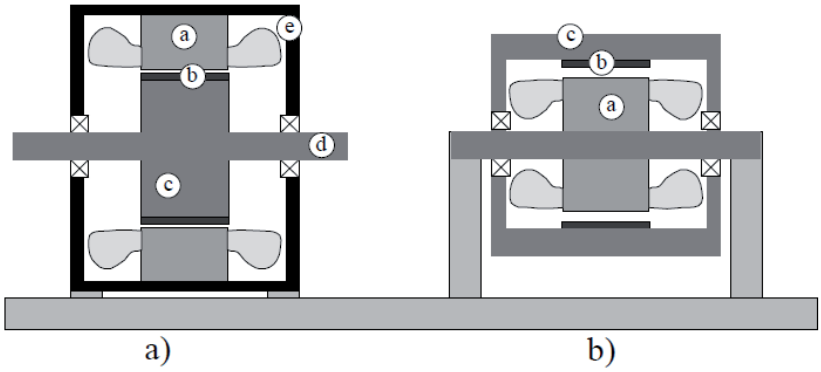

Figure 1.4. Inner rotor (a) and outer rotor radial flux (b) permanent magnet synchronous generator. a – stator, b – permanent magnet, c – rotor, d – shaft, e – frame of the machine.

From the given solutions, radial flux PM generators are the most used. Traditionally rotor solution is used that is similar to the classical induction machine and synchronous machine stator, where three phase winding is laid in the stator slots. This solution is relatively well established and offers good electrical parameters in generator mode. On the other hand the weight of the stator in such solution is relatively heavy. Solutions to decrease the stator weight are suggested in literature for such machines for better implementation in wind applications. One of the suggestions is the iron free stator where the stator is composed by only the windings [36, 37]. It is hard to construct a stator using this solution and the value of magnetic the flux in the air gap is relatively small. Another suggestion is the use of slotless stator construction [38, 39]. In that case the decrease of weight is smaller than in the case of iron free stator, but the weight remains still smaller than in the case of a traditional stator. Another advantage when compared to traditional stators is the absence of cogging torque and low phase inductance. PM rotor construction with salient poles, either in the shape of surface magnets or pole coils, resembles somewhat the classical technical solution of a hydro generator with high number of poles.

1.4.3 Construction of the rotor of radial PM excitation synchronous generator

Mainly two different permanent magnet layouts on the rotor of the generators are used in case of radial flux PM machines:

- Magnets are laid on the surface of the rotor as shown in Fig.1.5 a and c
- Magnets are laid in the slots that are carves the rotor as in Fig. 1.5 c, d…g.

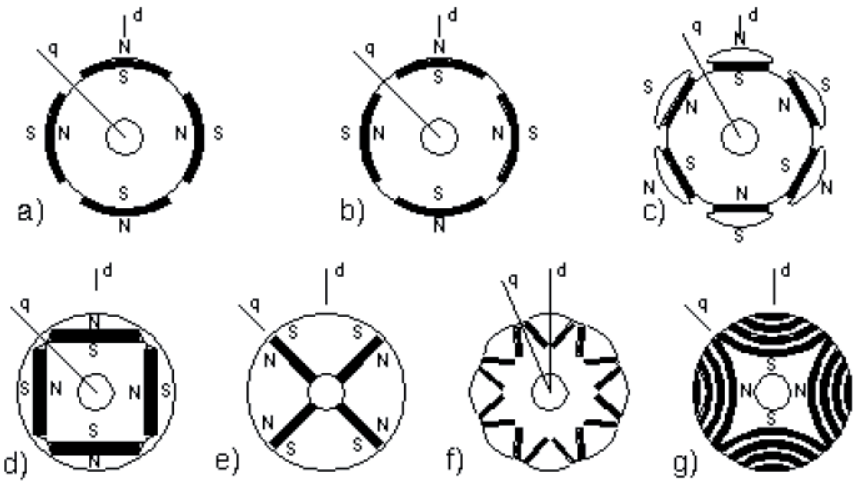

Figure 1.5. Rotor construction in case of different permanent magnet layouts: a) surface mounted magnets, b) magnets carved in the surface of the rotor, c) magnets mounted on the surface equipped with pole shoes to achieve sinusoidal current, d) tangential magnets laid inside the rotor, e) radial magnets laid inside the rotor, f) shifted magnets with sinusoidal curve pole shoes, g) permanent magnets with layer construction [40].

Such magnet layouts have their benefits and drawbacks. Advantages of the magnets mounted on the surface of the rotor are [8]:

- construction of the rotor is relatively simple both from the viewpoint of magnet layout and soft steel cylinder used as a base of the magnets;
- as the magnetic permeability of permanent magnets is low (close to air), air gap equivalent thickness of the PM generator rises for almost the thickness of the magnet. This leads to rise in the magnetic resistance of the air gap to armature reaction magnetic flux, which softens the armature reaction impact on the PM synchronous generator characteristics.

Disadvantages of the surface mounted magnets are as follows [8]:

- mounting magnets on the surface of the rotor poses a risk to the PM generator reliability, as magnets can be ripped off due to centrifugal and magnetic forces causing other magnets and eventually the whole generator to brake;
- magnetic flux density in the air gap drops due to relatively large air gap (especially in case of large PM generators) which lead also the efficiency of the generator to decrease;
- sinusoidal magnetic flux density distribution is hard to achieve, which is one of the key factors in sinusoidal voltage generation and decreasing the impact of higher harmonics in the stator winding of the PM generator.

There are different possibilities for interior magnets as shown on Fig. Figure 1.5. Different layouts can be used for different reasons. The goal can be improvement of the machine working characteristics, more effective magnet use as well as achieving constructional strength. In conclusion, advantages of interior magnet machine are:

- it is possible to concentrate the magnetic flux in the air gap. This is achieved with using PM with bigger surface area than the surface are of the pole. With concentrating the magnetic flux also the magnetic flux density in the air gap is increasing resulting in increase in generator output voltage. With higher output voltage it is achievable higher generator output power as the generator efficiency is increasing;
- due to magnetic flux concentration effect it is possible to use permanent magnets with lower magnetic properties which are cheaper price (e.g. ferrites);
- magnets can be fixed in place, which rules out the ripping off or breaking possibility due to centrifugal forces or malfunction.

In case of interior magnet machine disadvantages can also be pointed out:

- rotor construction is more complex compared to the solution, where magnets are mounted on the surface of rotor yoke;
- as direct air gap between poles situated on rotor and stator is smaller, effect of armature reaction to the magnetic field of the air gap and PM generator efficiency is somewhat stronger. There is a certain demagnetization risk in case of sensitive magnetic materials.

1.4.4 Main properties of permanent magnet materials

Usage of permanent magnets in generators grants the possibility of producing energy efficient machines that have made them attractive for the use in wind applications. Development of large industrial PM machines is still young and different solutions for improvement can still be found. There are four main magnetic materials that are industrially used: NdFeB, SmCo, AlNiCo and ferrite magnets. The main properties of these materials are described Table 1.1.

Table 1.1. Main properties of permanent magnet materials [41].

	BH_{max}(kJ/m^3)	B_r(T)	H_c(kA/m)
NdFeB	220-500	0.97-1.45	740-1000
SmCo	120-240	0.85-1.1	620-840
Ferrite	7-42	0.2-0.48	120-360
Alnico	10-35	0.6-1.16	40-120

Usually four main parameters are taken into account when choosing permanent magnets to be used in electrical machines: energy density BH_{max}, remanence density B_r, coersitivity H_c and temperature resistance.

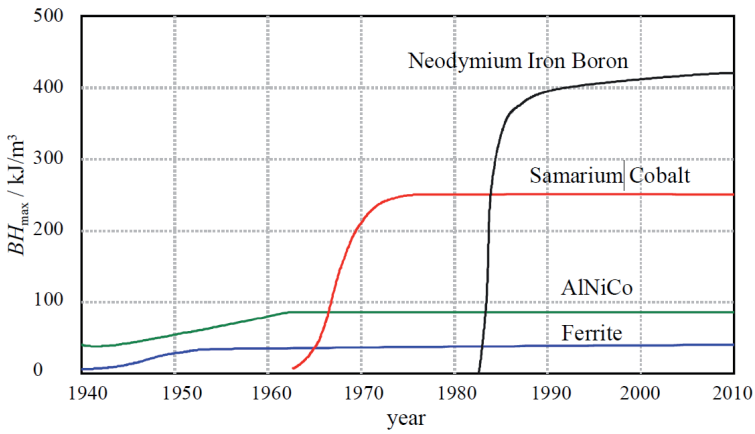

Figure 1.6. Development of magnetic materials based on energy productivity [42].

As it can be seen on Fig. 1.6 rear earth magnets (NdFeB and SmCo) have substantially higher energy density than AlNiCo and ferrite magnets. On the other hand, ferrite magnets that are the oldest magnets in the list are still being used in electrical machines due to their low price compared to other magnetic materials. Although both properties and price of SmCo magnets are usually lower than NdFeB magnets, they are used due to their temperature resistance in applications where NdFeB magnets cannot be implemented.

If one observes the development of NdFeB magnets on Fig. 1.6 it can be seen that from the moment of coming to the market it has been the permanent magnet material with the highest energy density. Although for a long time temperature resistance of NdFeB magnet posed a problem, there has been a major leap in corrosion protection and temperature resistance of the material during the last few decades [43]. Due to high energy density and remanence of NdFeB magnets, it has become one of the most used and preferred magnetic materials to be used in electrical machines. These types of magnets help to achieve sufficient excitation magnetic field in the PM generator air gap, being relatively small in size at the same time.

1.4.5 Permanent magnets using Halbach's array

Usually traditional permanent magnet layouts on the rotor steel (surface placement of magnets) are used in PM wind generators. In such case there is no problem of achieving sufficient excitation magnetic field when NdFeB magnets are used. Although, if low energy density magnets are desired to be implemented in the electrical machine, such as ferrite magnets, it is almost impossible to achieve sensible field strength using the given generator type. Additionally, mass of the generator would rise substantially due to the amount of magnet material. One of the possibilities to overcome this problem is to use special magnet layout, such as Halbach's array. It is possible to raise energy density of the machine with less magnets using Halbach's array [44, 45, 46], which means that it is possible to decrease the weight of the machine as well as

the price of magnets. In addition to that, in case of such magnet layout magnetic flux in the rotor closes through the permanent magnets, so no magnetically soft material underneath the magnets is needed [46, 47]. Due to that it is possible to change the iron used under the magnets to a substantially lighter and cheaper material.

In case of Halbach's array, radial magnets are placed between magnetic poles that help to direct the magnetic field in the desired way (Figure 1.7).

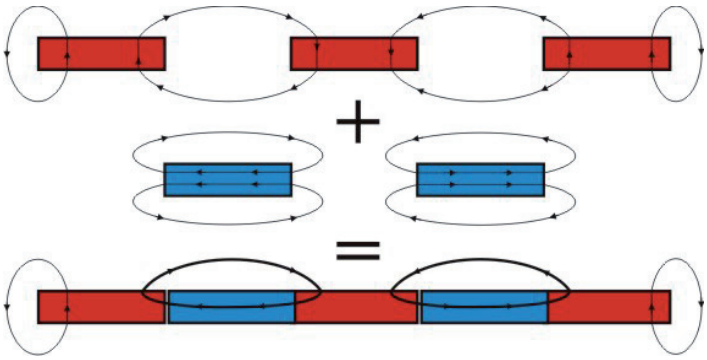

Figure 1.7. Principle scheme of magnets placed in Halbach's array.

Using Halbach's array substantially raises the magnetic flux density in the air gap and decreases the weight of the machine. Even usage of ferrite magnets in a slow speed generator is possible using this solution. On the other hand, even Halbach's array cannot help to achieve the weight of ferrite machine to match the weight of the same machine with NdFeB magnets.

There are certain risks that cannot be forgotten when Halbach's array is used. It is mechanically difficult to build a machine with such magnet layout and partial demagnetization of magnets can occur.

1.4.6 Demagnetization of permanent magnets

One of the risks when permanent magnets are used in electrical machines is the demagnetization of the magnets. There are many reasons why demagnetization can occur. One of the main reasons is magnetic field of generator armature reaction, which has the opposite direction to the excitation field and is created due to the load of the machine. Such demagnetization can occur either malfunction of the machine or when windings are short circuited [48, 49, 50].

Another possible reason for demagnetization that is often investigated in case of PM machines is the temperature caused demagnetization, as demagnetization curve of permanent magnets is highly dependent on the temperature of the magnet [50, 52, 53]. When the temperature of the permanent magnet exceeds a certain limit, there is always a risk that the working point of the permanent magnet will move over the knee of the demagnetization curve to the point which leads to irreversible partial or full demagnetization of permanent magnet.

In both cases demagnetization process can be described through the demagnetization curve of permanent magnet. Usually, electrical machines are designed to work so that magnets would be working on the point of maximum energy product. In case of machine overload or short circuit, the working point falls along the demagnetization curve. When the coercitive force of permanent magnet is low, there is a risk that the working point of the magnet will fall over the knee point of the curve, so that the magnet would partially or fully demagnetize. Figure 1.8 shows a typical permanent magnet demagnetization curve with the demagnetization process. When working point of the magnet P_1 moves to point P_2 due to outer magnetic fields (armature reaction magnetic fields), the remanence B_r decreases to B_r' and the magnet is partially demagnetized.

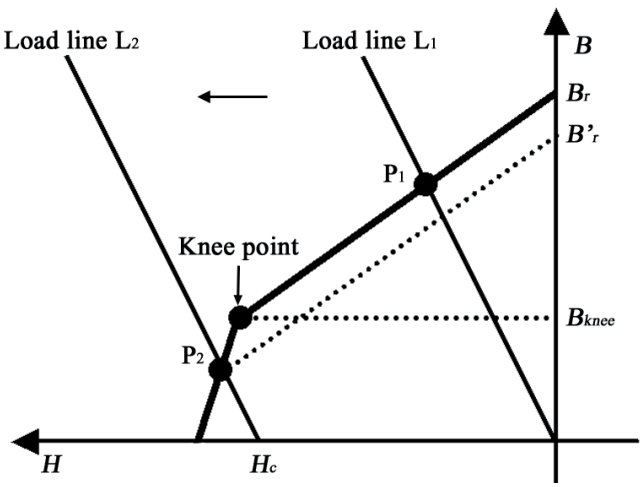

Figure 1.8. Demagnetization curve of a permanent magnet with working points [51].

Demagnetization curve of the permanent magnet depends also on temperature. Due to temperature, both coercitive force and remanence change. The change in temperature can be taken into account using the following equations [52]:

- Temperature coefficient of remanence:

$$\alpha_{Br} = \frac{1}{B_r} \cdot \frac{\Delta B_r}{\Delta T} \qquad 1.1$$

- Temperature coefficient of coercitive force:

$$\alpha_{Hc} = \frac{1}{H_c} \cdot \frac{\Delta H_c}{\Delta T} \qquad 1.2$$

Table 1.2 shows temperature coefficients of different magnets. It can be seen that usually permanent magnet properties weaken with the rise of temperature, except in the case of ferrite, where rising temperature raises coercitive force. This leads to a larger risk of demagnetization of magnets on higher temperatures.

Table 1.2. Temperature coefficients of permanent magnets.

Parameter	Symbol	Unit	Ferrite	SmCo	NdFeB
Temperature coefficient of remanence	α_{Br}	%/°K	-0,2	-0,03	-0,1
Temperature coefficient of coercitive force	α_{Hr}	%/°K	0,4	-0,23	-0,6…-0,4

In addition to the described situations, demagnetization of permanent magnets can occur during the time when magnets are placed in the machine. This problem can emerge due to special layout of the magnets (e.g. Halbach's array) [53]. In such case one permanent magnet is placed in the strong magnetic field created by other magnet that can result in partial demagnetization of one or the other permanent magnet.

1.4.7 Eccentricity of electrical machines

One of the essential parameters of an electrical machine during the design process is the air gap and its uniformity. Usually it is assumed during the design of a machine, that the air gap is distributed evenly and possible eccentricity is discarded. On the other hand, as slow speed machines are used in wind applications, it is quite hard to maintain an even air gap as the machine has large radius and is relatively thin.

Air gap eccentricity can be caused by different inaccuracies during the production of the machine, such as construction strength, manufacturing tolerances, bending of the shaft and bearings etc… [54]. Eccentricity can be found to some extent in all electrical machines and it has been thoroughly investigated. Researches have been made on how eccentricity affects losses [55], eccentricity due to asymmetrical magnetic forces [56, 57], diagnostics of eccentricity [58, 59, 60] etc.

Generally it is not known how much such problem affects the working parameters of electrical machines and how important it is to take eccentricity into account during design process of the machine. In case of PM machine, every magnet that creates a pole also creates a radial force that has an effect on the stator. When the air gap of the machine is evenly distributed, the sum of magnetic forces is zero and those forces can be discarded. On the other hand, if the machine has even a slight declination towards eccentricity, resulting magnetic forces are not zero and there is additional force affecting the bearings and shortening their lifetime. Distribution of magnetic flux also becomes asymmetric in case of air gap eccentricity, resulting in declination of real machine parameters from the designed ones. Declinations can be found in output voltage of the machine, current, as well as power that can be varying. Additionally, power distribution of the machine can become asymmetrical, which may result in overload of windings. Overloaded windings can lead to local overheating of windings, which can result in aging of winding insulation. Mechanical vibrations can also be the result of air gap eccentricity.

1.5 State of arte

During the past few decades usage of permanent magnets to create excitation field for electrical machines has substantially increased. This has happened mostly due to improvement of permanent magnet material properties and technical data; also the materials have become cheaper. One of the main forces that have led to development of PM machines is wind power industry, where PM machines fit very well due to their properties. There are numerous scientific researches and dissertations to prove this statement and give a good overview both from technical state of this field as well as possible development directions.

There are also many researches that are investigating slow speed electrical machines that are used in wind applications and list the advantages and disadvantages of their usage. Some of them are [5, 6, 9, 10, 11, 21, 61], where overviews of existing wind generator technical level and future trends are presented.

Requirements and optimization possibilities due to the specific working cycle of wind turbines are discussed in [23, 24], where peculiarities of windmill characteristics and possibilities how to optimize a PMSG according to them has been presented.

One of the main goals while designing a PM generator is the power density of the generator and possible rising of this parameter. There are many constructional solutions presented in the literature to lighten the weight of the generator. For example using the iron free solution [36] or a slotless machine can be a possibility [32]. Decreasing of magnetic mass through the usage of Halbach array to mount the magnets is also proposed as one of the possibilities to decrease both weight and cost of the machine [44, 45, 46].

Demagnetization of permanent magnets can occur in PM generators. Overcoming this problem and how to take this problem into account while designing the machine is described in [48, 49, 50]. Additionally when demagnetization occurs, permanent magnets create radial forces in PM machines that can lead to eccentricity of the air gap [54, 55].

Slow speed PM generators possibly suitable for the usage in wind applications have been the topic for many scientific papers and dissertations. Some of them are the PhD dissertation of Florence Meier [62] and dissertation of Maxime R.J.Dubois [6] as well as the dissertation of Aleksander Kilk [8].

One of the problems occurring during the design process of electric generator is always the setting of preliminary parameters and development of an exact machine according to the preferred solution. Usually existing solutions are used as the base of the design or loop calculations are used, during which every next loop is used to enhance the parameters to meet the expected result.

1.6 Goals and tasks of the thesis

The goal of this thesis was investigate the feasibility of a slotless low speed PM generator for windmills and develop the design methodology for such type of machine. The needed production of a concrete windmill is set as a base for

the design of the generator and preliminary parameters are set in accordance. The preliminary parameters of the generator help to find the parameters that make the generator suitable for the needed wind application. While choosing the generator construction, the goal has been set to find an optimal solution that would grant both light weight of the generator and would be free of cogging torque. Additionally, as permanent magnet demagnetization and air gap eccentricity can occur in PM machines, possible risk of those faults in the given generator has been investigated in this thesis.

During the preliminary analysis it was found that many problems of engineering calculations and design peculiarities have to be taken into account while the needed generator is developed. During the research made for the design of the generator, designed to be used in windmills it was found that a set of problems have to be solved or specified and those problems set the main tasks of this thesis.

The main research tasks to be achieved are as follows:

1. analysis of the current technologies of the generators used in windmills (chapter 1.4).
2. investigation of the generator parameters set by the windmill and by the generator output which will be the generator preliminary design parameters. (Chapter 2.2.1 and 2.2.2).
3. analysis of the possible generator construction choice for windmills (chapter 2.2.3).
4. based on the generator construction choice and the preliminary design parameters development of the generator dimensional design methodology (chapter 2.2.4).
5. investigation and develop design methodology for the generator magnetic field calculation (chapter 2.3), electromotive force calculation (chapter 2.4), generator loss and output characteristic calculation (chapter 2.5) and generator thermal calculation.
6. practical verification of the calculation methodology on the test prototype generator (chapter 3).
7. analysis of the generator with different permanent magnets (chapter 4).
8. analysis of the generator manufacturing tolerances effect on the generator: the generator eccentricity (chapter 5.1), permanent magnet demagnetization (chapter 5.2).

Further sections present the most important results achieved in this doctoral research, including both the scientific and practical novelties.

Scientific novelty

The scientific novelty of the doctoral thesis includes:

- proposal of new type slotless permanent magnet slow speed generator for windmills;
- development of design proses for the generator based on the windmill parameters;

- new calculation methodology for the slotless permanent magnet slow speed generator;
- method for analyzing the demagnetization during the manufacturing of the generator.

Practical novelty

The practical novelty of the doctoral thesis includes:

- new slotless permanent magnet slow speed generator;
- method for calculating the slotless permanent magnet slow speed generator for windmills;
- experimental investigation of the proposed generator regarding its output characteristics;
- method for analyzing the generator eccentricities;
- method for analyzing the permanent magnets demagnetization during the manufacturing the generator.

Dissemination of results and publications

The results of the doctoral thesis have been presented by the author at 16 international conferences. The author has published 11 international scientific papers directly associated with the thesis. Seven of them are available in the IEEE database and one has been published in the international peer-reviewed journals.

2 Designing methodology

2.1 Background of the design

Small scale windmills are gaining more popularity and due to that, the requirements for the technical level set for those windmills are also increasing and becoming stricter. The main task of small windmills is to supply electric energy for summer houses and small cottages. Mostly solutions available on the market are used in the windmills. On the other hand, choosing of the correct generator depends directly on its usage in the windmill, where it must grant the right energy productivity and be technically as optimal as possible. This thesis investigates generator design according to specific need of energy productivity in small windmill.

A novel low-speed slotless generator solution is chosen to be under investigation as a suitable generator. Preliminary design parameters of the generator are set based on wind turbine parameters and needed annual energy consumption of a typical household.

In this chapter design parameters of the investigated machine are set and calculation model is developed. Magnetic and electric parameter calculations as well as thermal behavior of the machine are taken into account while developing the calculation model.

2.2 Design process and parameter identification

To design a generator, it is important to define what the machine will be used for, which defines the generator preliminary data. As mentioned before, the generator investigated in this thesis is meant for the use in windmills, producing electrical energy for households. The windmill is equipped with a frequency converter to be connected to the grid or load batteries. The windmill must then fit the wind characteristics and it must be possible to connect it with the converter. Based on those requirements it is possible to set the needed preliminary parameters to start the design process. Firstly, the wind turbine sets the rated power and rotational speed of the generator. Secondly, the converter, used with the windmill, sets the output voltage of the generator. Next chapter describes how the preliminary parameters of the generator design are found.

2.2.1 Power and rotational speed from wind

One of the most important parameters of the generator is the power. To find the needed power of the generator, one must rely on generator's potential use and its peculiarities. As the generator is meant only for the use in small windmills, the required energy productivity of small windmills must be found.

The main application field of small windmills is their use in households, where they are used to produce either all the needed electrical energy or to decrease the amount of electricity consumed from the grid. Problem with the windmill is that its output power is almost uncontrollable. In case of no wind, the windmill is not able to generate power. This leads to the situation, where

other energy sources must be used to ensure electricity supply for the household. This means that it is not possible to design a windmill based only on the momentary consumption but consumption of a certain time gap must be looked at.

There have been many researches that investigate the habits and energy need of households [63, 64]. Those researchers have found that the average annual energy consumption of a household in Estonia and neighboring countries is between 2 and 10 MWh/y. Table 2.1 shows some of those average values in different countries. This is one of the preliminary data used in design of the generator. In other words, annual energy productivity of the generator must be equal to the annual average energy consumption of one household plus the conversion and accumulation energy losses.

Table 2.1. Average energy consumption of households in Estonia and some other countries in 2006 [65] (Nordic countries the electricity consumption includes heating).*

Country	Consumption, kWh/y
Estonia	4 814
Lithuania	2 468
Latvia	2 658
Iceland*	30 003
Norway*	23 255
Poland	2 699
France	6 824
Sweden*	14 457
Germany	6 405
Slovakia	4 376
Finland*	16 321
Denmark	6 278
Czech Republic	5 557
USA	13228
Russian Federation	5350

The power that a windmill can achieve depends on numerous different aspects. Those are for example climatic aspects – not only wind speed but also wind density affects wind power. The kinetic energy of the wind per second P_{wind} can be found according to flowing equation of fluids and gases [66]:

$$P_{wind} = \frac{1}{2}\rho_{air} S v_w^{\ 3} \qquad 2.1$$

where, ρ_{air} is air mass density
S is surface area of the blades
v_w is the wind speed

However, this equation does not describe directly the power that the windmill is able to produce. To find the mechanical power of the windmill on its shaft, it is necessary to consider productivity of the blades used in the windmill. The productivity of the blades is described using the blade power factor C_p. The maximum blade power factor is set by Betz' law, which sets it to 16/27 (or 59.3%). This is the maximum theoretic value [66]. The best blades used in windmills achieve a value of C_p of 0.45-0.5, which are around 75-85% of the theoretical maximum [66]. Yet, this maximum power factor depends on a certain wind speed and rotational speed of the blades. In the whole wind speed spectrum, the C_p of the windmill changes depending on the shape and number of the blades. To find the productivity of the windmill, it is necessary to know the C_p of the blade in the whole speed range.

The most used blade type in windmills is the three blade horizontal solution. As an example Fig. 2.1 shows the dependence of three bladed windmill power factor on blade tip speed ratio to blade pitch angle. It can be seen from this Fig. 2.1 that C_p depends highly on the blade pitch angle β to the wind as well as rotational speed of the blades (λ_{tip} is the blade tip speed ratio according to wind speed) and wind speed. Due to this, it is relatively difficult to find an accurate C_p. On the other hand, it have to be remembered that a windmill has three important wind speed values that describe the windmill properties – wind speed that starts the windmill, rated wind speed of the windmill (usually it is the wind speed where C_p has the maximum value), and maximum wind speed of the windmill that it can handle while working, above this speed the windmill is shut off.

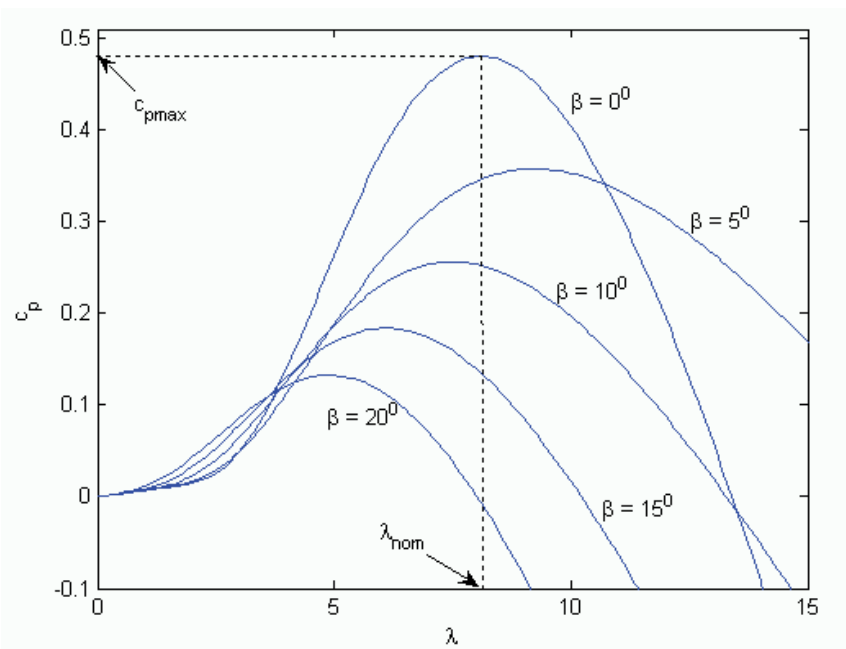

Figure 2.1. Dependence of wind turbine power factor on wind speed [67].

To find the annual productivity of the wind, wind information is needed. These are values that are possible to measure. Measuring is one of the most important ways of gaining accurate information while building a wind park. On the other hand, meteorological observations have shown that statistically the annual wind speed is distributed according to a specific function on which the generator parameters in this thesis rely. Statistic distribution, more specifically Weibully's distribution described by its density function *ρ(v)* (2.2) and cumulative distribution function *f(v)* (2.3), is the information which has been taken into account for the calculation of the generator in this thesis:

$$\rho(v) = \left(\frac{k}{\lambda}\right)\left(\frac{v}{\lambda}\right)^{k-1} e^{-\left(\frac{v}{\lambda}\right)^{k}} \qquad 2.2$$

$$f(v) = 1 - e^{-\left(\frac{v}{\lambda}\right)^{k}} \qquad 2.3$$

where k is shape parameter
λ is scale parameter
v is average wind speed

Weibully's distribution, where its shape factor is equal to 2 is considered to be one of the most common wind speed distributions [66]. In this case Weibully's distribution simplifies and matches Rayleigh's distribution. Rayleigh's distribution is the simplest wind speed distribution functions, as only average annual wind speed must be known to describe it. In this case, wind function can be described using the following equations:

$$\rho(v) = \left(\frac{\pi}{2}\right)\left(\frac{v}{\bar{v}}\right) e^{-\left(\frac{\pi v}{4\bar{v}}\right)^{2}} \qquad 2.4$$

$$f(v) = 1 - e^{-\left(\frac{\pi v}{4\lambda}\right)^{2}} \qquad 2.5$$

where $\bar{v}$ is mean wind velocity.

According to equations 2.4 and 2.5 probable wind speed presence probability can be composed. This is presented on Fig. 2.2 where can be seen wind speed Rayleigh's distribution on different average wind speeds.

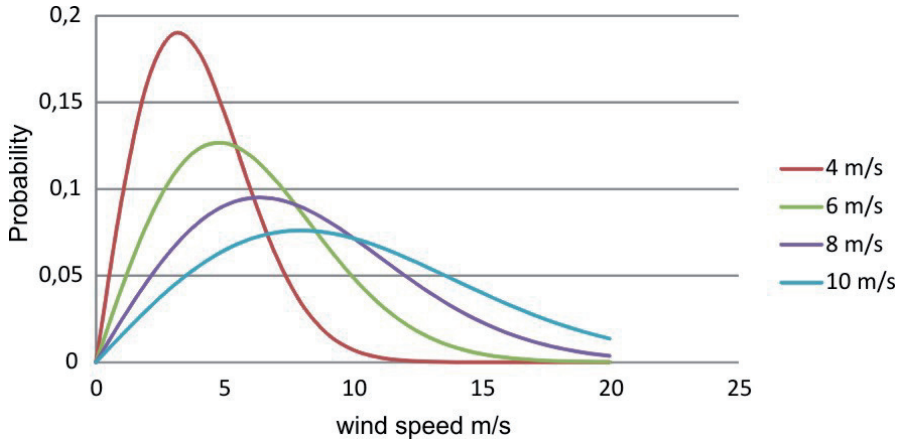

Figure 2.2. Relative distribution of wind speed on different average wind speeds.

Using equation 2.12.1 and taking wind turbine blades power factor C_p into account, turbine power P_{turbin} function equation can be found as follows:

$$P_{turbin}(v) = \frac{1}{2}\rho_{air} C_p S v^3 \qquad 2.6$$

Now, equivalent power of the windmill can be found, that considers wind speed distribution law described before. Equivalent power P_{ekv} can be written as an integer:

$$P_{ekv}(v) = \int_{v_1}^{v_2} P_{turbin}(v) \cdot \rho(v) \cdot dv \qquad 2.7$$

From this it is possible to find productivity factor of the windmill c, which is the ratio of equivalent power (Eq. 2.7) to rated power of the windmill:

$$c = \frac{P_{ekv}}{P_n} = \frac{1}{P_n}\int_{v_1}^{v_2} P_{turbin}(v) \cdot \rho(v) \cdot dv \qquad 2.8$$

As both equivalent power and rated power equations use wind pressure and area of windmill blades, which are constant, those values are reduced. This means that to find productivity factor of the windmill, only average wind speed, rated speed of the designed windmill and probable distribution of the wind must be known.

From this considering the annual energy consumption and productivity factor as well as the needed electrical rated power P_n^e can be found and it can be written as follows:

$$P_n^e = \frac{W_a}{c \cdot 8760 \cdot h}, \qquad 2.9$$

where, W_a is annual energy consumption.

According to equation 2.9 Fig. 2.3 shows which windmill is needed to supply an annual consumption of a household based on its annual productivity according to average annual wind speed (average annual energy consumption of a household is considered to be 5000 kWh). To define the power there were made some assumptions based on commercially available wind turbine power characteristics. The assumption is made, that the rated power of the windmill is achieved at wind speed 12 m/s (usually varying from 11 to 13 m/s), the windmill starts at wind speed of 3 m/s and shuts down at 25 m/s. From 3 m/s to 12 m/s the windmill produces the power according to the blades characteristics, over the 12 m/s the windmill output power is constant (windmill rated power).

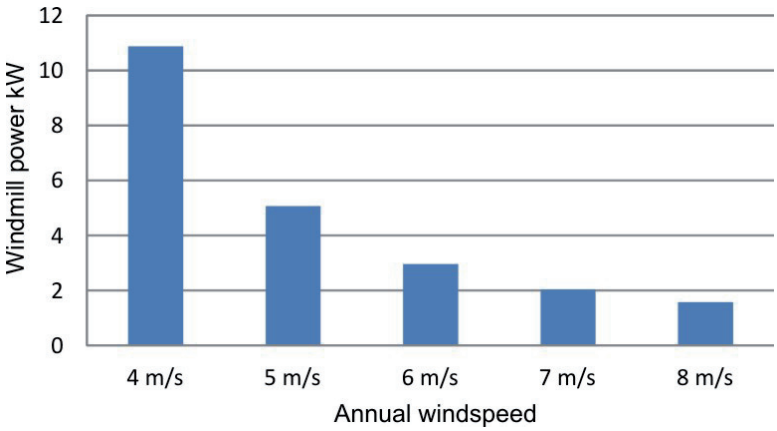

Figure 2.3. Rated power to which the windmill must comply according to the average annual wind speed when the needed annual energy is 5000kWh.

Powers shown on Fig. 2.3 describe the rated output values of the windmill. To set the power of the turbine one must know the efficiency of the windmill system. This efficiency must consider all the generator losses, which are bearing, copper, iron and aerodynamic losses as well as converter losses. Those losses cannot be found accurately before the design of the system, but they can be approximated based on efficiency values of existing systems. It can be approximated that efficiencies of grid converters are between 94 and 97% depending on the producer and power level [68, 69]. The generator efficiency depends highly on the generator type and power level. The efficiency of low speed PM generators at the power of 5 kW is between 75 and 85%. Knowing the efficiency and needed output power, the needed power of the turbine can be calculated:

$$P_n^t = \frac{P_n^e}{\eta_g \cdot \eta_m} \qquad 2.10$$

where, P_n^t is windturbine nominal power

η_g is generator efficiency

η_m is converter efficiency

When the wind turbine power is known, its parameters can be set. The main parameters of a wind turbine are air pressure, wind speed, blade productivity factor, and area that the blades cover. Those parameters can be also seen in Eq. 2.6. Air pressure and wind speed are the parameters that can be set as rated parameters. Typically, windmills are designed according to blade parameters and rated parameters are chosen at the highest blade productivity factor, which is achieved at a certain maximum tip speed ratio. Tip speed ratio λ_{tip} is the ratio between blade tip tangential speed u and wind speed v_w:

$$\lambda_{tip} = \frac{u}{v_w}. \qquad 2.11$$

Figure 2.4 shows, blades reach their maximum productivity at different tip speeds. From the Fig. 2.4 it can be read that three-bladed windmill has the highest C_p that is achieved at a relatively high tip speed ratio (at the rated speed of the blades that is around 12 m/s, blade tips move at the speed of 84 m/s). This is one of the reasons why three-bladed windmills are preferred. When more blades are used it is possible to achieve a higher starting torque of the windmill, but as their productivity is less than the one of three-bladed windmills, such windmills are rarely used. When the number of blades is decreased, the productivity factor is also relatively good as it is in case of three-bladed windmills, but on the other hand, rotational speed rises significantly, which sets new and severe requirements on the construction of such windmills. Additionally, noise will be relatively high and the starting torque will decrease.

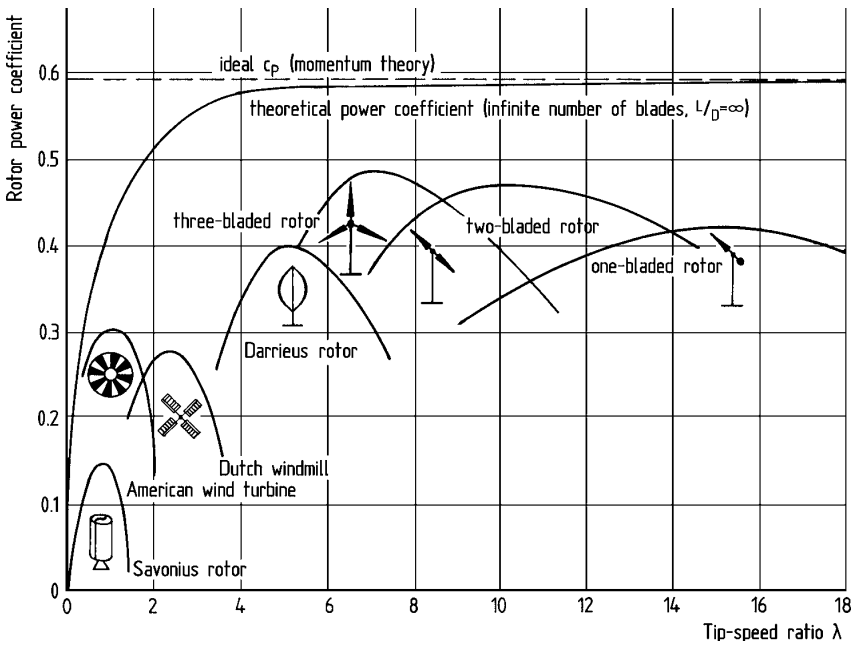

Figure 2.4. Productivity factors of the blades at different tip speeds

Using Eq. 2.9 and 2.6 with rated wind speed of the windmill, assumed productivity factor of the blades, air density and tip speed ratio, the rotational speed of the turbine n_n can be found as follows:

$$n_n = 60 \cdot \lambda_{tip} \cdot \sqrt{\frac{\rho_{air} \cdot C_p \cdot v_w^5}{8 \cdot P_n^t \cdot \pi}} \qquad 2.12$$

In this chapter the needed preliminary design parameters of the generator, such as rated power and rotational speed of the generator have been set. Additionally, data that is needed to find the mentioned parameters is presented. Based on the discussion above and Fig. 2.3, the output power of the generator is set to 5 kW for a rated wind speed of 12 m/s, which makes the annual energy productivity of the generator to be 5000 kWh. Based on Eq. 2.12, the rated rotational speed of the generator was found to be 230 rpm.

2.2.2 Voltage and current requirements from the inverter

In the previous chapter, it was shown how to find the needed power and rotational speed for generator design. In addition to these parameters, output voltage and current of the generator must also be found. Setting of these parameters is described in this chapter.

There are different ways how to utilize the energy gained from a windmill. In case of small windmills, typically three solutions or combinations of them are used. The cheapest and simplest solution is to convert the energy directly to heat. Usually, energy coming from the generator is used directly to heat water. Other solutions are to accumulate the energy in batteries or feed it to the grid.

As the output power of the windmill depends directly on the characteristics of the blades, the windmill must be able to work with various rotational speeds to generate the maximum amount of power at different wind speeds. On the other hand, the output voltage of the windmill depends directly on its rotational speed. Based on this, it is not possible to connect the windmill simply directly to a load resistance or to the grid. To connect the generator to load system, the output of the generator must be adjusted. The most common solutions to do so is to use of an inverter, in which case the output parameters of the generator must fit with the input parameters of the inverter.

There are various inverter topologies in use in case of windmills. These have been described in numerous scientific publications [70, 71, 72]. When the windmill is connected to the grid, the output of the inverter must be in accordance to the parameters of the grid. Small windmills are usually connected to the low voltage (LV) grid, in which case the grid voltage is 230/400 Vac and the frequency is 50 Hz or 60 Hz. Typically, inverters raising the voltage are used in windmills. This means that due to the converting process of the inverter, output voltage of the generator must be lower than the output voltage of the inverter even when the windmill is rotating faster than its rated rotational speed. Due to this, the maximum rotational speed of the windmill must be known. To simplify, it will be assumed that the rotational speed of the windmill can exceed

its rated rotational speed by 10%. As the rotational speed and voltage of the windmill are directly connected, it can be assumed that the rated voltage of the windmill should be about 10% lower than the output voltage of the inverter. In the case of 400 V inverter output voltage the generator rated voltage will be 360V. As the output power of the generator must be 5 kW, then the rated output current of the generator is 8.4 A. By calculating the generator output current there is taken into account that the inverter has a diode bridge rectifier with power factor 0.96.

Now, the rated voltage and current of the windmill have been set. From here, it is possible to determine the mechanical parameters of the generator.

2.2.3 Choice of generator design

There are various types of generators in use in windmills. Oldest and the most common type of generators in use in wind applications is the induction machine [73]. Such solution generally needs some type of transmission to be used, which decreases the reliability of the machine. To increase the reliability, directly drive windmills have been gaining popularity. Mainly PM machines are in use in such windmills [74].

While choosing the construction of the generator, one has to remember that the generator has to be suitable for the use in windmills and following design requirements must be met 75]:

- Simple construction,
- Light weight,
- Slow rotational speed,
- High output power,
- Changeable rotational speed,
- Small starting torque,
- Low cost.

Direct drive generators that are used in windmills are large, heavy and expensive compared to the generators that are used in windmills with transmission [76]. On the other hand, direct drive windmills offer significantly higher reliability as less mechanically wearing parts are in use. The weight of the direct drive windmill is large, as standard generator solution is used that is based on slow speed hydro generators [8]. When choosing the generator topology, one of the goals is to construct a generator as lightweight as possible, this would be suitable for the use in direct drive windmills. Due to this, the use of PM machine has been chosen, as this grants the possibility to use energy efficient machines and makes them attractive to the use in windmills. Development of industrial magnets is still a young industry and the optimal implementation to electrical machines is not fully developed yet. This gives many possibilities to engineering research in the field.

Electrical part of the generator can be divided to active part and passive part. Active part in the generator consists of magnetic field source that can be either electromagnet or a permanent magnet, and windings to which electrical

energy is generated. Passive part is used to direct the magnetic field and to get large energy density in the air gap. Both active and passive parts have similar weight densities – iron 7870 kg/m^3, copper 8940 kg/m3 and NdFeB magnet 7500 kg/m^3. Generally electrical machines have been designed so that the weights of active and passive parts divide equally in the machine. As passive part is needed only to direct and strengthen the magnetic field and is not needed for the generation of energy, theoretically it can be discarded for example in the stator. In that case, magnetic field density in the air gap decreases significantly, but using rear earth metals, it is possible to get at least 0.25 T field [36]. This is enough for the electrical machine to be built and gives the opportunity to build a light weight construction and large diameter machines. The result is a generator that weighs around 20-30% less compared to similar design machines with iron cores. Efficiency of such iron free machine is higher than 90% [36].

Preliminary construction in this thesis is the generator with iron free stator. When the iron free construction was investigated, it was found that it is sensible to use stator yoke made of iron as such solution would have similar characteristics as the iron free construction. Additionally, such solution grants a better magnetic flux density in the air gap and it is simpler to build construction wise. Finally it was found, that the best generator solution in a direct drive windmill is the generator construction shown on Fig. 2.5, which is the slotless PM three phase generator.

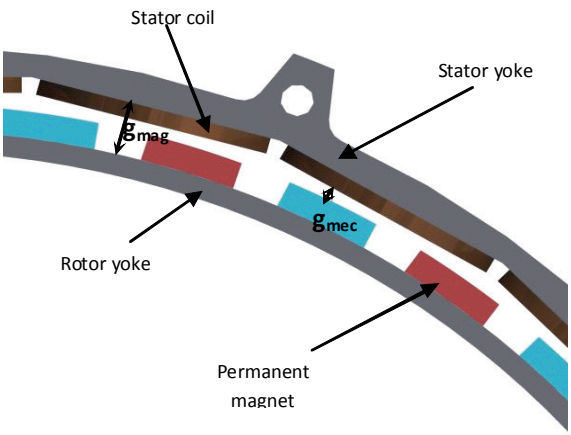

Figure 2.5. Principle schematic of the chosen generator

Such solution gives the opportunity to build large radius, slow speed, and light weight machines equipped with rear earth magnets and having low starting torque. The low starting torque comes from the construction as ferromagnetic layers in both rotor and stator have practically the same area. This means that magnetic resistance of the machine remains the same in every position of the rotor and no cogging torque can occur. Absence of cogging torque is important, as in case of the windmill, the generator is working mostly on low torque

compared to the rated torque, which means that cogging torque may cause unwanted speed fluctuations (vibrations) or even restrict the generator to start.

2.2.4 Generator radius and thickness

To set the mechanical dimensions of the generator, afore found generator power and rotational speed must be used. Knowing those values, it is possible to find the needed generator torque that the machine must achieve to generate the wanted amount of electric power. Mechanical torque of the generator is found using the following equation:

$$\tau = \frac{P}{\omega} \tag{2.1}$$

where, τ is torque,

P is power,

ω is angular velocity.

Torque achieved by the generator can be found according to Maxwell stress tensor σ:

$$\sigma = \frac{1}{\mu_0}\begin{bmatrix} B_x^2 - B^2/2 & B_x B_y & B_x B_z \\ B_y B_x & B_y^2 - B^2/2 & B_y B_z \\ B_z B_x & B_z B_y & B_z^2 - B^2/2 \end{bmatrix} \tag{2.2}$$

According to the theory, the strength of the magnetic field between objects in vacuum created a magnetic tension σ_r on the surface of the object that can be described as:

$$\sigma_r = \frac{1}{2\mu_0} B^2 \tag{2.3}$$

where, σ_r is magnetic field tension,

μ_0 is permeability of vacuum,

B is magnetic flux density.

This tension is oriented in the same direction as the force and creates equal perpendicular stress. When those values are divided to normal and tangential components according to the investigated object, tangential stress tensor can be found:

$$\sigma_{\tan} = \frac{1}{2\mu_0} B_n B_{\tan} \tag{2.4}$$

where σ_{tan} is magnetic field tangential tension,

B_n is magnetic flux density normal component,

B_{tan} is magnetic flux density tangential component.

From this, the linear current density A in the air gap that produces the needed tangential field strength can be found according to Ampere's law:

$$\oint H \cdot dl = Ady \tag{2.5}$$

where A is the linear current density and l is the length of the magnetic path.

Assuming that the normal direction magnetic flux density B_n is created by a permanent magnet, it can be written that:

$$B_n = \mu_0 H \tag{2.6}$$

Replacing Eq. 2.6 and 2.5 to Eq. 2.4 it can be seen that the stress tensor is as follows:

$$\sigma_{\tan} = B_n A \tag{2.7}$$

This Equation stands for the values that are independent from time. As the generator has rotating sinusoidal fields, the Equation can be written to be dependent on time:

$$\sigma_{\tan} = B_n \sin(\omega t) A (\sin \omega t) \tag{2.8}$$

From this, the average value of tangential stress is:

$$\sigma_{\tan} = 0{,}5 B_n A \tag{2.9}$$

Equation 2.9 gives the tangential magnetic stress in the air gap. To find the torque achievable by the machine, the stress tensor must be multiplied by the area of generator active part and radius of the air gap. Hence, the generator torque can be found:

$$\tau = Fr = \sigma_{F\tan} Sr = 0{,}5 B_n A 2\pi r^2 l \tag{2.10}$$

where F is force, r is radius.

From Eq. 2.10 it can be seen, that the torque the generator can achieve depends on two values besides its dimensions – the magnetic flux density in the air gap and the linear current density. The magnetic flux density in the air gap is set by the permanent magnets. It can be approximated that while designing the generator, the dimensions of the magnets are chosen so, that the working point of the magnet would be in the maximum point of energy productivity. It varies in case of different magnets and depends on the demagnetization curve of the

permanent magnet. Fig. 2.6 shows a demagnetization curve of an NdFeB permanent magnet that is planned to use in the given machine type.

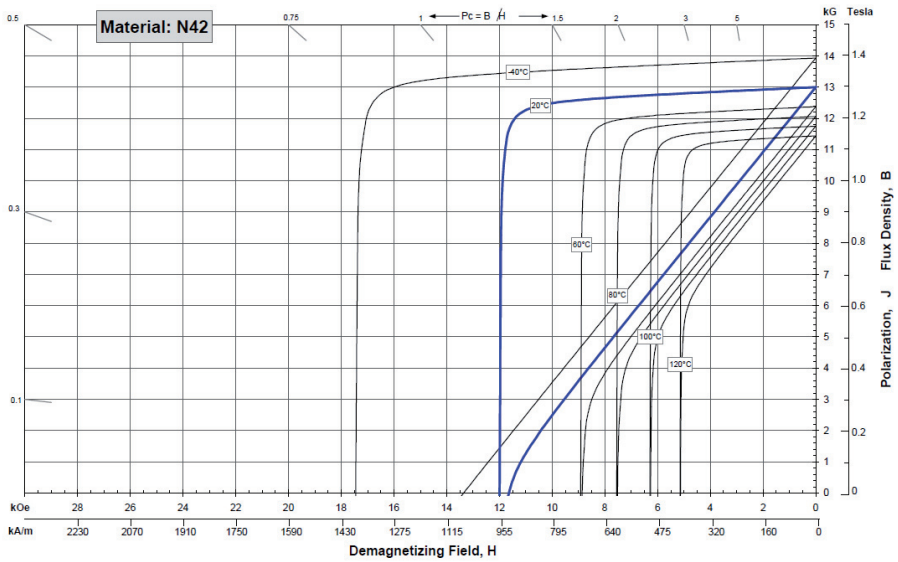

Figure 2.6. Demagnetization curve of a permanent magnet.

It can be seen from the demagnetization curve that the working point of the magnet could be between 0.5-0.7 T (point where BH is highest). According to this parameter, the maximum desired magnetic flux density in the air gap of the designed machine is set to 0.6 T. Using the magnetic flux density, it is possible to find the relative dimensions of the machine. For this purpose, one pole pair section of the machine is used as shown on Fig. 2.7.

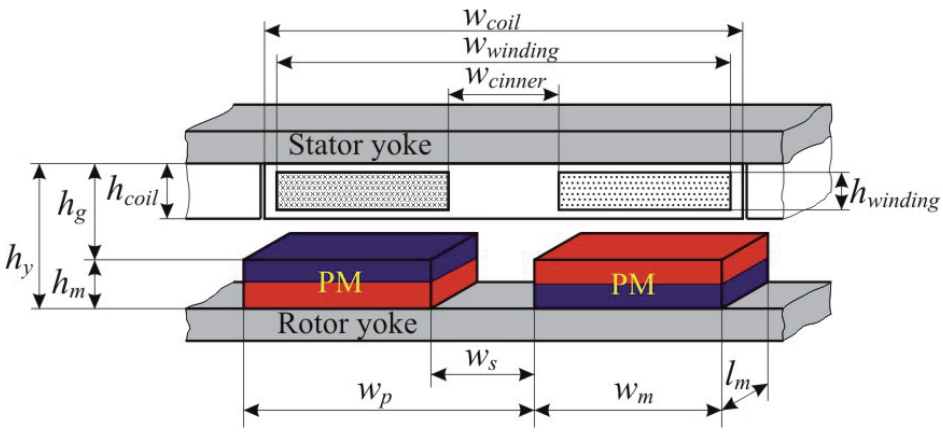

Figure 2.7. One section of the generator.

To set the relative dimensions of the machine, a simple reluctance network is used for the magnetic field calculations. In the investigated construction, the path of the magnetic circuit can be divided into three parts. First, the main

magnetic path, that goes from the rotor to stator. Second, the magnetic flux leakage paths that are situated over the top of the magnet and leaking from one magnet to another. Third is the magnetic flux leakage path over the magnet edges. Different paths of the magnetic flux are shown on Fig. 2.8.

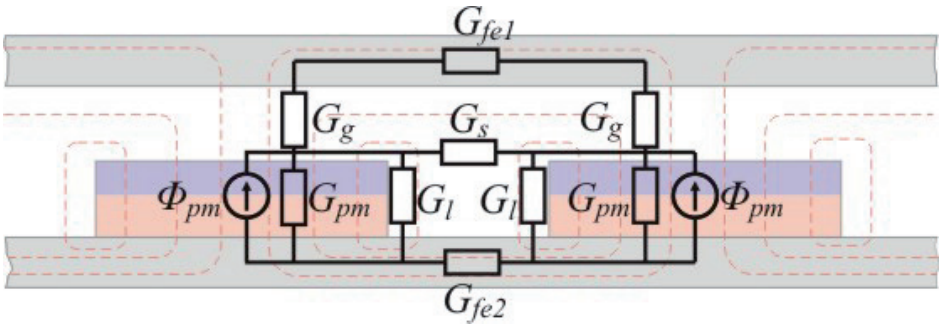

Figure 2.8. Closing paths of magnetic field in one pole pair of the investigated machine.

According to Fig. 2.8 a magnetic circuit can be composed that is shown on Fig. 2.9. From there it can be seen that the magnetic circuit consists of four areas of magnetic conductivity – permanent magnet conductivity P_{pm}, leakage conductivity over the edge of the magnet P_l, leakage conductivity between magnets P_s and air gap conductivity P_g.

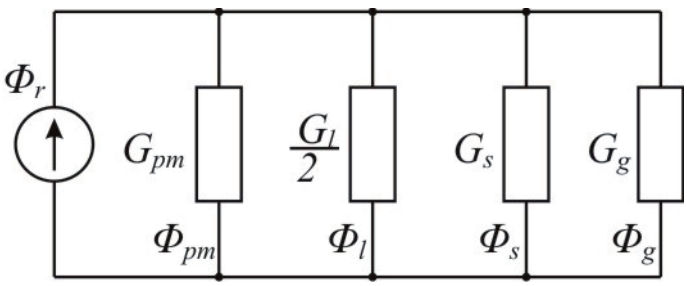

Figure 2.9. Equivalent circuit

Magnetic conductivity G is calculated as:

$$G = \mu \int S dx \tag{2.11}$$

where S is the cross-section are of the flux path and x is the flux path length.
According to Eq. 2.11 the permanent magnet conductivity can be found according to the dimensions of the magnet and its permeability μ:

$$G_{pm} = \mu \frac{l_m w_m}{h_m} \tag{2.12}$$

To find the conductivity of the closing path from the top of the magnets, the following equation must be used:

$$G_s = \frac{\mu_0 l_m}{\pi} \int_0^{\frac{w_m}{2}} \frac{dx}{x + \frac{h_m}{\pi}} = \frac{\mu_0 l_m}{\pi} \cdot \ln(1 + \frac{\pi w_m}{2h_m}) \qquad 2.13$$

To find conductivity between the magnets, the following formula can be used:

$$G_l = \frac{\mu_0 l_m}{\pi} \int_0^{h_g} \frac{dx}{x + \frac{w_s}{\pi}} = \frac{\mu_0 l_m}{\pi} \cdot \ln(1 + \frac{\pi h_g}{w_s}) \qquad 2.14$$

And last, the air gap conductivity can be found as follows:

$$G_g = \mu_0 \frac{l_m w_m}{h_g} \qquad 2.15$$

When the circuit on Fig. 2.9 is solved, the magnetic flux density in the air gap can be found:

$$B_g = B_r \frac{G_{pm}}{G_\Sigma} \qquad 2.16$$

where the G_Σ is the sum of the conductivities.

When solving Eq. 2.16, the studied generator magnetic field and relative dimensions can be found according to the type of permanent magnet and value of the magnetic flux density in the air gap. The calculations are based on NdFeB magnet N42 (*Figure 2.6*) and the magnetic flux density in the air gap was chosen to be 0.6 T. When finding the relative dimensions of the construction it was kept in mind that all the dimensions would be based on the length of a single pole w_p. Additionally it was taken into account, that the length of the magnet w_m forms 2/3 of the whole pole. This dimension was set based on literature and the magnet-pole ratios of PM machines described there. When solving the equivalent circuit (*Figure 2.9*), the relative dimensions of magnetic circuit of the investigated generator was computed. They describe the magnet length ratio to pole length w_m/w_p, whole air gap length ratio to pole length h_y/w_p and magnet height ratio to whole air gap length h_m/h_y. Note that the whole air gap consists of the magnet height, the mechanic air gap and the winging height. The computed values are shown in Table 2.2.

Table 2.2. Relative dimensions found during magnetic field calculations.

Dimension ratios	Ration
w_m/w_p	0.67
h_y/w_p	0.37
h_m/h_y	0.5

These beforehand computed relative dimensions are replaced in the rest of the design equations with the following constants:

$$k_p = \frac{w_m}{w_p}, \qquad k_g = \frac{h_y}{w_p} \cdot \frac{h_m}{h_y} \tag{2.17}$$

where k_p describes the magnet length ratio to the pole length, and k_g describes the air gap ratio to the pole length.

Other value that set the generator torque according to Eq. 2.10 is the linear current density. This is determined mainly by the cooling of the generator. As passive cooling is planned to be used in the designed generator and due to the characteristics of the wind generator its rotational speed is low, it can be assumed that the cooling possibilities are not the best. Hence, the planned current density is chosen to be conservatively low 4.5 A/mm^2 [77]. Additionally, the linear current density of the generator is chosen to be 20 kA/m [77].

The linear current density of an electrical machine can be expressed as follows:

$$A = \frac{JS}{w_{coil}}. \tag{2.18}$$

It can be seen that, the linear current density depends on the current density J that was set earlier, the area of the active part of the winding S and the whole length of the winding w_{coil}. The whole length of the winding can be found according to pole length w_p, the number of poles p and number of coils n_c:

$$w_{coil} = \frac{p}{n_c} \cdot w_p. \tag{2.19}$$

To determine the active area of the winding, the generator relative dimensions calculated from the magnetic field calculations are used. In addition to that, constants are used, that describe the insulation surrounding the winding (k_{tiso}, k_{niso} *and* k_{coil}) and the ratio between the winding whole length and the winding window length $k_{inn/out}$. Those constants are:

$$k_{tiso} = \frac{w_{windig}}{w_{coil}} = 0{,}97, \quad k_{niso} = \frac{h_{winding}}{h_{coil}} = 0{,}86,$$
$$k_{coil} = \frac{h_{coil}}{l_g} = 0{,}7, \qquad k_{inn/out} = \frac{w_{cinner}}{w_{coil}} = 0{,}25, \tag{2.20}$$

where k_{tiso} is the coefficient of the isolation thickness on the sides of the winding depending on the width of the winding,

k_{niso} is the coefficient of the isolation thickness on top and under the winding depending on the thickness of the winding,

k_{coil} is the coefficient of the winding thickness depending on the thickness of the winding in the air gap,

$k_{inn/out}$ is the ratio between whole winding length and winding window length.

When choosing the insulation constant, it was taken into account that physically it is impossible to place the windings directly next to each other and the mass in which the winding is casted is also the mean with which the winding is closed to its position. The winding thickness constant is chosen according to the final physical air gap size. This dimension depends highly on the precision of the building of generator construction. The more accurately the machine is built, the smaller air gap can be allowed. When choosing the inner and outer dimensions of the winding, the winding distribution factor was taken into account, so that it would be as optimal as possible with respect to manufacturing tolerances.

The generator winding active area can be calculated in terms of the aforementioned constants:

$$S_{coil} = h_{coil} k_{nisa} (w_{coil} k_{tiso} - w_{cinner}) \tag{2.21}$$

The height of the winding can be found using the constants and the magnet pole length:

$$h_{coil} = w_p k_g k_p \tag{2.22}$$

The winding window can be found using the magnet pole length:

$$w_{cinner} = w_{coil} k_{inn/out} = \frac{p}{n_c} w_p k_{inn/out} \tag{2.23}$$

Replacing Eq. 2.23, 2.22, 2.21 into Eq. 2.18, the generator linear current density equation is formed:

$$A = J w_p k_g k_p k_{niso} (k_{tiso} - k_{inn/out}) \tag{2.24}$$

From the Eq 2.24 it can be seen that the linear current density of the generator depends only on the current density, the pole length and the constants that were defined during the magnetic field calculations. This Eq. 2.24 determines directly, what the length of the generator pole must be, so that the generator would be able to achieve the desired torque:

$$w_p = \frac{A}{J k_g k_p k_{niso} (k_{tiso} - k_{inn/out})} \tag{2.25}$$

With this, the first mechanical dimension of the generator has been set. For the studied machine it was found that the length of the pole w_p has to be 57 mm. Using the length of the pole and the defined constants, the length l_m and height

h_m of the magnet, air gap dimensions h_g and winding height h_w can be calculated.

To find other needed dimensions, the rotational speed of the generator and the electric frequency has to be used. Traditionally, the generators nominal frequency is set by the grid frequency 50 Hz. As the generator under investigation is meant to be used in a windmill where the output is rectified with a diode bridge, it is not necessary to use the grid frequency in this case. For choosing the generator output frequency there have to be considered two aspects. The higher the frequency is, the better the magnetic field conversion to electrical energy is, meaning that less magnetic flux is needed in the machine. But on the other hand the iron losses in the machine depend on the frequency and with higher frequency the losses in the machine also go higher. Taking these two conditions into account for the studied machine the nominal frequency is chosen higher than the grid frequency. Higher frequency was chosen because one of the aims was to design light weight machine. Also as the studied generator is a slotless machine were the stator iron part is much smaller than in conventional machines, it can be assumed that the iron losses do not affect strongly the total losses of generator. This assumption will be justified later in the loss calculation. Besides, the generator is designed to work in a windmill where most of the time it is working at lower frequencies than the nominal one. Based on this, during the design, the frequency is set around 77 Hz at nominal rotational speed. Knowing the rotational speed n_n and the generator frequency f_n, it is possible to find the number of pole pair in the given generator:

$$p = \frac{2f_n}{n_n} \cdot 60. \tag{2.26}$$

It was found from Eq. 2.26 and the parameters calculated above that the optimal number of pole pairs in the studied generator is 20.

Most costly material for PM machine is the magnet. So it is important to predict the amount of magnet material needed for the machine. Knowing the number of poles, it is possible to approximate the needed volume of magnets. The volume of all the magnets in the generator is:

$$V_m = 2k_p k_g \cdot \frac{\pi\tau}{0{,}5AB_n p^2}. \tag{2.27}$$

Knowing the number of poles and the length of one pole, the generator radius can be found:

$$r = \frac{pw_p}{2\pi}. \tag{2.28}$$

From here, the generator width can be found, that is needed to achieve the desired torque. For that Eq. 2.10 is used:

$$l = \frac{\tau}{0{,}5 B_n A 2\pi r^2}. \qquad 2.29$$

To determine the length of the machine, it must be taken into account that the machine is built to have three phases. Hence, symmetry must be present:

$$n_c = 3q, \qquad 2.30$$

where q is the number of phases and n_c is the number of generator windings.

As three phase system is used in the machine, a shift between the phases must be granted. In the given machine three phase symmetry is achieved when the angle between phase windings is 60^0, 120^0 or 240^0. Hence the following equation must hold:

$$\sin\left(\frac{2p}{n_c}\right) = \left|\frac{\sqrt{3}}{2}\right|. \qquad 2.31$$

Additionally, as concentrated windings are used in the machine, the length of one winding must not exceed 360 electric degrees:

$$\frac{2p}{n_c} < 1 \qquad 2.32$$

From Eq. 2.31 and 2.32 a comparison Table 2.3 is compiled, where the solution for poles and windings that are suitable for this machine is presented.

Table 2.3. Choosing of suitable poles and windings according to criterion presented in Eq. 2.31 and Eq. 2.32.

$n_c \backslash p$	10	12	14	16	18	20	22	24	26
3	-	-	-	-	-	-	-	-	-
6	-	-	-	-	-	-	-	-	-
9	-	-	-	-	-	-	-	-	-
12	Ok	-	-	-	-	-	-	-	-
15	Ok	-	-	-	-	-	-	-	-
18	-	Ok	-	-	-	-	-	-	-
21	-	-	Ok	-	-	-	-	-	-
24	-	-	-	Ok	-	Ok	-	-	-
27	-	-	-	-	Ok	-	-	-	-
30	Ok	-	-	-	-	Ok	-	-	-
33	-	-	-	-	-	-	Ok	-	-
36	-	Ok	-	-	-	-	-	Ok	-

Combinations between poles and windings suitable for the machine were found. When choosing the number of windings, it must be done so that the induced electromotive force in the winding would be maximal. For that one winding must be investigated. The winding consists of two parts – beginning and end.

While choosing the winding it is assumed that the vector sum of the electromotive force induced in the beginning and end of the winding would have a maximum value. Fig. 2.10 presents a fundamental electromotive force distribution, where the first winding is placed in the magnetic field with the angle α and final winding is placed in the magnetic field shifted from the beginning by an angle $\alpha+\theta_{endcoil}$. The angle of the end winding can be found using electrical angle of one winding, which can be found as follows:

$$\theta_{coil} = \frac{2p}{n_c} 2\pi + \alpha \qquad 2.33$$

Position of the end winding is found using the generator constants calculated before:

$$\begin{aligned} w_{endcoil} &= k_{inn/out} w_{coil} + \left(\frac{k_{inn/out} w_{coil} - w_{coil}}{2} \right) \\ &= w_{coil} \left(\frac{k_{inn/out} w_{coil} - 1}{2} \right) \end{aligned} \qquad 2.34$$

Using Eq. 2.33 and 2.34 the electrical angle of the end winding can be found:

$$\theta_{endcoill} = \frac{2p}{n_c} 2\pi \left(\frac{k_{inn/out} w_{coil} - 1}{2} \right) + \alpha \qquad 2.35$$

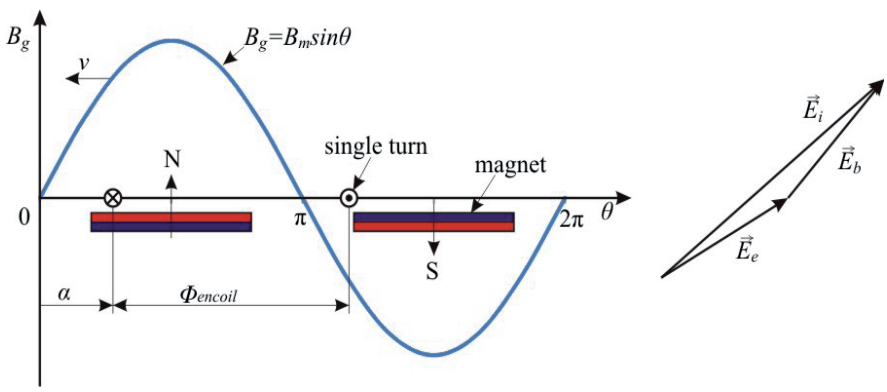

Figure 2.10. Placement of the beginning and end of the winding in magnetic field and electrical angle of the winding.

Knowing the electrical angle of the beginning and end of the windings, the sum of induced electromotive force in relative units can be found.

$$\vec{E}_i = e^{j\alpha} + e^{j\alpha+\phi_{edcoil}} \qquad 2.36$$

According to Eq. 2.36 Table 2.4 is compiled. It shows the induced electromotive force values to the winding in relative units.

Table 2.4. Induced electromotive force values to the winding in relative units.

$n_c \backslash p$	10	12	14	16	18	20	22	24	26
6	-	-	-	-	-	-	-	-	-
9	-	-	-	-	-	-	-	-	-
12	1,991	-	-	-	-	-	-	-	-
15	1,866	-	-	-	-	-	-	-	-
18	-	1,866	-	-	-	-	-	-	-
21	-	-	1,866	-	-	-	-	-	-
24	-	-	-	1,866	-	1,991	-	-	-
27	-	-	-	-	1,866	-	-	-	-
30	1,259	-	-	-	-	1,866	-	-	-
33	-	-	-	-	-	-	1,866	-	-
36	-	1,259	-	-	-	-	-	1,866	-

It can be seen from Table 2.4 that in case of such machine construction, a machine with the pole ratio of 0,666 can always be built. The exception is the 20 pole pair machine, where also 24 windings can be used, in which case the ratio is 0,833. As the number of pole pairs was set to 20 before, then according to Table 2.4 the number of windings is chosen to be 24.

Knowing the number of coils, the length of the coil can be set according to Eq. 2.19 and it was found to be 92 mm. With this the preliminary parameters of generator design have been set. Table 2.5 shows the summary of these results, which were based on the design methodology of the generator.

Table 2.5. Preliminary parameters of the generator under investigation.

Name	Sign	Unit	Value
Generator power	P	kW	5 (6)
Rotational speed	n_n	p/min	230
Torque	τ	Nm	249
Number of poles	$2p$		40
Radius of air gap	R	mm	680
Width	l	mm	57
Number of coils	Q		24

2.3 Magnetic field calculation

One of the most important parameters for a generator is the magnitude of the main magnetic field. Main magnetic field determines the rate of energy that the generator is capable to convert and it provides the magnitude and waveform of the induced electromotive force (EMF). Additionally the magnetic field rotating in the machine is the source for hysteresis and eddy current losses in the iron. In the following, two different methods to calculate the magnetic field are proposed. First calculations are carried out analytically by using vector potential calculation method as this allows fast calculation of static magnetic fields. Second method for magnetic field calculations is using finite element method (FEM), which by its nature is rather much slower method for calculation.

However it provides means to determine the magnetic field in the full geometry and in addition it allows dynamic magnetic field calculations which with other calculation methods (like analytical method) would be mathematically very complex and time-consuming.

2.3.1 Magnetic field calculation principles

To study and analyze the magnetic fields in an electrical machine a number of different methods are available [78]:

- In principle, it is possible to determine the magnetic field quantities analytically by solving the Maxwell equations in the geometry of the machine. However in the real devices and models this is often too complex. Direct magnetic field analysis methods are used very rarely, and even in such cases significant simplifications are made.
- If the model is symmetrical, Maxwell's equations can be implemented in 2-dimensional geometrical model rather than using 3-dimensional model. In 2-dimensional model the effect of the third geometrical dimension is taken into account using approximation equations. Sometimes it is also possible to simplify magnetic fields descriptions by representing those using scalar potentials instead of vector potentials. For the evaluation of scalar potentials, Laplace or Poisson equations are used.
- In some geometry configurations, it is possible to use conformal transformations when analytically solving magnetic field equations. In this case the geometrical model will be provided in 2-dimensional from on a plane described in grid coordinates of complex plane z. Using such geometry and boundary conditions, the model will be transformed with conformal mapping to a new plain w. The magnetic scalar potential on z plane is replaced with w plan magnetic field complex potential using special conversion equations.
- Using Maxwell equations, the current, flux and power density distributions can be modeled mathematically very accurately. In order to determine the numerical quantities, different widely used methods include:
    - finite difference methods;
    - finite element methods;
    - finite volume method;

  and many others. Modern software uses mainly finite elemental methods which allow relatively precise analysis of the field distribution for geometrical models using parameters of materials and pre-defined boundary conditions (examples of such software packages include Comsol Multiphysics, Maxwell, ANSYS, Infolytica, MagNet, FEMM, and others).

– Magnetic field can also be studied experimentally. However, this method can be applied only on the particular built machines or models and there are practically not many possibilities to study the field distribution inside the model.

Electromagnetic field distribution in PMSG can be characterized by Maxwell's equations. Maxwell's I law (Ampère's circuital law) describes how the magnetic field *H* vector is related to the current density *J*:

$$\nabla \times \vec{H} = \vec{J}. \tag{2.37}$$

Maxwell's II law (though electromagnetic induction law was first discovered by Faraday, Maxwell provided its mathematical formulation) states that a time-varying magnetic field *B* is always accompanied by a spatially-varying, non-conservative electric field *E*, and vice-versa:

$$\nabla \times \vec{E} = -\frac{\partial \vec{B}}{\partial t}. \tag{2.38}$$

Additionally to supplement Maxwell's equations, several derived formulations can be used:

the magnetic flux density continuity relation

$$\nabla \cdot \vec{B} = 0, \tag{2.39}$$

the electric current density continuity relation

$$\nabla \cdot \vec{J} = 0, \tag{2.40}$$

and materials constitutive equations

$$\vec{B} = \mu_a \vec{H} = \mu_r \mu_0 \vec{H}, \tag{2.41}$$

and

$$\vec{J} = \sigma \vec{E}. \tag{2.42}$$

The field distribution according to equations 2.41 and 2.42 depends on the electromagnetic properties of the environment where:

$\mu_0 = 4\pi 10^{-7}$ is permeability of vacuum,

μ_r is relative permeability of the material,

σ is conductivity.

2.3.2 Vector potentials

Prior to evaluating the magnetic field in the studied generator model using vector potential method, some initial conditions have to be defined. First, let us

assume that permanent magnet provides ideal sinusoidal magnetic field distribution in the air gap and it is moving with constant speed. Second, let us assume that the length of a generator pole is much smaller than the width of the generator. In this case, it can be considered acceptable if the generator magnetic field is analyzed in 2-dimensional geometry on one plane. In such case the problem can be expressed as vector potential A, where x and y components become zero for a 2-dimensional solution and we use A as the z-axis component. Configuration used to calculate the magneto motive force (MMF) is provided in Fig. 2.11 where Y_1 represents rotor yoke thickness, Y_2 represents thickness of rotor yoke along with permanent magnet thickness, Y_3 is total thickness of rotor yoke, permanent magnet and air gap thickness.

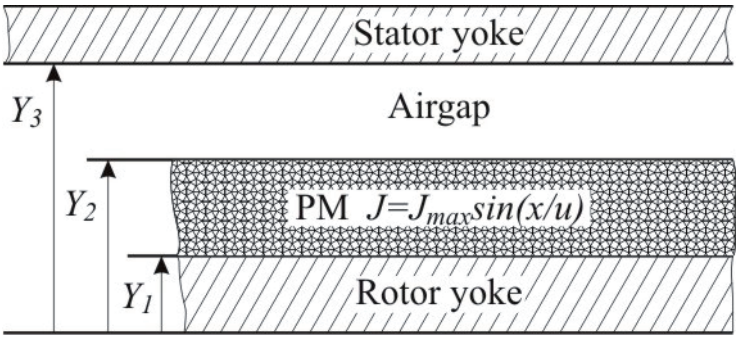

Figure 2.11. Generator magnet flux model for vector potential calculation.

To determine the excitation field of the machine the excitation current density distribution has to be defined first, for a permanent magnet having magnetic field density B_r this can be expressed using equation [79, 80]:

$$J = \frac{4B_r \sin(\alpha)}{\pi u \mu_{rec} \mu_0} \qquad 2.43$$

where J is the equivalent current density

α is the wavelength calculated as $\alpha = \frac{\pi w_m}{2w_p}$

u is the wavelength calculated as $u = \frac{\pi R}{p}$

Within this thesis, our target is the magnetic field distribution within the area where the coils are placed; this is between Y_2 and Y_3 in Fig. 2.11. In this area the vector potential is determined by [[81] J.R. Bumby, E. Spooner, M. Jagiela, "Equivalent Circuit Analysis of Solid-rotor Induction Machines with Reference]:

$$\overline{A} = \frac{y}{(Y_3 - Y_2)} \left\{ A_{2,1} \left(e^{\frac{Y_3}{u}} - e^{\frac{Y_2}{u}} \right) - A_{2,2} \left(e^{-\frac{Y_3}{u}} - e^{-\frac{Y_2}{u}} \right) \right\} \qquad 2.44$$

The magnetic flux density can then be found using a relation of vector potential A and wavelength u:

$$B = \frac{A}{u} \qquad 2.45$$

To account for the higher harmonics in the magnet flux density, it has to be taken into account that the wavelength depends on the harmonic number. The higher the harmonic order the shorter is the wavelength *u*. Taking this into account it is possible to find all the harmonics separately solving the vector potential equation Eq. 2.45.

For the studied machine, the distribution of magnetic flux density determined with the vector potential method is provided in Fig. 2.12 where the fundamental harmonic magnetic flux density distribution over one pole is presented. As seen from Fig. 2.12 the vector potential method has provided a fundamental harmonic maximum flux density magnitude of 0.645 T, this is slightly greater than the value of 0.6 T selected in the section describing the generator's parameter identification.

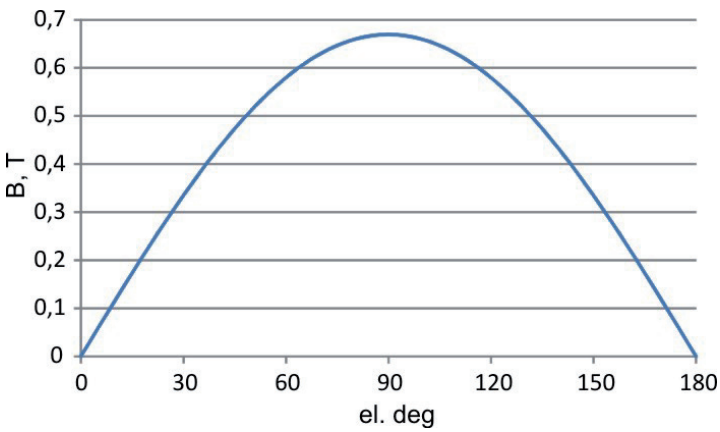

Figure 2.12. Spatial distribution of fundamental harmonic of the generator magnetic flux density.

Using the vector potential method, also the higher harmonics where determined for the studied machine and are shown in Fig. 2.13. Only odd harmonics where studied up to 9th harmonic order as these are the main harmonics that may strongly affect the generator output electromotive force. The magnitude of the harmonics is listed in Table 2.6.

As it can be observed from Table 2.6, the highest magnitude is seen for the 5th harmonic, providing significant influence for the main magnetic flux density, as it is nearly 5% of the fundamental flux density. There is noticeable effect from 3rd and 7th harmonics also, with magnitudes of 1.5 % compared to the

fundamental harmonic. Less effect is provided by the 9th harmonic being is only 0.2% of the fundamental harmonic. As this significant harmonics affect the generator operation considerably it would be beneficial to introduce changes to the permanent magnets shapes so that it would provide more sinusoidal waveform. For the studied generator, the intended use of power electronic converter removes the requirement for perfectly sinusoidal output. This, guaranteeing of sinusoidal output it is not further studied within this thesis.

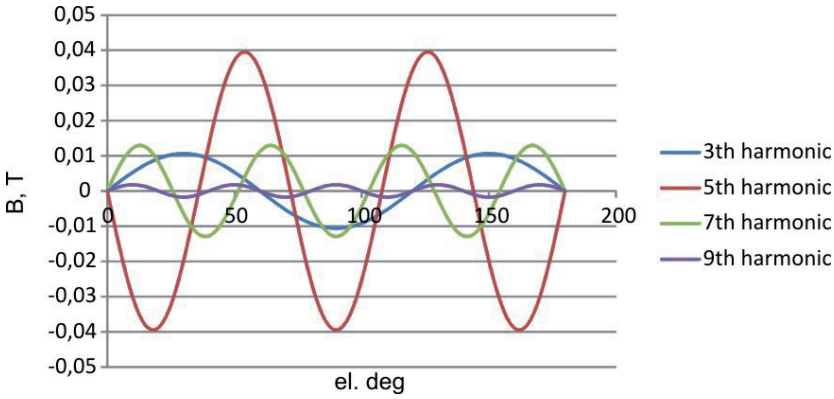

Figure 2.13. The higher harmonics of the generators magnetic flux density distribution over the length of one pole.

Table 2.6. The magnitude of the harmonics.

Harmonic order	Magnetic flux density magnitude B, T
1	0,646
3	0,011
5	-0,040
7	0,013
9	0,002

To determine the total magnetic flux density waveform in the generator air-gap all harmonics waveforms have to be summed up. For the studied generator the final magnet flux density spatial distribution over the length of one pole is provided in Fig. 2.14, where the final maximum flux density value of 0.63 T can be observed. The vector potential calculations still providing greater value for the magnetic flux density magnitude compared to initial value defined previously, even if all harmonics were taken into account.

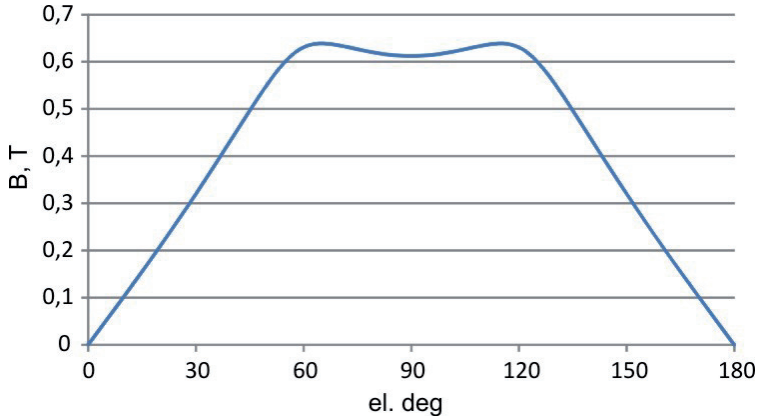

Figure 2.14. Total spatial distribution of the magnetic field in the air gap, over the length of one pole.

2.3.3 Finite element method

There are two reason why finite elemental method (FEM) is used in this study. First, for the vector potential method analytical calculations, several simplifications in mathematical model were introduced and FEM calculations could be used to validate the results from the vector potential calculation method. Second, FEM calculation enables in addition to static field calculations to carry out dynamic field calculations, which are rather complex in analytical approach. Dynamic calculations are necessary for the analysis of permanent magnet generator cogging torque. In addition it also enables to study generator iron losses.

If the generator pole length is significantly longer than the pole width, it would be sufficient to carry out the generator magnetic field analysis in one plane as a two-dimensional task. Relying on this, also the studied generator FEM calculations are performed in two-dimensional approach. As the studied generator radius is significantly greater than the pole length, it is also possible to simplify the magnetic field calculations by assuming the machine to be linear. According to the simplifications described above, the studied machine plane model was constructed; it is shown in Fig. 2.15. Since the machine poles distribution is symmetrical, then it's enough to carry the magnetic field calculations with half of the magnetic pole where the field symmetry is ensured with the boundary conditions. If applying to the magnetic field calculation the windings then the symmetry can be achieved with five poles for chosen construction. That's also the reason why all magnetic field calculations are carried out with 5 poles.

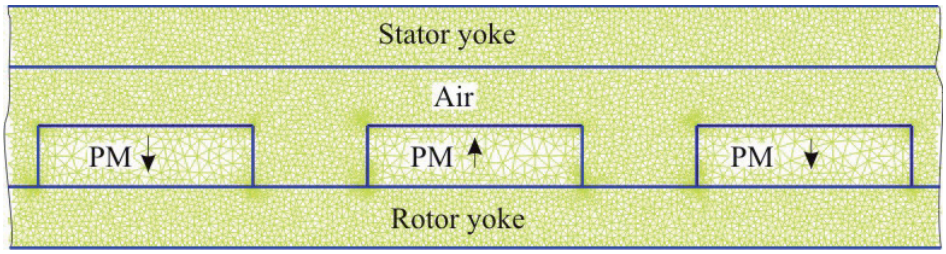

Figure 2.15. Generator in-plane model for the FEM calculations (only 3 poles are shown but the model consists of 5 poles).

For the studied generator, the FEM calculations were carried out using freeware software FEMM 4.2 [82]. This software allows solving two-dimensional in-plane magnetic field tasks. For the calculation the mesh was created with 12675 nodes. Created mesh can be seen in Fig. 2.15. FEM calculation results of the magnet flux density distribution and flux lines are shown in Fig. 2.16. From the calculation results, the maximum magnet flux density of 1.4 T in the generator rotor yoke was indicated and a maximum magnet flux density for the stator yoke of 1.1 T was found. As the saturation point for the electrical steel and iron is greater than the calculated values in yokes, it can be concluded that the generator iron parts will not be saturated. The magnetic flux density distribution in the air gap over one pole according to FEM calculations is presented in Fig. 2.17. From Fig. 2.17 it can be seen that the maximum magnetic flux density is 0.63 T, corresponding to the results obtained previously by analytical calculation.

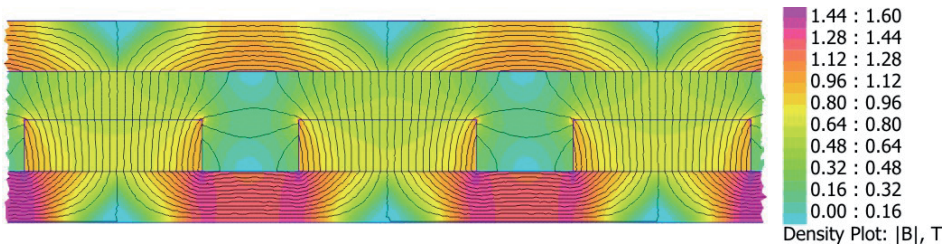

Figure 2.16. Computed distribution of the magnetic flux density. (only 3 poles are shown but the model consists of 5 poles).

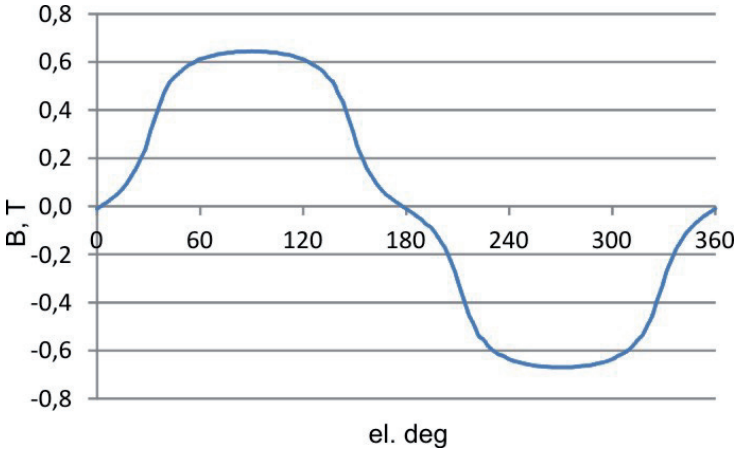

Figure 2.17. The magnetic flux density spatial distribution over the length of a single pole pair, in the radial direction.

A comparison between the analytical vector potential and FEM calculations is shown in Fig. 2.18 with magnetic flux density distribution over the length of one pole. In Fig. 2.18 the curve (1) is obtained with the analytical vector potential calculation and curve (2) is obtained using the FEM calculation. As it can be seen from Fig. 2.18, the curves differ but the amplitude values closely correspond to each other. The reason for the difference between the curves can be attributed to vector potential calculation specific questions, where not all possible higher harmonics were not included.

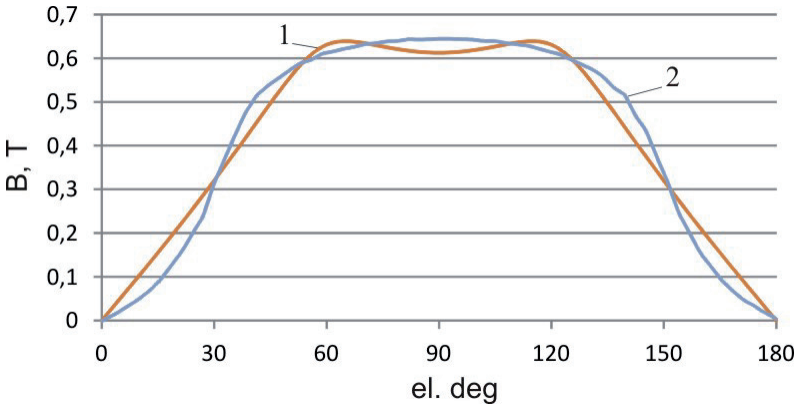

Figure 2.18. Magnetic flux density distribution over one pole. (1) is acquired with vector potential calculation and (2) is acquired with FEM calculation.

2.3.4 Electromagnetic Force

This chapter is focusing on the magnetic forces caused by the fundamental harmonic magnetic field. Such forces can be divided into two parts:

- Forces in generator radius direction (radial forces)
- Forces along the air-gap circumference (tangential forces)

Radial forces in generator are required to be examined for two reasons. First, as this force is applied directly to generator chassis, the requirements to the stiffness of the generator components have to be determined. Secondly, knowledge of the magnitude of these forces is required during the generator assembly when the rotor is mounted with the stator.

As a basis for determining the radial forces, the magnetic field integral over the surface can be used:

$$F = \frac{1}{\mu_0} \int\int dA \sigma \cdot n \qquad 2.46$$

where n is the unit vector perpendicular to the surface A and σ is the Maxwell stress tensor which can be found as:

$$\sigma = \frac{1}{\mu_0} \begin{bmatrix} B_x^2 - B^2/2 & B_x B_y & B_x B_z \\ B_y B_x & B_y^2 - B^2/2 & B_y B_z \\ B_z B_x & B_z B_y & B_z^2 - B^2/2 \end{bmatrix} \qquad 2.47$$

Assuming that the magnet flux in the generator is only provided by the permanent magnet and it is passing through the stator yoke only in the radial direction. As the calculations are carried out in 2D plane then the z directional component can be neglected and taking that all the flux is going in radial direction the x directional component is zero and in the calculations there have to be used only y directional components. For the studied machine by solving the equation 2.47, the magnitude of the force with which each magnet is pulling the stator is ~300 N, provided that the generator air gap is at its nominal size.

The total radial force applied to generator is obtained by summing the forces from all the magnets. As the magnets on the generator are evenly distributed around the rotor and the surface of the stator is smooth the sum of the radial forces is zero. However if the generator air gap is not uniform then a radial force component arises which in turn adds additional load to the generator bearings. The generator air gap eccentricity and resulting forces are described in more detail in chapter 5.1 Eccentricity.

The second force component examined in the work was the tangential force resulting from the generator uneven magnetic reluctance in different rotor positions. Because of this force the generator rotor always tries to reach a position where the reluctance of the generator is the smallest. The fluctuation in the reluctance is called cogging and the resulting torque cogging torque.

If the generator stator surface would be uniformly smooth then there wouldn't be any cogging torque present. In the studied machine the stator is almost uniformly smooth, however for the easier coil assembly the stator yoke is straightened in the locations where the coils are assembled. This cases the stator yoke inner surface to be not circular but rather a polygon consisting of 24 corners as shown in Fig. 2.19. Consequently, it can be assumed that relative to the rotor position the machine reluctance changes slightly and there can be some

cogging present.

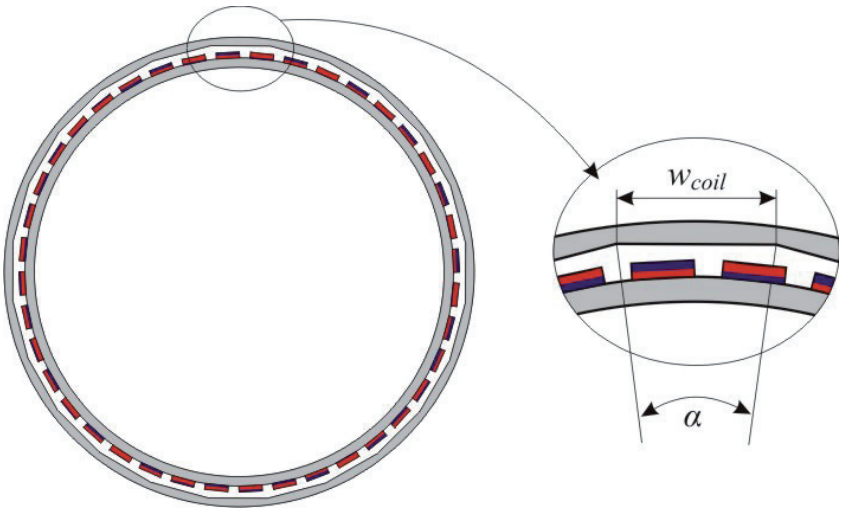

Figure 2.19. Geometry of a stator for the placement of windings.

The general method to calculate the torque ripple is based on the rate of change with the angular position θ of the co-energy W' in the air gap [86]:

$$T = \frac{dW'}{d\theta} \tag{2.48}$$

Where the energy can be found according to:

$$dW' = \int \frac{B_\theta^2}{2\mu_0} dV \tag{2.49}$$

This method requires an accurate modeling of the air gap and usually the analysis is carried out by FEM modeling and calculations. As the generator is symmetrical then there is no need to make the calculations over the full rotor rotation but it is enough to make the calculations with the angle of one coil step after which the reluctance will repeat itself. In the studied machine one coil step is 15 degrees of mechanical rotor movement. This means that for the machine studied, it is enough to analyze the cogging torque over this region. 15 degrees of rotor mechanical movement corresponds to the electrical angle variation of 270 degrees. For the analysis, FEM magnetic field calculation was applied and carried out with rotor electrical angle steps of 9 degrees from range 0…270 degrees of electrical angle. At each such step the torque acting on the rotor was calculated. In order to achieve higher result accuracy of the torque, the number of elements in FEM calculation was 5 million, which was still reasonable to use based on the calculation time. Calculation result is provided in Fig. 2.20 and it can be seen that the torque value is changing while the value itself is relatively small. Referring to the same figure it is presented that the maximum torque value obtained is 2 Nm and the pick-to-pick value is 3 Nm.

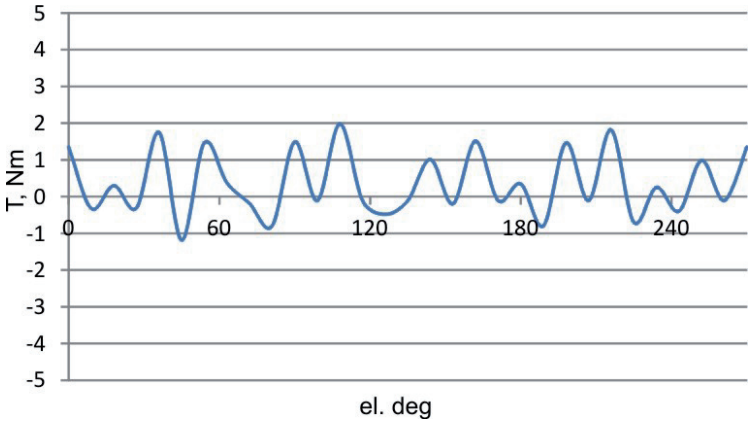

Figure 2.20. Magnetic torque relative to the rotor position at no-load operation.

The FEM calculation precision is largely determined by the relative size of the elements and the force obtained from calculation is relatively small. To verify if the results were valid, recalculations were done for some points with different number of elements (number of elements was increased). While the obtained results provided numerical values up to two times different the absolute value itself was not exceeding the 2 Nm value. Based on this, it can be concluded that the calculation results were merely calculation precision related noise. As the highest value for the torque found from the modeling is relatively small considering main torque values, it was decided that there is no need for carrying out more precise calculations. The studied generator nominal shaft torque is ~250 Nm which means that maximum cogging torque is 0.8 %. As the maximum cogging torque is relatively small compared with nominal torque it can be concluded that the designed machine is basically free from cogging torque.

2.3.5 Conclusion

In the above, an analytic magnetic field calculation model was presented for the slotless machine investigated. Comparison of the results found by applying analytical methods versus results found by FEM proves that the analytical methods may be applied to calculate the flux density created by the permanent magnets in the air gap. Calculations carried out on the magnetic field harmonics presented that the highest component is the 5th harmonic. The calculations were also carried out to find the mechanical forces generated by the magnetic field. Calculations of the machine cogging torque were carried out and found that in this type machine this is negligible.

2.4 EMF calculation

Creation of electromotive force (EMF) is described by Faraday's law, which states that any change in the magnetic flux of a coil of wires will cause a voltage to be induced at the coil terminals:

$$E = w\frac{d\phi}{dt} \qquad 2.50$$

Assuming that a wire is moving with the speed v through spatially sinusoidal distributed magnetic flux density and the length of a wire being l_m then EMF can be found according to:

$$E = \frac{B}{\sqrt{2}} v l_m \qquad 2.51$$

The magnetic flux density used in equation 2.51 was defined in previous chapter, however the end effect of the magnets was not taken into account. The flux density is approximately constant over a stator yoke and decreases gradually to zero along the shaft of the machine as an effect of the edge field. Such edge field is included in the fundamental flux of the machine and it participates also in torque formation. In an analytic approach, the lengthening of the machine caused by the edge field can be approximated by the equation [77].

$$l' = l + 2g, \qquad 2.52$$

where l' is the effective length of the core, l is the length of magnet and g is the air gap height.

2.4.1 Winding factor

Coils used in the studied generator are concentrated windings which are placed in the generator air-gap. The physical layout of the coils is shown in the Fig. 2.21.

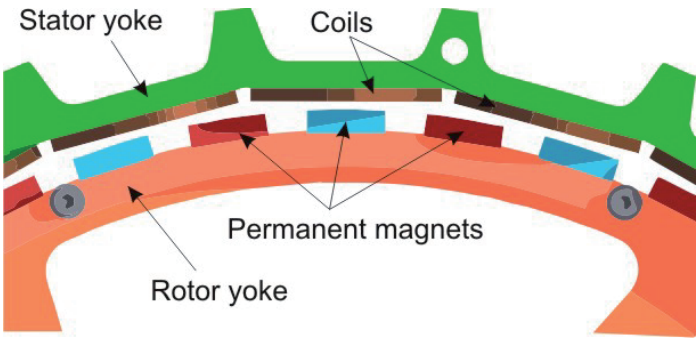

Figure 2.21. Geometrical layout of a coil of the generator studied.

Coils are not wound from an infinitely thin wire but they have specific dimensions and the beginning and end of a wire which area can be geometrically situated in the magnetic field which have phase shift. These shifts have to be taken into account when calculating then EMF. Such conditions are accounted with two factors: pitch factor and distribution factor.

The coil consists of several wires distributed over the width of the coil w_c as shown in Fig. 2.22. Because of this, the voltages induced within these turns of

wires are shifted electrically. As the coil EMF is the vector sum of all wires voltages, it is not possible just to sum the voltages but also the voltage shift described with distribution factor k_d has to be taken into account.

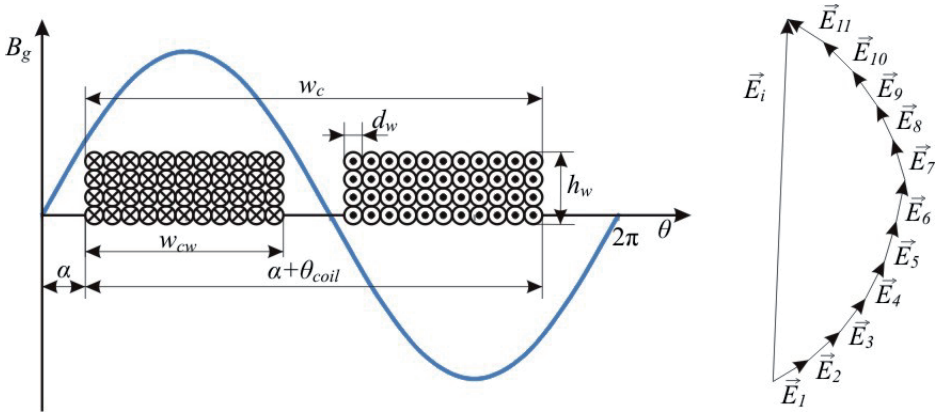

Figure 2.22. Winding shape and magnetic flux density (left) and the vector sum of induced voltages in different wires (right).

To find the distribution factor the electrical angle σ_s representing the width of coil has to be defined first:

$$\sigma_s = \theta_{coil} \frac{w_{cw}}{w_c} \tag{2.53}$$

There are several papers which describe the methods to find the distribution factor when the distribution angle is known [83, 84]. Assuming magnetic flux having sinusoidal distribution the coil distribution factor can be found by integrating over the surface of the coil:

$$k_d = \int_0^{\sigma_s} \sin(\sigma_s) d\sigma_s = \cos\left(\theta_{coil} \frac{w_{cw}}{w_c}\right) \tag{2.54}$$

The beginning and end of the coil can be shifted electrically in geometrical space as explained in Chapter 2.2.4 and shown in Fig. 2.10 Because of this the voltage sum may be reduced and has be taken into account with the pitch factor k_p.

To find the pitch factor first the electrical angle between the coil beginning and end has to be determined. This angle ε can be found for the particular machine accordingly:

$$\varepsilon = \theta_{coil} \frac{w_{cw} + w_{cinner}}{w_c} \tag{2.55}$$

Knowing the angle, the pitch factor can be found as suggested in [77]:

$$k_p = \sin\left(\frac{\varepsilon}{2}\right) \qquad 2.56$$

The winding factor is obtained with multiplying the pitch and distribution factors of the generator:

$$k_{wn} = k_d k_p \qquad 2.57$$

The winding factors for the investigated machine for the magnetic field first harmonic with the chosen parameters were pitch factor ~1 and distribution factor 0,858. It can be seen from equations 2.53 and 2.55 that the winding factors on the studied machine depend on the coil inner (winding window) and outer width and the pole length. These parameters were previously defined in the design of the generator. As the coil winding window width used here was chosen not specifically calculated, it needs verification if this was the optimal choice. To verify that, the value chosen was close to optimal in the point of view of winding factors, comparative analysis has been made with different coil inner width with results shown in Fig. 2.23.

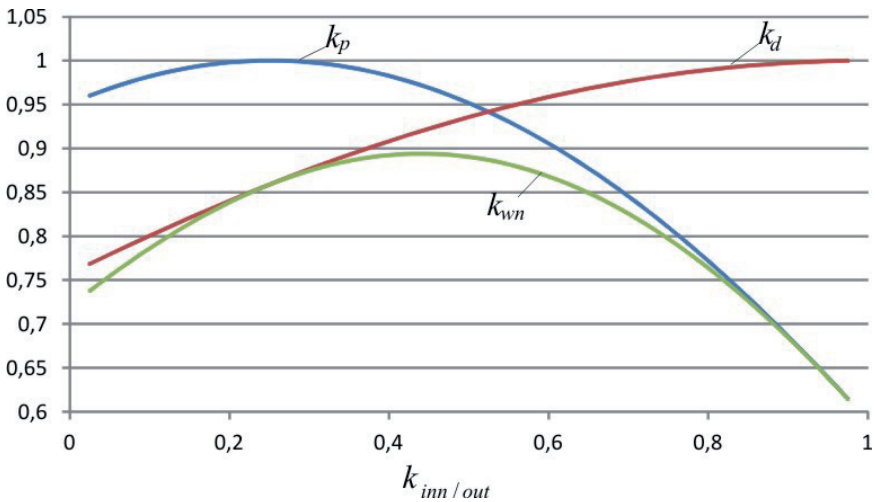

Figure 2.23. Coil factors in relation to the ratio of the inner width of the coil to its outer width.

From Fig. 2.23 it can be seen that the highest winding factor is reached when the coil inner width is 45 % of the coil outer width. For the investigated machine the coil inner with was chosen as 25 %. The difference between these values arises because in the real machine design, the choice of the coil inner width has to take into account that not only the highest winding factor are needed but also the coil active cross section area should be the highest possible. To reach the highest active cross section the coil inner width should be at minimum. Taking this into account and looking at the Fig. 2.23 it can be seen that when the winding factor is decreasing after the optimal point the pitch factor is also decreasing but the distribution factor is increasing. From this point

of view it can be said that the optimal coil inner width can be defined when the distribution factor is the highest. In this way a quite good winding factor and also good coil active cross section are provided. Based on this and looking at the Fig. 2.23 it can be seen that the coil inner width should be ~25 % from coil outer width which means that also the coil inner width chosen in the start of design process was nearly optimal.

2.4.2 Coil windings

In order to determine the magnitude of electromotive force induced into generator coils, the number of turns in the winding is crucial. Finding the number of turns needed for the generator windings is based on the required generator output voltages that were defined in Chapter 2.2.2.

For the studied machine, which is a silent pole permanent magnet machine, the equivalent circuit for one phase can be defined as shown in Fig. 2.24 a. Based on the equivalent circuit, the phasor diagram is shown in Fig. 2.24 b.

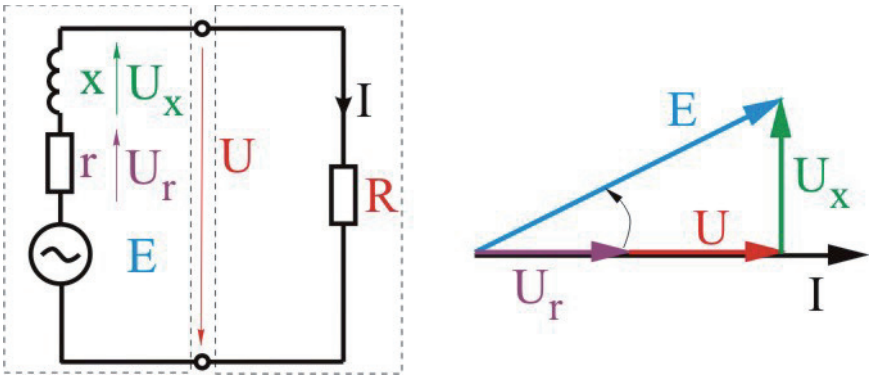

Figure 2.24. Equivalent circuit of a generator and respective vector diagram.

From the equivalent circuit as well as the phasor diagram it is evident that the generator output voltage depends on the coil resistance and coil inductance. From the phasor diagram the generator's EMF can be found according to the equation:

$$E = \sqrt{(U + RI)^2 + (XI)^2} \qquad 2.58$$

In order to find the electromotive force, the generator coil resistance R and inductance X have to be found first. Calculation of these parameters is presented in the next chapters.

2.4.2.1 Coil resistance

Determining the resistance of the coil relies on the coil dimensions which are shown in Fig. 2.25. The coil active cross section area and active length was found previously in the Chapter 2.2.4. In order to provide all coil parameters, the coil end winding parameters have to be taken into account besides the

previously given parameters. End winding dimension calculation is based on the assumption that the end windings are forming a semi-circle with inner radius r_s and outer radius r_v, and that the end winding cross section area is the same as the active part cross section area.

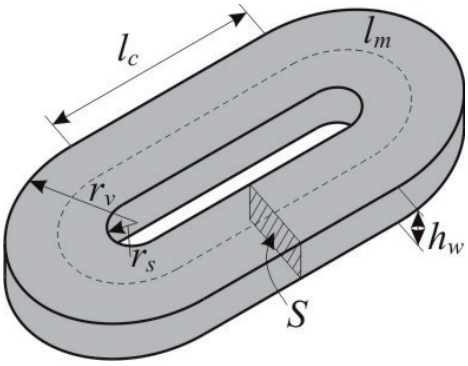

Figure 2.25. Illustration and dimensions of the generator coil.

The coil cross section area defines the space where the coil wires are located. Since the coil wires consist of isolation besides the active part, and in the studied machine circular wires are used then it is not possible to fill the coil cross section area completely with active material. This area reduction is taken into account with the fill factor k_f. Typically the fill factor for round wire is 0.4…0.6, in studied machine the fill factor is chosen as 0.5.

To find the average length of a single turn, the coil is split in two: wire straight part, which is the winding active part and circular part from the end windings. The average length of the end winding can be found as:

$$l_{laup} = \int_{r_s}^{r_v} \pi r dr = \pi \frac{r_v + r_s}{2} \qquad 2.59$$

Based on equation 2.59 and adding straight wire section length l_c the average winding length can be calculated:

$$l_m = 2l_c + \pi \frac{r_v + r_s}{2} \qquad 2.60$$

Knowing the winding average length and the coil cross section area the coil resistance can be found according to:

$$R_c = \rho \frac{l_m}{k_f S} w \qquad 2.61$$

where w is the number of turns and ρ is the wire resistivity.

Wire cross section area can be found from the coil cross section area and number of turns according to:

$$S_w = \frac{k_{täide} S}{w} \qquad 2.62$$

2.4.2.2 Inductance of the windings

To determine the required number of turn's simplified method is used to define the inductance of the coil.

Using simplifications, the generators coil can be observed as solenoid winding which is in the generator air gap. Assuming that the magnetic permeability of iron is infinitely large, the coil inductance can be found according to:

$$L_w = \frac{w^2 \cdot l_{iron}(r_v + r_s)\mu_0}{h_{cap}} \qquad 2.63$$

It can be seen from Eq. 2.61 and 2.63 that both the generator coil resistance and inductance values depend on the number of turns of wire in the coil.

Generators EMF can be found in two different ways. First, it can be determined based on generator output with coil resistance and inductance as given in equation 2.58. Additionally, it has to be taken into account for the studied machine that generator has 24 coils which are connected in series as three phase system. It means that in the studied machine there are 8 coils connected in series per phase. Taking the number of coils connected in series n_{coil} into account and substituting the coil resistance and coil inductance, the EMF can be calculated as:

$$E = \sqrt{(U + \rho \frac{l_m}{k_{täide} A} w^2 \cdot n_{coils} \cdot I)^2 + (\frac{w^2 \cdot l_{iron}(r_v + r_s)\mu_0}{h_{cap}} \cdot n_{coils} I)^2} \qquad 2.64$$

EMF can also be calculated based on equation 2.51. It can be observed from the equation that the EMF depends on the rate of change of the magnetic flux density. To find the generator EMF with this equation, the winding factor k_{wn}, the number of winding turns w and the number of coils in series n_{coils} have to be taken into account besides the magnetic field density. In such case the EMF can be calculated as:

$$E = 2 \cdot Bvl_m \cdot k_{wn} \cdot w \cdot n_{coils} \qquad 2.65$$

Solving these two equations (2.64 and 2.65) it is possible to find the necessary number of turns in the generator coil. For the test machine it was found that 86 turns per coil are needed and according to the equation 2.62 respectively the winding wire cross-section are is found and based on this the wire thickness was found to be 1.12 mm.

2.4.3 EMF and harmonics

All necessary parameters to find the generator EMF were previously introduced. According to equation 2.65 the generators fundamental harmonic EMF is found.

From the generator magnetic field calculation it was determined that the higher harmonics are also present besides the fundamental harmonic of the magnetic field. As not only the fundamental harmonic will be induced in the generator coils but also the higher harmonics, it needs observation on how much the magnetic field higher harmonics affect the generator EMF. All harmonics for EMF can be calculated separately from the magnetic field with equation 2.65. The EMF calculation depends on the frequency of the magnetic field. Also the winding factors are depending on the frequency of magnetic field. As with the higher harmonic the magnetic field frequency is higher than for all harmonics the EMF has to be calculated separately with new winding factor parameters. The final EMF can be found with summing up all harmonics components.

$$E_n = \sum_{i=1}^{n} 2 \cdot B_i v l_m \cdot k_{wni} \cdot w \cdot n_{coils} \qquad 2.66$$

Using equation 2.66, the generator EMF harmonics were found and have been shown in Fig. 2.26 where the a) is showing the higher harmonics separately and b) is the sum of all harmonics.

a)

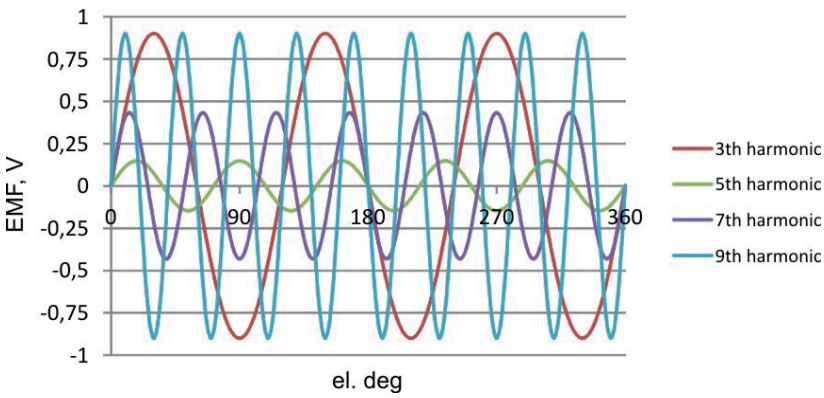

b)

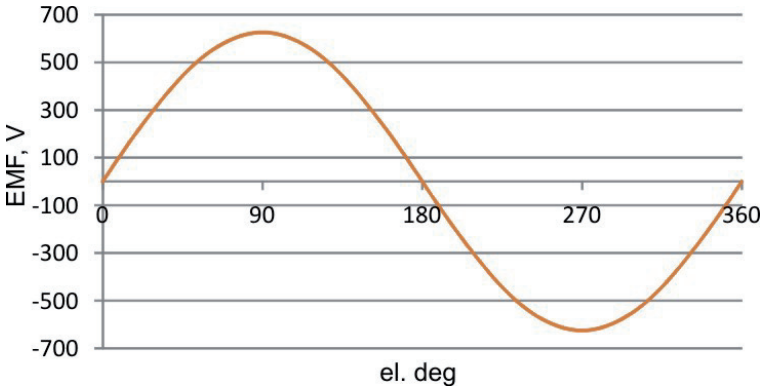

Figure 2.26. Electromotive force of the generator where a) is higher harmonics electromotive forces and b) is the sum of harmonics.

2.5 Loading and losses

Losses occur always with energy conversion and are usually released as heat into the surrounding environment. Because of this the mechanical energy provided to the machine always has to be higher than the electric energy output. The relation between the output electrical power P_{el} and input mechanical power P_{meh} gives the generator efficiency:

$$\eta = \frac{P_{el}}{P_{meh}} \qquad 2.67$$

The losses that occur in a generator can be divided into four categories:

- mechanical losses
- eddy current losses
- hysteresis losses
- resistive losses

Mechanical losses are a consequence of different frictions in the machine. In the studied machine this would be bearing friction and windage. The studied generator is a low speed generator and thus windage losses could be neglected. Bearing losses depend on the bearing quality and the generator rotation speed. According to manufacturer data from SKF, the bearing losses can be found as [77]:

$$P_{be} = 0{,}5\Omega\mu F D_{bearing} \qquad 2.68$$

where Ω is the angular frequency, μ is the friction coefficient (typically 0.0010-0.0050), F is the bearing load and $D_{bearing}$ is the inner diameter of the bearing.

For the studied machine the bearing losses are also minor and can be neglected from the loss calculation.

Resistive losses (sometimes called Joule losses) are losses in the generator conductors. In PM machine these losses accrue only when the generator is loaded as these losses are present only when the current is flowing through the coils.

Hysteresis loss and eddy current loss, also known as iron losses, are caused because of the alternating magnetic fields.

2.5.1 Eddy current loss

Eddy current losses are everywhere where alternating magnetic field penetrates through electrically conductive environment. In the studied machine there are three places where these losses occur: stator yoke, rotor yoke and coil wire. In the rotor the magnetic field changes because of reluctance variation in generator when generator is moving. In Chapter 2.3.4 the cogging torque was studied and it was shown that the change in the reluctance in the machine is small. Based on this it can be said that eddy current losses in the rotor are minor and because of this they are not investigated within this work.

Eddy current losses in the stator are the reason why the stator yoke is made from laminated electrical steel. The thinner the electrical steel is the smaller are the eddy current losses. One limit how thick the electrical steel can be is that all magnetic flux would penetrate through the lamination or in other words there will be no skin effect. The maximum lamination thickness at which all magnetic field penetrates the lamination can be calculated as [77]:

$$\delta = \frac{1}{\sqrt{\pi f \mu \sigma}} \qquad 2.69$$

From equation (2.69) it can be seen that the skin depth δ depends on the frequency f, the material magnetic permeability μ and the material conductivity. On the studied machine it was found according to equation 2.69 that the maximum lamination thickness where the skin effect can be considered neglible is 0.6 mm. Based on this result and commercially available laminations, the lamination thickness of 0.5 mm was chosen for the generator.

If there is no skin effect in lamination the eddy current losses in the stator yoke can approximately calculated as [77]:

$$P_{skin} = \frac{B^2 (2\pi f d)^2}{24\rho} \cdot V \qquad 2.70$$

It can be seen from the equation that the eddy current losses depend on the magnetic field density B, the rotational speed of the magnetic field f, the lamination thickness d, the material resistivity ρ and the volume of material V. According to equation 2.70 the studied machine stator eddy current losses were 48 W.

As there are eddy current losses in the stator iron there are also eddy current losses in the generator coils. According to equation 2.69 it was found for the studied machine that the maximum coil diameter can be 7.5 mm when only negligible skin effect is present. Previously it was found that the suitable coil winding wire diameter is 1.2 mm then with the present coil design, the skin effect can be neglected. Assuming 1.2 mm winding wire diameter for the studied machine, the total coil eddy current loss of 121W is found according to the equation 2.70. Compared with the iron eddy current loss this value is almost three times higher. This is a consequence of the air gap winding design, which results in low flux density in the iron but on the other hand the flux density in the winding is considerable when compared with conventional slotted machines.

As eddy current loss depends on the wire diameter, by decreasing the wire diameter in the coil it is possible to decrease these losses. It is possible to decrease the wire diameter by using parallel wires in the coil. A comparison of the coil eddy current losses with different number of wires in parallel is provided in the Fig. 2.27. It can be seen from the figure that already with two parallel wires the eddy current losses decrease by 2 times. Adding more wires in parallel would decrease the loss even further but it makes building the wire more complex as using parallel wires means that single wire diameter will be smaller. With this the fill factor will decrease and also the labor cost to make the coils increases. Taking this into account two parallel wires were chosen, for the studied machine with single wire diameter of 0.85 mm.

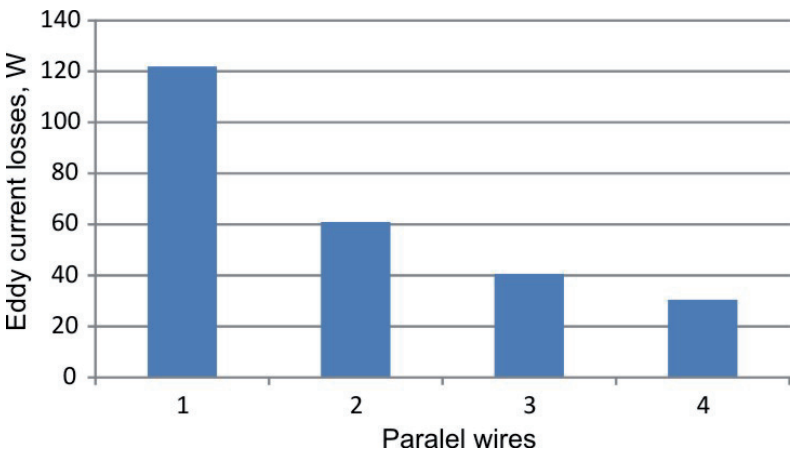

Figure 2.27. Eddy current losses in generators winding in relation to number of single wires used in the winding in parallel.

2.5.2 Hysteresis loss

In all ferromagnetic materials, the flux density lags behind the magnetic field intensity throughout the whole cycle of magnetization and demagnetization.

This lagging phenomenon occurring in the material is called hysteresis. The loss caused by this effect is termed hysteresis loss P_{hys}. The magnetic energy dissipated is converted into heat and is permanently lost. This lost energy (W_h) is the area enclosed by a hysteresis loop [85]:

$$W_h = V_{mat} \oint HdB \tag{2.71}$$

As the magnetic field changes with the generator fundamental harmonic frequency f then also the hysteresis power P_h dissipated changes accordingly. Taking this into account the losses can be calculated as:

$$P_h = fW_h \tag{2.72}$$

In this equation the V_{mat} is the volume of associated material. However, it is difficult to quantify the area of hysteresis loop due to the nonlinearity of the B-H characteristic. For the magnetic materials used in electric machines, a well-known approximate relation first presented by Charles Steinmetz is used to evaluate the area of the loop:

$$A_{loop} \approx k_{hys} B_{\max}^{\beta} \tag{2.73}$$

where B_{max} is the maximum flux density, k_{hys} is an empirical constant that depends on the ferromagnetic material and β is Steinmetz index that varies from 1.5 to 2.5. With this approximation, the hysteresis loss in a given volume of material can be calculated as:

$$P_{hys} = fV_{mat} k_{hys} B_{\max}^{\beta} \tag{2.74}$$

Using the equation 2.74 it was found that the studied machine has 74 W of hysteresis losses at nominal speed.

2.5.3 Copper loss

Generator copper losses P_{copper} are defined as:

$$P_{copper} = I^2 R \tag{2.75}$$

where I is the current in the coil winding and R is the coil resistance. Coil resistance is defined with generator construction and can be found according to the equation:

$$R = \rho \frac{l}{A} \cdot w \tag{2.76}$$

where l is the coil wire average length, A is the wire cross section area, ρ is material resistivity and w is the number of turns in the coil.

When calculating the coil resistance the wire material conductivity dependency on the temperature has to be taken into account, it is calculated as:

$$\rho = \rho(1 + \alpha \Delta T) \qquad 2.77$$

where the α is the temperature coefficient.

Assuming the generator nominal load the generator copper losses were found in relation to the coil temperature, provided also in the Fig. 2.28. Assuming that the generator nominal working temperature is 80 C° there is 895 W copper loss when the generator is working at nominal load.

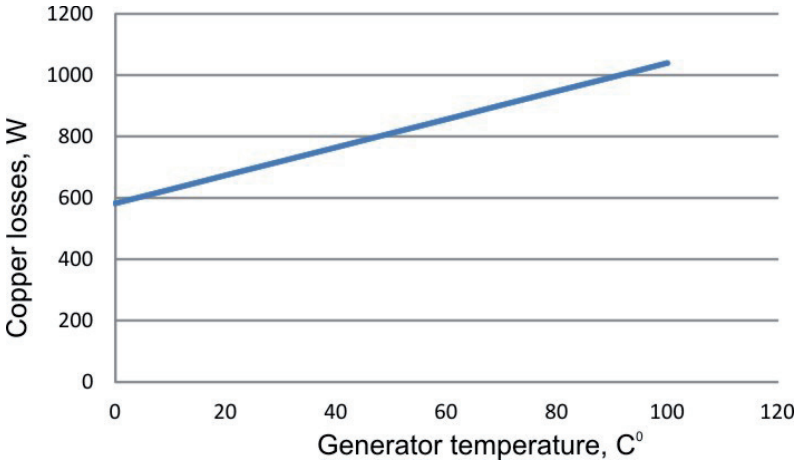

Figure 2.28. Active losses in a generator in respect to the operating temperature.

2.5.4 Output power and efficiency

In the studied machine the copper losses are dominating at nominal load as can be seen in Fig. 2.29. This was an expected result as this type of machine is missing teeth, resulting in a flux path through the core, which much smaller than in a conventional slotted machine.

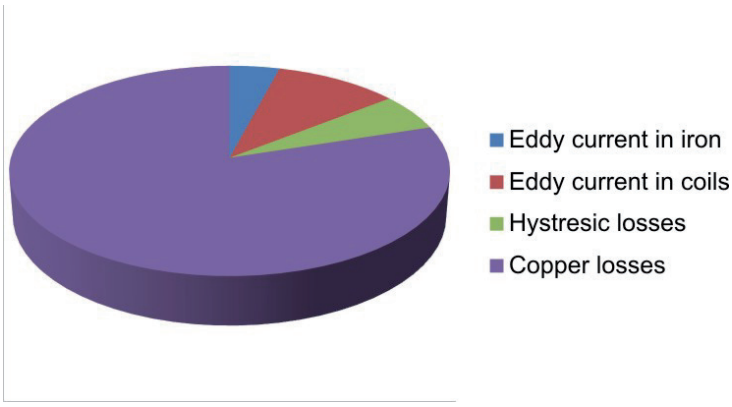

Figure 2.29. Proportions of different losses in the generator at rated load.

The studied generator is intended for use with wind turbines where the rotation speed is not constant. As the hysteresis loss and eddy current loss depend on the rotating speed these losses were analyzed at different rotational speeds. Result of the analysis can be seen from Fig. 2.30 where it can be seen that the hysteresis losses are in linear dependency from the rotational (green line) speed but eddy current losses rise more rapidly (blue line represents eddy current loss in wire and red line is eddy current loss in stator yoke).

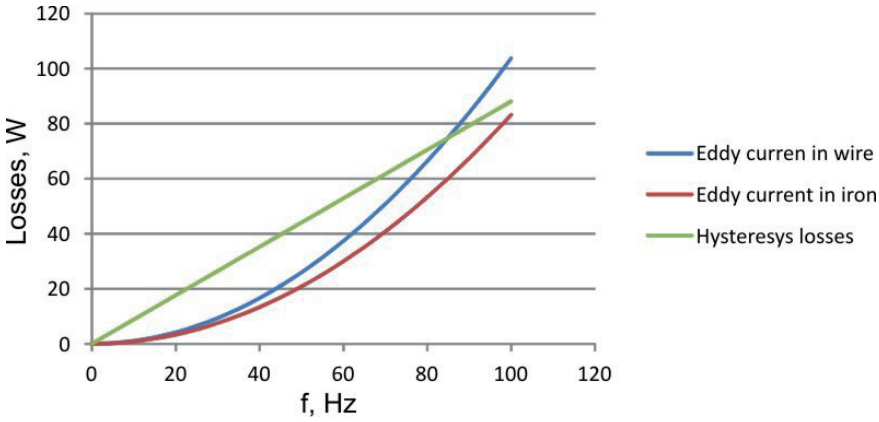

Figure 2.30. Eddy current and hysteresis losses in relation to generators working frequency.

Copper losses are not related to the rotation speed but are affected from the generators load. To study the generator load the nominal rotational speed was observed first. It was assumed that the generator is loaded only with active load. Result of the analysis is shown in the Fig. 2.31 where generator output voltage, (blue line) generator output power (red line) and efficiency (green line) are provided. It can be seen from the Fig. 2.31 that with load increase the generator output voltage is dropping and is almost 23 % less compared to EMF at nominal rotational speed.

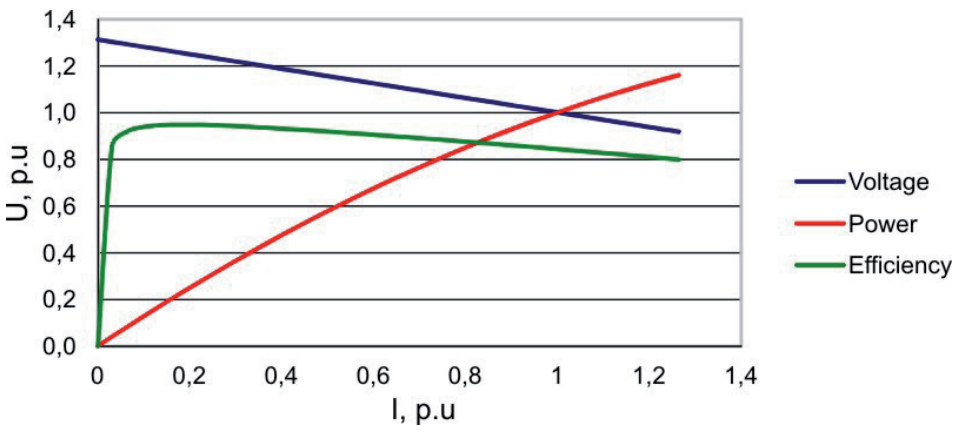

Figure 2.31. Generators load characteristics at nominal rotation speed.

Generator efficiency at nominal load and nominal rotation speed is 82 % as shown also in Fig. 2.31. It can be seen from this figure that it is not the point where the generator has it maximum efficiency. At nominal speed the generator efficiency is increasing with lighter loads and it achieves a maximum of 95% at 0.2 p.u. load. As the generator is not intended to work at constant load but at rather smaller loads also the generator rotational speed is often lower. From this reason analysis was made to find out how the generator efficiency is affected from different rotational speeds. Result of the analysis is shown in Fig. 2.32.

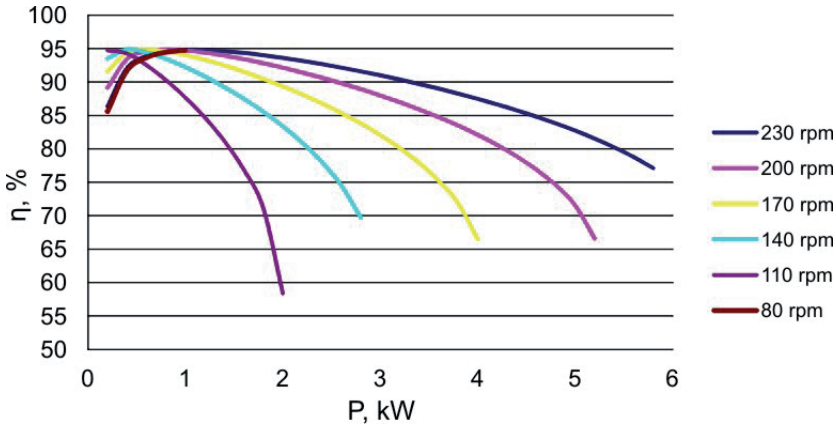

Figure 2.32. Generator efficiency at different rotating speeds and loads.

The generator loading is directly influenced by the wind turbine where the blades produce specific maximum power for different rotational speeds. This is reflected on the generator input power curve as shown in Fig. 2.33 (red line) and while the calculated generator output power (green line) and efficiency (blue line) are compared. It can be seen from the Fig. 2.33 that the generator maximum efficiency reaches 86 % when the generator power is 0.25 p.u. which is achieved with wind speed of ~5 m/s. Referring to Fig. 2.2 it can be seen that this is the point where the generator is working most of the time.

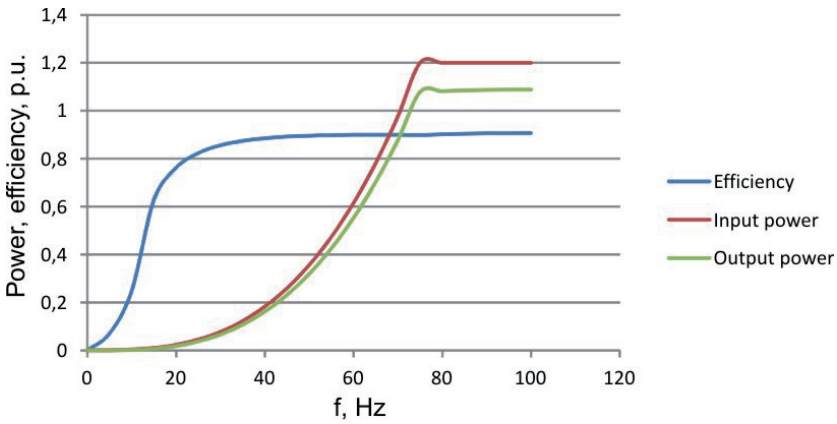

Figure 2.33. Generator output power and efficiency in relation to the operating frequency.

2.6 Thermal design

The thermal characteristics of an electrical machine are important as temperature rise in the winding defines the power that can be obtained from the machine. In permanent magnet machines, the temperature is important also as permanent magnet characteristic depends strongly on the temperature, which in turns affects the generator output characteristics. Also with temperature rise in permanent magnet machine there is a high risk to demagnetize the magnet. Typically, the temperature limit for NdFeB magnet is below 120 ˚C. This limit can be raised with special alloys but usually it is quite expensive and used only in special machines. Also, typically permanent magnets are bonded on the rotor where there is also a risk with higher temperatures that the glue may lose its properties resulting in loose magnets which may damage the machine. The winding resistance is also temperature dependent and with temperature rise losses in the winding will rise. Also there are limits for winding isolation and what temperature it can handle.

There are many different calculation methods, which can be used to calculate the machine temperature. Mainly, there are in use lumped parameter thermal model. Also in recent years there has been some trend to use more FE models to calculate the thermal characteristics of machines. In this thesis, the thermal network has been used as explained bellow.

2.6.1 Heat transfer

Heat transfer can be classified as:

- Convection
  - Natural
  - Forced
- Radiation
- Conduction

Heat transfer from machine to the environment through convection depends on both the surrounding environment temperature T_{amb} and the machine surface temperature T_{sur} from where the temperature is transferred. The dissipated power P_{con} due to the convection is defined as [87]:

$$P_{con} = hS(T_{sur} - T_{amb}) \tag{2.78}$$

where h is the heat transfer coefficient

S is the surface area

The most problematic task is to find a heat transfer coefficient h for the studied machine. With simple surfaces, like plains or pipes, it is possible to calculate this value but more complex surfaces like electrical machine common method

to find h is based on experimental measurement. Forced air convection is the most common cooling method for the electrical machine where heat transfer coefficient is between 10 to 100 W/(m^{2}K). In the studied machine there is used passive cooling, but as the generator is located in the windmill, where the wind is forced over the generator surface then the machine cooling can also be looked as forced air cooling. The studied machine surface can approximately be looked as cylindrical in which case the h can be calculated as:

$$h_{con} = 9{,}6v^{0{,}8} \tag{2.79}$$

In this equation the v is the airflow speed on the surface of the machine. On the outer surface of the machine it can be taken as equal to the wind speed. As in the machine also the wind can go through the air-gap then in the inner surface of machine the airflow speed is the vector sum of wind speed and additional speed from generator rotation.

Dissipated power P_{rad} due to the radiation can be calculated as [87]:

$$P_{rad} = \varepsilon_{sur}\varsigma S(T_{sur}^4 - T_{amb}^4) \tag{2.80}$$

where ε_{sur} is emissivity of the surface and

ς is the Stefan-Boltzmanin constant, 5,6703x10^{-8} W/m^{2}K^4

The emissivity of the surface is a quantity which depends on the material of the surface. For example black painted surface emissivity is typically 0,9 whereas for the polished steel surface it may be below 0,3[88]. As can be seen from the equation already a small difference in the temperature can give a good heat transfer as the temperature difference is in the exponent of 4.

Convectional heat transfer can be described with partial differential equation known as diffusion equation [87].

$$\nabla^2 T = \frac{\partial^2 T}{\partial x^2} + \frac{\partial^2 T}{\partial y^2} + \frac{\partial^2 T}{\partial z^2} \tag{2.81}$$

For the thermal analysis of electrical machines applying Eq. 2.81 causes a complex boundary value problem with several unknowns related to the contacts between the different parts. Therefore, simplifying the considered problem and using a thermal equivalent circuit to describe the heat transfer problem is often appropriate [87]. Also in this thesis is used equivalent circuit method to find the machine temperature.

2.6.2 Thermal resistance network

In calculating the generator temperature there was taken two thermal paths were the heat transfers to the environment. The heat is given away from the outer and inner surface of stator. The power that has to be dissipated to the environment

comes from copper loss, eddy current loss in coil and in iron and hysteresis losses. Based on the generator thermal analyses, thermal resistance network was grated that is given in the Fig. 2.34. Thermal analyses for the machine are carried out only at steady-state. The nodal temperature of the network is calculated as:

$$T = G^{-1}P \tag{2.82}$$

where T is nodal temperature vector, G is the thermal conductivity matrix and P is the loss vector. The thermal conductivity matrix is defined as:

$$G = \begin{bmatrix} \sum_{i=1}^{n} \frac{1}{R_{1,i}} & \frac{1}{R_{1,2}} & \cdots & -\frac{1}{R_{1,n}} \\ -\frac{1}{R_{2,1}} & \sum_{i=1}^{n} \frac{1}{R_{2,i}} & \cdots & -\frac{1}{R_{2,n}} \\ \vdots & \vdots & \ddots & \vdots \\ -\frac{1}{R_{n,i}} & \frac{1}{R_{n,i}} & \cdots & \sum_{i=1}^{n} \frac{1}{R_{n,i}} \end{bmatrix} \tag{2.83}$$

where $\sum_{i=1}^{n} \frac{1}{R_{n,i}}$ is the sum of thermal conductance connected to a particular node. The loss matrix P is defined as:

$$P = \begin{bmatrix} P_1 \\ \vdots \\ P_n \end{bmatrix} \tag{2.84}$$

Defining the thermal resistance is based on the heat conductance and is found as:

$$R_{th} = \frac{l_i}{\lambda_i S_i} \tag{2.85}$$

where l_i is the length of a particular path described by a thermal resistance

λ_i is the thermal conductivity of the material

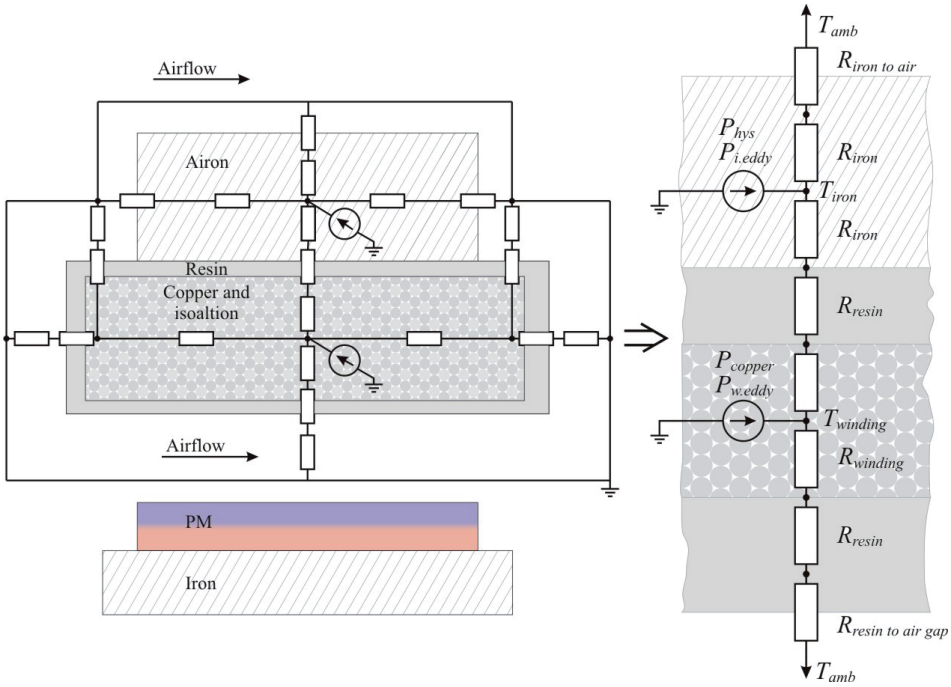

Figure 2.34. Equivalent circuit of temperature for the generator

Thermal conductivities in the machine are taken as constants within the same material but different for different materials. In the Table 2.7 are given thermal conductivities used in the calculations.

Table 2.7. Thermal conductivities.

Material	λ_i [W/mK]
Electrical steel	38,7
Copper wire	395
Isolation	0,8

Knowing the surfaces where the temperature is dissipated and the contact thermal conductivity, it is possible to find the contact thermal resistance from one surface to other as:

$$R_{th,con,i} = \frac{1}{h_i S_i} \qquad 2.86$$

where h_i is the contact thermal conductivity

It is difficult to find the exact contact thermal resistance as the contact conductivity depends on surface roughness, material pressure and also from manufacturing tolerances [87].

Thermal calculation are done in the static case but as copper losses in the coil depend from the temperature, where the losses are increasing with temperature, the thermal calculation are done in an iterative way, where in every cycle there is updated the copper loss value. The calculation process was carried out until the generator windings temperature had reached a stable state.

Thermal calculation analyses where carried out only on the stator as there are the main losses. Losses in the rotor are from fluctuating magnetic field resulting in eddy current and hysteresis losses. As previously studied, this magnetic field fluctuation is minor and also the losses in rotor are minor and can be neglected. Mainly the rotor is wormed up by the stator temperature which is transferred to rotor by convection and radiation. In the studied generator calculation, it was found that at normal machine operation the stator temperature is up to 95 ˚C, it means that also the rotor temperature will not be higher. As this temperature is not vital for permanent magnets then in generator design proses it is not important to do rotor thermal calculations unless it is necessary for some other designs.

2.7 Conclusion

In this chapter the main considerations related to the modeling of the slotless permanent magnet slows speed generator are provided. The procedure to parameterize the generator for windmill has been developed. This procedure can be generalized for all type of wind generators. Analytic design procedure for the generator has been given where analytic magnetic field calculation is verified with 2D FEM calculations. As the generator analytic design procedure is mainly considered for preliminary design purpose, some simplifications are included in the given computation model. In the magnetic field calculation the generator construction is given in-plan as the radius of the air gap is much larger than the pole width. In the generator loss calculation, the losses in rotor are neglected as they were expected to be minor. Also in the thermal calculation the thermal resistance network has been limited. Despite the simplifications, a reasonable accuracy of the design results can be expected.

3 Prototype machine and test results

It was found that for the windmill it is suitable to use slotless permanent magnet generator. Based on the study, prototype generator was built, suitable for annual energy production in a specific windmill. According to the design parameters, prototype generator was constructed, which can be seen in Fig. 3.1. Goal for building the prototype was to control the developed design methodology and also to study generator behavior at operation. Besides the generator parameter study, idea for building the generator was to study the generator mechanical parameters and also implementation of it to the windmill to study the windmill operation. Windmill where the prototype generator is used is given in Fig. 3.2. In the thesis only the generator electrical test results are given, windmill and generator mechanical parameters tests are left out as they are irrelevant based on the thesis study.

Figure 3.1. Prototype generator.

Figure 3.2. Prototype generator used in a windmill

To study the prototype generator, a test bench was constructed, where the generator was driven with a motor and different parameters were measured. During the tests, magnetic parameters in the generator air gap, coils parameters, generator output parameters at no load and load were studied.

3.1 Construction of the prototype

When the prototype generator was constructed it was known that it will be implemented to a 5 kW windmill. This type of windmill blades at rated wind speed 12 m/s are rotating with the speed of 230 rpm. As the generator is directly driven, which means its shaft is directly connected to the blade shaft, its nominal rotational speed will also be 230 rpm. Rotational speed also gives generator pole pairs number according to the output frequency.

Prototype generator had 20 pole-pairs, which gives the generator output frequency of 76.7 Hz. The generator poles were constructed from NdFeB magnets type 45N with dimensions 35x55x10 mm. To get smoother magnetic flux in the generator air-gap, the magnets surface was not straight but curved with the radius of 342.5 mm. On the rotor yoke there were made slots for magnets with depth of 0.5 mm for easier magnet placement. The magnets were bonded to the rotor slots where the rotor yoke thickness was 15 mm. The width of rotor yoke was chosen to be 66 mm and rotor radius was 664 mm. Constructed rotor is given in Fig. 3.3

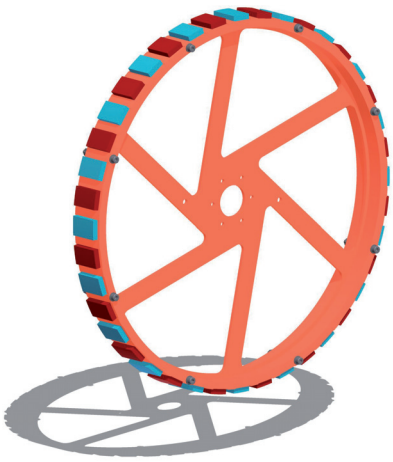

Figure 3.3. Schematic of the rotor.

Generator coils where constructed from 2 parallel round copper wires with diameter 0.85 mm and isolation class F. Maximum coil width was chosen to be 84 mm and inner width minimum 22 mm. Maximum height of the coil was chosen to be 7 mm. Straight length of the coil was chosen to be minimally 54 mm. Total length of the coil maximum 140 mm. Total number of coils in the generator 24. Coils in the generator were connected in serial into three phase system. Connection schematic is given in Fig. 3.4.

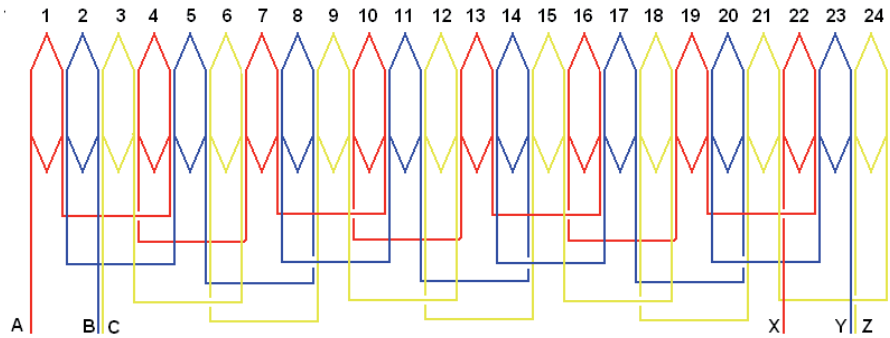

Figure 3.4. Connection schematic of generator windings

Coils were fixed on the stator with compound. Stator yoke was built from electric steel with sheet thickness 0.5 mm. Total stator yoke thickness was 65 mm and inner diameter 704 mm. Outer diameter of the stator was chosen to be 716 mm. Additionally, 24 cooling ribs with a thickness of 16 mm for better cooling were placed on the yoke. Mechanical air gap of the generator was found to be 2.5 mm. Schematic of the constructed stator is presented on Fig. 3.5.

Figure 3.5. Schematic of the stator.

3.2 Experimental set-up

A test bench was constructed to test the prototype machine where both the tested machine and driving machine were placed. The machines were connected to each other using a V-belt and the connection was tightened. Figure 3.6 shows the tested machine that is connected with the driving machine.

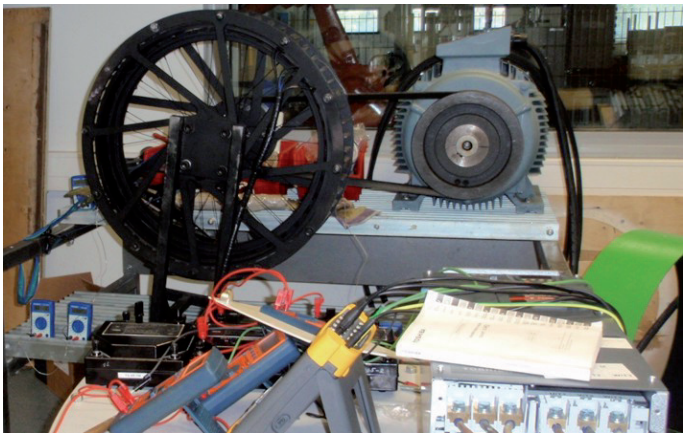

Figure 3.6. Test bench of the generator

A driving machine, 30 kW induction motor was used in the test bench. Rotational speed of the machine was controlled using a frequency converter. As the rated rotational speed of the induction machine was 960 rpm, whereas the rated speed of the tested generator was 230 rpm, the driving machine was chosen to have much more power than the rated power of the tested generator.

During the tests, the generator was rotated using the driving machine and the generator output was measured. At no load tests, the generator voltages were registered and output voltages were recorded using an oscilloscope. During load tests, the generator output was loaded using symmetrical resistive load and both output voltages and currents were recorded. As an induction machine was used, which characteristics were not known and it was not possible to measure transmissible torque in the transmission circuit, it was also not possible to determine the input parameters of the generator during the tests. Due to that, iron losses and efficiency have not been investigated during the tests.

3.3 Magnetic field

Magnetic field measurement was carried out on the prototype machine were the magnetic flux density radial component B_r was measured with a teslameter. For the measurement, the teslameter probe was put into the generator air gap so that the sensor was located at the center of the air gap on the surface of the stator. The magnet flux density was measured at different rotor positions. Measurement result is given in Fig. 3.7 where the flux density distribution over one pole can be seen. As the generator stator yoke inner surface is relatively smooth then it is not needed to repeat the measurement in different stator positions. Flux density is the same in every position as in this type of generators the magnetic reluctance does not depend on the rotor position. Difference in values in different stator positions can come only if the air gap is not uniform, which was not the case in the prototype machine.

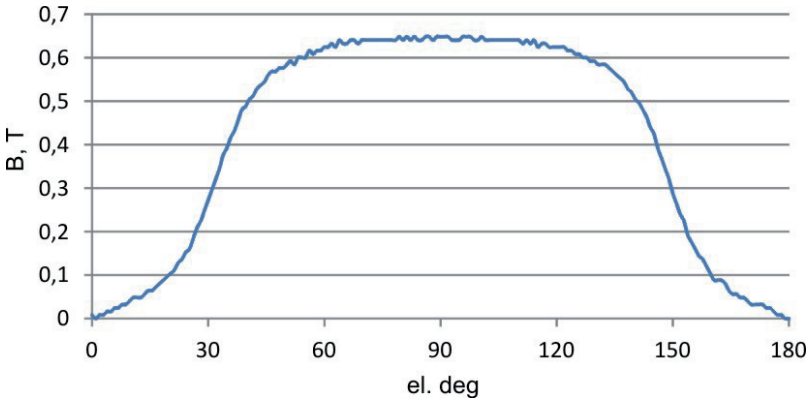

Figure 3.7. Measured primary magnet flux density in the generator air gap over one pole.

There were several reasons for measuring the magnetic field density in the air gap. One was to control that all magnets are mounted correctly. Another reason was to find out how much the magnets differ from each other. From the measurement it was found that from pole to pole there is a slight difference between the maximum flux density values with a maximum deviation of 0.015 T. The difference comes from the permanent magnets as they differ from each other slightly because of manufacturing tolerances.

Another aim for measuring was to verify that the calculation methodology results correspond to measured values. Comparison between the measured value and the calculated one can be seen in Fig. 3.8 where a) is the measured curve, b) is result of FEM calculation, c) is result of analytic calculation and d) is the first harmonic from analytic calculation. As it can be seen from the Fig. 3.8, the measured and FEM calculation results correspond with each other very well. Analytic method gives slightly different magnetic flux distribution over one pole because in the calculation not all harmonics were taken into account. But as the maximum value for the flux density is similar to the measured value, it can also be used for machine calculation.

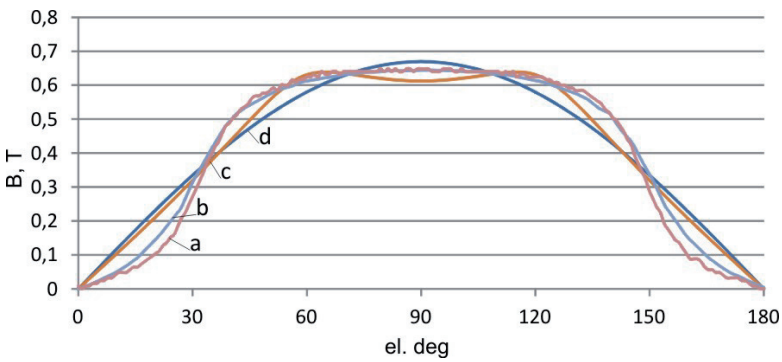

Figure 3.8. Magnet flux density over one pole. a measured, b calculated with FEM, c analytic calculation, d first harmonic with analytic calculation.

3.4 Coil resistance

The aim for measuring the coil resistance was to control that all coils are wounded correctly and also to verify that the calculation methodology for coil resistance is suitable for this type of coils. Difference between the coil resistances can cause uneven power distribution in the generator which can cause vibration in the machine and also some section of the coil can overheat.

The coil resistance was measured by loading the coil with DC current and measuring the input voltage and currents. This method was used as the generator winding resistance is small and with simple ohmmeter the measuring error would be high. To lower the measuring error the measurement was done in three different voltage levels. The Current used in the test was kept low so that the coil temperature would not change during the measurements. Testing was done in room temperature 25 ˚C. Testing schematic is given in Fig. 3.9.

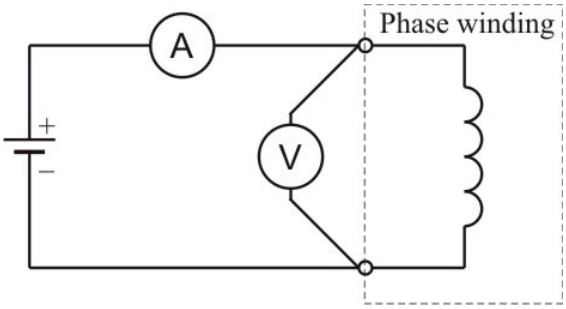

Figure 3.9. Schematic for measuring coil resistance.

From the measurement it was found that all coils resistances at room temperature are 2.6±0.5 Ω. Calculated coil resistance at room temperature was 2.8 Ω. Difference from calculated and measured value is coming from the fact that coil end winding were taken as circular but in reality the end windings can be made shorter which also results in smaller resistance. As the difference is not so big then it can be said that the calculation method for coil winding is good and can be used for this type of coil. Also as the generator copper losses depend on the coil resistance, its good result if real value is a bit smaller then calculated value.

3.5 Open circuit test

The aim for the open circuit test was to control that all generator phases are connected correctly and that phase and line voltages would not differ from each other. Also as the open circuit voltage corresponds to the generator EMF then this test allows verifying the generator EMF calculation methodology.

Open circuit test was carried out in two different generator winding temperature, first at the room temperature 25˚C and after generator load test at generator rated temperature 80˚C. During the test, the generator output phase and line voltages were measured at different generator rotational speed. Test

results are given in Fig. 3.10 where measured line voltages and calculated value are presented.

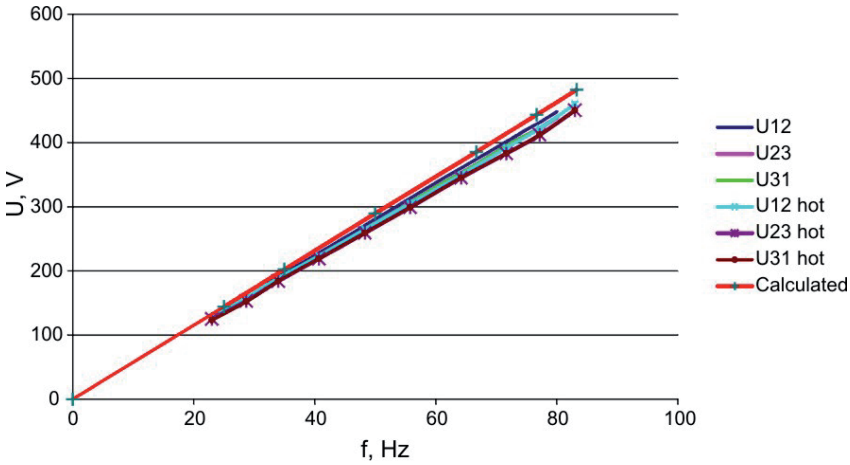

Figure 3.10. Generator open circuit voltage. Red line is calculated and others are measured

As it can be seen from the Fig. 3.10 the EMF at nominal temperature 80˚C is smaller than when the generator is working at room temperature 25˚C. Voltage decrease at higher temperature is expected because of permanent magnets. The problem is that when the permanent magnet temperature is rising then its remanence is decreasing resulting in a decrease in the magnetic flux density and because of this also a decrease of the EMF.

It can be seen from the Fig. 3.10 that there is a slight difference between the line voltages, which could not be seen in phase voltages. The difference between the line voltages is coming from the generator manufacturing process. While in conventional slotted machines the windings goes in slots and fix the winding into exact position, in slotless machine there is always a risk of miss placing of the windings. In slotless machine the windings are put in the air gap and there is nothing that would fix them into exact position, which may result in slight misplacement (a few millimeter drift from its original place) of winding during the generator construction. Because of that the phase angle may not be exactly 120 degrees resulting in difference in line voltages even if the phase voltages are equal.

Also as it can be seen from Fig. 3.10, the generator measured voltage is slightly smaller than the calculated values. There are many reasons why the value may be different. As the permanent magnets may vary little bit from each other (measured deviation was 0.15 T) then also the generator EMF may be slightly different. Also in the generator EMF calculation the effect from magnet edges was calculated with approximate equations. As explained previously, the winding in the generator may be slightly misplaced resulting also in generator EMF etc. But as the difference between the calculated values and the measured ones is 5% at generator nominal rotational speed then it can be said that the EMF calculation is precise enough for designing the generator.

With open circuit test also generator EMF waveform was captured with an oscilloscope. The resulting waveform is given in Fig. 3.11 where it can be seem the measured value and calculated value. As can be seen from the Fig. 3.11 the calculated value corresponds well with measured value. Also it can be said that the voltage waveform is sinusoidal and the higher harmonics cannot be seen except for the every high ones.

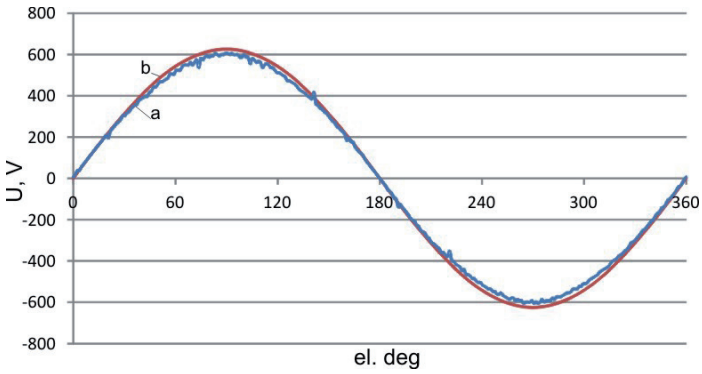

Figure 3.11. Generator open circuit phase voltage waveform. a measured, b calculated.

3.6 Load test

Generator load test was carried out to investigate its output characteristics and behavior during the loading. Also this test allows validating the calculation methodology. As the studied generator is planned to be used in windmills where it works at different speeds then also the tests were carried out at different generator rotational speed.

First the load test was done at the generator nominal rotational speed where the load curves where studied at machine room temperature and at machine nominal temperature. The machine was loaded with a resistive load and in different load points the generator output voltage and current were measured. The generator load test results are given in Fig. 3.12, where the load test with machine working at room temperature, machine working at nominal temperature and the calculated curve can be seen. As it can be seen from the figure the generator output voltage is decreasing with higher loads and at nominal load point it is 17% smaller than the EMF. When the generator is working at nominal load the load curve is smaller than when generator is working at room temperature. This is because the induced EMF is smaller at higher temperatures as explained in no load test then also it stays lower at load test. Also as the winding resistance is temperature dependent where with higher temperature the resistance is higher resulting in higher generator losses and also higher drop in the generator output voltages.

Comparing the test result with calculated value, it can be seen from Fig. 3.12 that the calculated curve is decreasing more with the load than the measured one. While at no load the calculated voltage was 5 % higher than the measured one, at nominal load the measured voltage is 5 % higher than calculated value.

The difference between the calculated and measured values as well as the difference between no load and load is coming because of the winding resistance. As the measured winding resistance was smaller than the calculated one, with load test the voltage drop in the winding is smaller too. Additionally the difference may be added from the simplifications made for winding inductance calculation as also the inductance is defining the voltage drop in the generator. But as the calculated and measured value deviation is at maximum 5 % then it can be concluded that the tested curves in the figure corresponds quite well with the calculated values which means that developed calculation methodology can be used for this machine type.

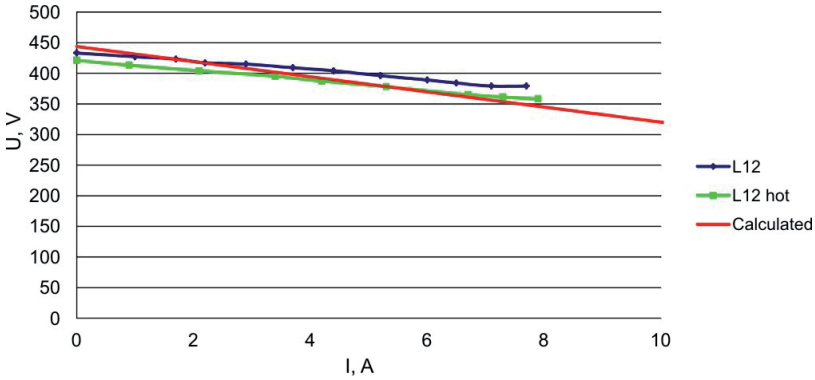

Figure 3.12. Generator output voltage at different loads.

With the load test also the generator power curve corresponding to current was registered which can be seen from Fig. 3.13. Here it can be seen that there is a slight difference between the calculated and measured values, but as the difference is not very big, it can be concluded that the curves are corresponding with each other quite well.

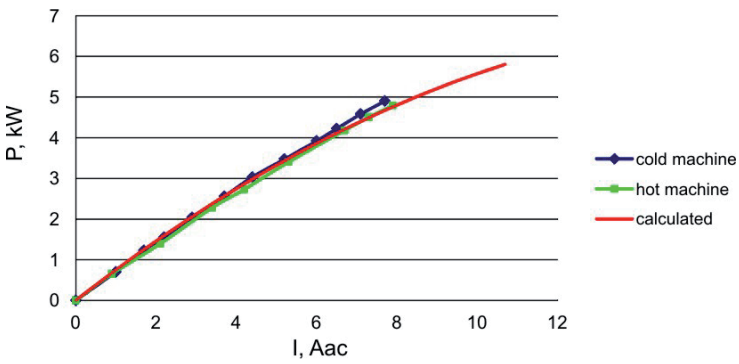

Figure 3.13. Generator output power at different loads.

3.7 Temperature measurements

There were two purposes for the generator temperature tests. The generator windings and permanent magnets are temperature sensitive resulting in wire

isolation destruction and permanent magnet demagnetization when overheated. It was important to control that the machine would handle the nominal load and would not overheat. Also testing the generator temperature was carried out to control the temperature calculation methodology.

The problem with temperature testing at the test bench was the generator cooling system. The generator cooling system was designed to work in the wind where the wind is blowing over the generator outer surface and through the generator air gap. This means that at the test bench there should be cooling fans which ensures the stable airflow at a speed of 12 m/s over the generator surfaces at the generator nominal power. But the test bench did not enable to use the fans. Because of this for making the temperature test at the test bench there was made an assumption that the generator is designed to work with passive cooling system. This also means that the generator nominal power will be lower. For this, new generator temperature calculations were made with new convection heat transfer coefficient h_{con}. For machines with passive cooling the convection heat transfer coefficient is between 1 and 10 W/(m^{2}K). With the new h_{con} it was found the generator power, where the generator achieves stable temperature of 95 ˚C, which corresponds to the generator nominal working temperature. It was found from the calculations that the generator with passive cooling has the nominal power of 4 kW.

Temperature testing was carried out with loading the generator with constant 4 kW resistive load. The temperature was measured with 10 min time steps starting at the generator room temperature 25 ˚C and ended when the generator achieved stable temperature. Coil temperatures were measured with indirect method based on the winding resistance changes. For copper wire it is possible to find the temperature from the wire resistance change according to the equation:

$$T = \frac{R \cdot (T_0 - 245)}{R_0} - 245 \qquad 3.1$$

where T_0 is the ambient temperature,

R_0 is the winding resistance at ambient temperature.

R is the resistance at given temperature.

With this measuring technic it has to be taken into consideration that it gives the winding average temperature. Some hotspots in the winding will be with higher temperatures.

The temperature test result is given in Fig. 3.14. With passive cooling and 4 kW load the generator achieves the stable temperature at 75 ˚C when the ambient temperature was 25 ˚C. The heat up time was approximately 2 hour. The generator is designed to work at a maximum ambient temperature of 40 ˚C. As the ambient temperature was 15 ˚C lower than the maximum ambient temperature the difference has to be added to the generator stable temperature. Taking this into account we achieve from the test, the generator nominal

temperature of 90 ˚C. The calculated temperature was 95 ˚C giving 5 ˚C difference from the measured value. As the measured coil resistance was smaller then also the copper losses in the generator are smaller resulting in lower temperature. Also the difference may be affected by the convection heat transfer coefficient as this value was taken approximately. But as the difference between the calculated and measured values is 5 % and the calculated value is higher it can be concluded that the used calculation method is suitable for the generator temperature calculation.

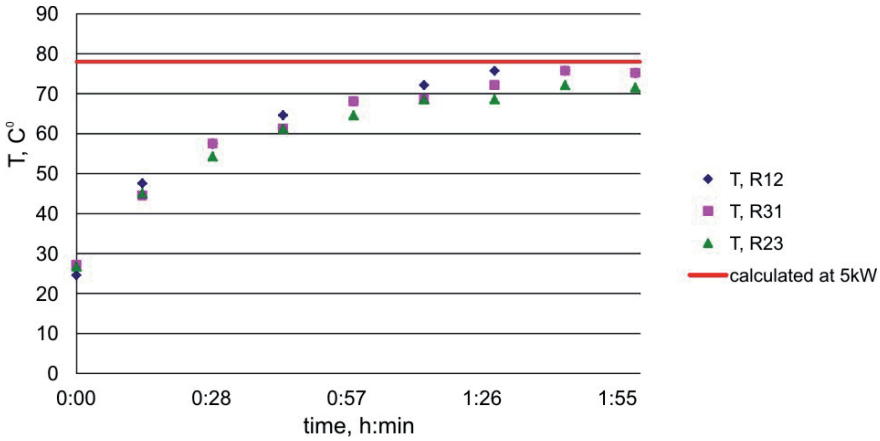

Figure 3.14. Generator temperature test result.

3.8 Conclusion

A 5 kW slow speed slotless generator is designed and constructed. Comparison of the calculation and measured values for the prototype machine shows, generally a good correlation and a high level of accuracy. The difference between the MMF can be explained by the magnet manufacturing tolerances which may affect the experimental result significantly. Also the analytical method did not take into account all the harmonics which results in a difference in the MMF. If exact MMF waveform is needed, the FEM calculation has to be used but as analytic calculation is much quicker calculation method and gives good accuracy, the analytic method is preferred. Difference in the winding resistance can be explained by the winding construction and manufacturing tolerances. The copper wire diameter can vary especially for the small diameter wires resulting in difference in the calculation. Also constructing the end winding can be different from the one used in the calculations. The end winding calculation method have to be renewed in the future where is known exactly how the coil end winding are constructed. Difference in the induced EMF comes from the difference from the MMF. Difference in generator output line voltages is coming from the coil manufacturing proses. When positioning the coils into the generator there is a risk that they are shifted slightly from their original positions resulting in shifts between the phases. This is high risk for this type of machine and has to be studied further. Difference in coil load curves

can be explained by the difference in coil resistance and also by the simplified inductance calculation. With the temperature calculation it is difficult to find accurate temperature coefficients, which results in differences between calculated and measured values. In the future more temperature test should be performed and from this, accurate temperature coefficients should be found. Also as the test bench did not allow doing the test with forced cooling, in the future the fans have to be implemented to the test bench.

Based on the results obtained in this study it can be said that the developed analytic calculation methodology gives sufficient accuracy for the design of slow speed slotless permanent magnet generator. This method can be used with reasonable exactness for the design of other similar generators. It could also be used for optimization purposes as it is quick and requires very little data.

4 Generator with different permanent magnets

As the prices of NdFeB magnets have been very unstable during the generator design proses, possibilities of using other magnetic materials in this generator have been researched.

Besides the NdFeB magnets there are commercially available three types of magnet materials that can be used in the generator: samarium cobalt magnets (SmCo), alnico magnets (AlNiCo) and ferrite magnets. From this range SmCo magnets has the highest energy density. AlNiCo magnets have high remanence, but as their coercivity H_c is relatively low, there is a high risk of magnet demagnetization. Usage of such magnet in a generator is complicated and not desired and not studied further is this thesis. Ferrite magnets have the lowest energy density from those materials. But the ferrite magnets price is the lowest and as they have wide linear demagnetization curve, their usage in the generator was studied as one alternative magnetic material for NdFeB magnets.

Using the SmCo magnets instead of the NdFeB magnets there were made assumption that the generator stator will be the same as it is in NdFeB generator. This requirement can be fulfilled in case the magnet flux density in the air gap is the same as in NdFeB generator.

In the design there was chosen Sm2Co17 grade 28 magnets which demagnetization curve is given in Fig. 4.1. The remanence of SmCo magnet is smaller than NdFeB magnets and to get the same amount of energy from them SmCo magnets have to be bigger. To keep the air gap parameters the same in the calculation it was chosen to change only the height of magnet. It was calculated that in order to get the same magnetic properties in SmCo machine as in NdFeB machine, the thickness of the magnets must be raised 1.2 times. This means 1.12 times growth in generator weight. A prototype generator was built and test result were the same as for NdFeB machine.

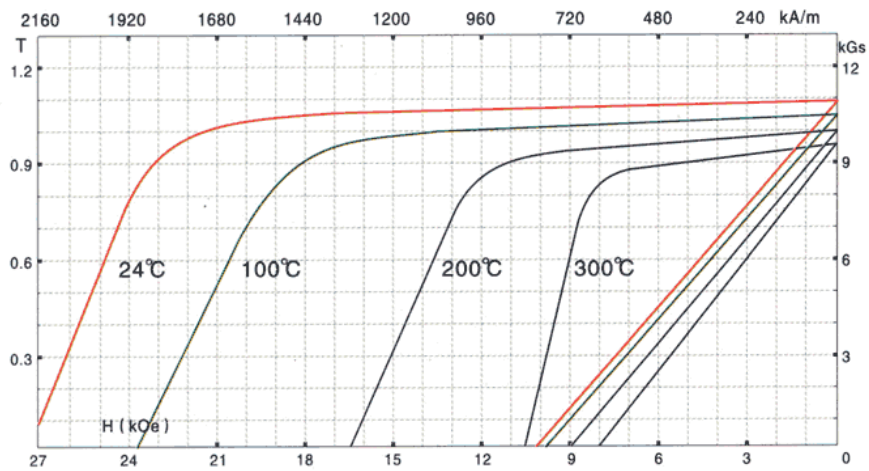

Figure 4.1. Demagnetization curve used to design SmCo machine.

As another possible solution, the usage of ferrite magnets in the generator was studied. As the energy density of ferrite magnets is small and their remanence is low, it is almost impossible to gain a reasonably strong field in this generator using traditional layout of the magnets. To raise the magnetic flux density in the air gap, special layout solutions of the magnets were researched. One of the possibly sufficient solutions turned out to be the Halbach array. In this solution radial magnets are fitted between the poles of the magnets, which help to guide the magnetic field in desired way. This solution helps to significantly raise the magnetic flux density in the air gap and gives a realistic possibility of using ferrite magnets. One of the disadvantages of that solution is that compared to rear earth elements more magnetic material is needed for transporting the same amount of energy through the air gap. This raises the weight of the generator. At the same time ferrite magnets are considerably cheaper compared to rear earth magnets. The grade Ceramic 8 ferrite magnets were used in this study with a demagnetization curve given in Fig. 4.2.

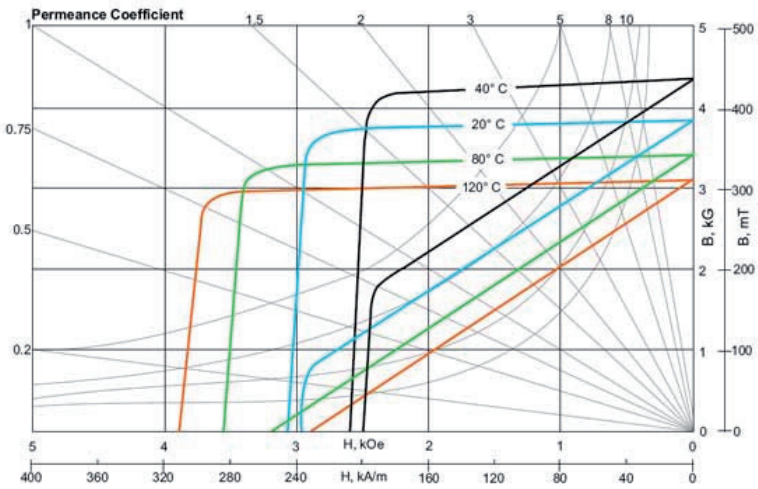

Figure 4.2. Demagnetization curve used to design ferrite machine.

With magnetic field analyze on the studied machine construction it was found that the maximum magnetic flux density achievable with Halbach array is 0.37 T, which is 44 % less than in the case of NdFeB magnets. Due to this fact it is not only necessary to use more magnetic materials, but the generator also must be wider to achieve the same output parameters as in case of rear earth element machines. If the generator air gap diameter is kept the same as in the case of NdFeB machine, it was found that the generator width will increase 62 %. Also the magnet height will increase 400 % compared to the NdFeB machine. The total weight of magnets will increase eight times. But as ferrite is significantly cheaper than rear earth magnets, the price of the machine is still competitive with rear earth material machines. The drawback with this solution is that the studied generator construction loses the weight advantage compared to the conventional machines.

4.1 Conclusion

Study was made of using different magnets in the generator. It was found that it is possible to use lower grade magnets then NdFeB magnet but with this the weight of machine is rising. In case of using the SmCo magnets instead of NdFeB magnets the magnet volume is raising almost 2 times but the NdFeB generator stator can still be used. With ferrite magnets in Halbach array it was found that there is not possible to use NdFeB stator, as with ferrite magnets it is not possible to obtain the required flux density in the air gap. Using the ferrite, the generator stator has to be wider and to get the same amount of power the ferrite magnet mass has to be 62 % higher compared with NdFeB machine.

5 Analyses of manufacturing tolerances

5.1 Eccentricity

One of the key issues in the generator design is the air gap and its uniformity. Air gap eccentricity is usually not taken into account during the design process of conventional generators, but as the generator under investigation has a large radius and is relatively thin, it is expected that there can be problems occurring due to air gap eccentricity rising from the low mechanical stiffness of the generator construction. This chapter is dealing with such possible problems from the point of view of analyzing the effect of the eccentricity on the operation parameters of the generator such as the induced voltage waveform and the mechanical stress acting on the stator and rotor of the machine.

Air gap eccentricity can be related to different manufacturing inaccuracies, such as construction tolerances, bearings, and shaft bending [54]. The eccentricity appears to some extends in all electrical machines and it has been studied from different points of views e.g. as related to its effect on the losses [55] or unbalanced magnetic pull [56], [57] or how to diagnose the fault [58], [59], [60]. However, it is not clear how much does a problem like this affects the performance of the electrical machines and is it important to take it into account during the design process. If one looks at a permanent magnet machine, then every magnet that is situated on the rotor causes some radial force that affects the stator. If the air gap has a uniform width, then the resultant of these forces in all the construction of the machine equals to zero. On the other hand, if there is some eccentricity in the air gap, the resulting force is different from zero and the additional force start to affect the bearings, which means faster wearing. Another aspect related to the eccentricity is that the magnetic flux density in the air gap will be asymmetrical, which causes a deviation of the electrical parameters of the machine from the designed ones. This can result in the deviations of the output voltage and current and also oscillations in the power of the machine. The oscillating power can cause unequal distribution of the load, which in turn causes local hot spots and wearing of coil insulation. Additionally, air gap eccentricity always results in excessive mechanical vibrations.

This chapter investigates the cases of static and dynamic air gap eccentricities in the low speed slotless permanent magnet generator. The investigation has been performed through analytical methods in order to better understand how the eccentricities affect to the machine. The methodology of how to consider the possible eccentricity faults in the analysis of the machine has been described and analytical calculations have been carried out and comparison with measurements made on a prototype machine has been presented. The measurements on the prototype have been made for a healthy machine only and for the purpose of validating the analytical methodology.

5.1.1 Type of eccentricities

Air gap eccentricity can be caused by inaccurate construction as well as different problems during the exploitation. Fig. 5.1 shows possible types of eccentricity. A healthy machine (Fig. 5.1a), static eccentricity (SE) (Fig. 5.1b), elliptic eccentricity (EE) (Fig. 5.1c) and dynamic eccentricity (DE) (Fig. 5.1d and 5.1e) are shown on the figure.

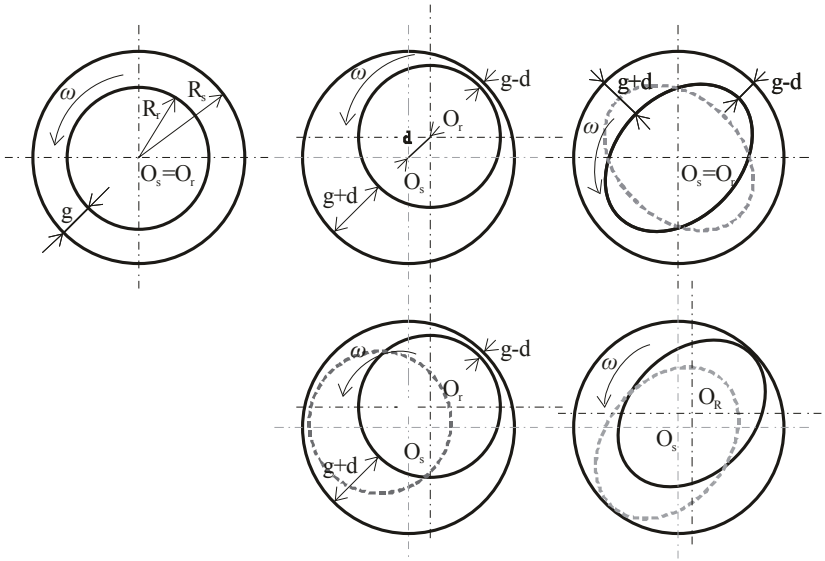

Figure 5.1 . Rotor eccentricity: a) healthy; b) static; c) elliptic; d) and e) dynamic. Other eccentricities mode emanating from the deformation of the stator can also occur but they are not investigated here

Static eccentricity

In the SE fault, the rotational axis of the rotor coincides with the rotor symmetry axis, and it is displaced from the stator symmetry axis. Although the air gap distribution around the rotor is not uniform, it is time independent. The SE degree (δs) is defined as follows:

$$\delta_s = \frac{\left| O_s O_w \right|}{g} \qquad 5.1$$

where O_s is the stator symmetry center, O_w is the rotational center, and g is the air gap length. Fig. 5.2 (a) shows the position of the stator and rotor in the cross section plan of the machine in the case of SE. β_s is the initial angle of the SE and the vector O_sO_w is the static transfer vector. This vector is fixed for all angular position of the rotor.

.

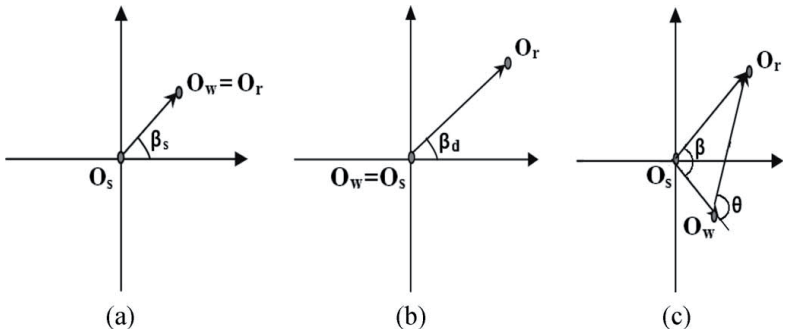

Figure 5.2. Position of stator and rotor cross sections under (a) SE, (b) DE, and (c) EE in the stator reference frame.

In a SE fault, the width of the air gap can be determined using the following equation:

$$g = R_s - R_r + \sqrt{R_r^2 - (d \cdot \sin\beta)^2} \qquad 5.2$$

where R_s is the stator radius and R_r the rotor radius.

Elliptic eccentricity

In case of elliptic eccentricity the center points of the rotor and stator symmetry are matching, but due to the elliptic shape of the rotor, non-uniform air gap still exists. In such case, the deviations caused by the eccentricity changes in time.

The width of the air gap in the case of elliptic eccentricity can be found using the following equation:

$$g(t) = R_s - \sqrt{\left[(R_r + d)\cos(\frac{\omega t}{p} - \beta)\right]^2 + \left[(R_r - d)\cos(\frac{\omega t}{p} - \beta)\right]^2} \qquad 5.3$$

where R_r is the radius of cylindrical rotor, d expresses the deviation of the ellipse from the circular shape and p is the number of rotor poles. Note that the angle β changes in time.

Dynamic and mixed eccentricity

Dynamic eccentricity is a situation where the center point of rotor symmetry is shifted depending on the stator center and the rotation of rotor is performed around the center point of stator symmetry. In such case the air gap eccentricity is a time-varying phenomenon. The DE degree (δ_d) is defined as follows:

$$\delta_d = \frac{|O_w O_r|}{g} \qquad 5.4$$

where O_r is the rotor symmetrical axis, and vector $O_w O_r$ is the dynamic transfer vector. This vector is fixed for all angular positions of the rotor, but its angle

varies in time as the rotor rotates. Fig. 5.2(b) shows the DE, where β_d is the initial angle of the DE.

Mixed eccentricity means that the center points of the rotor, the stator and the rotational symmetry are all shifted from each other. This means that both static and dynamic eccentricities are present in the generator. Mixed eccentricity is the result of static and dynamic transfer vectors and in that case MD degree (δ_m) can be defined:

$$\begin{aligned}\delta_d &= \frac{\left|O_w O_r\right|}{g} \\ &= \left|\frac{O_s O_w}{g} + \frac{O_w O_r}{g}\right| \\ &= \sqrt{\delta_s^2 + \delta_d^2 + 2\delta_s \delta_d \cos\theta}\end{aligned} \qquad 5.5$$

In case of mixed eccentricity the width of the air gap depends on the mechanical position and it can be found as follows:

$$g(t) = R_s - \delta_m g \cos\left(\frac{\omega t}{P} - \beta\right) - \sqrt{R_r^2 - \delta_m^2 g^2 \sin\left(\frac{\omega t}{P} - \beta\right)} \qquad 5.6$$

5.1.2 Stress and electrical parameters

Knowing the width of the air gap according to the mechanical angle, the magnetic flux density in the air gap corresponding to each pole can be calculated. This can be done by using a vector potential:

$$\vec{B} = \nabla \times \vec{A} \qquad 5.7$$

To know how large is the force that permanent magnets influence the stator with and also considering that $\mu_{iron} >> \mu_0$, so that magnetic force is acting on the surface of the iron, Maxwell stress tensor can be used:

$$f_r = \sigma_{rr}^{air} - \sigma_{rr}^{iron} \approx \frac{1}{2\mu_0} B_g^2 \qquad 5.8$$

where f_r denotes the radial traction.

To find radial unbalanced force acting on the rotor center integrating radial force density along the rotor surface can be determined as in:

$$F_r = \int_0^{2\pi} f_r \cdot r d\theta \qquad 5.9$$

When calculating the generator EMF it is assumed that the magnetic flux is uniform for the all the generator coils and thus the calculation of EMF in one coil is enough. In the case of eccentricity, every coil has to be considered as an

independent case and the EMF for each coil has to be calculated. The EMF can be calculated using:

$$emf = \oint_c (v \times B) \cdot dl \qquad 5.10$$

where v is the speed of magnetic field.

5.1.3 Eccentricity calculation results

Based on the parameters of the generator under investigation and the above presented analytical expressions, the angular variation of the air gap was first calculated under different eccentricities. Figure 5.3 show the dimensions of the air gap in case of different eccentricities. Calculations have been done assuming that in case of static eccentricity the offset of the rotor symmetry center point compared to the stator symmetry center point is 2 mm. It is the same in the case of dynamic eccentricity and considering also that the mechanical angle is changing with the angular position. In case of elliptic eccentricity, the offset of the ellipse from the circle is also set to 2 mm.

In the case of static and dynamic eccentricities it can be seen that one maximal and one minimal air gap is emerging in the generator. Also the location of the air gap is asymmetrical. With some simplifications, the location of the air gap can be looked at as a sine function in such case.

In case of elliptic eccentricity two maximal and minimal values are forming, which are located symmetrically with respect to the mechanical angular position of the generator. With some simplification it can be looked at as a double sine function.

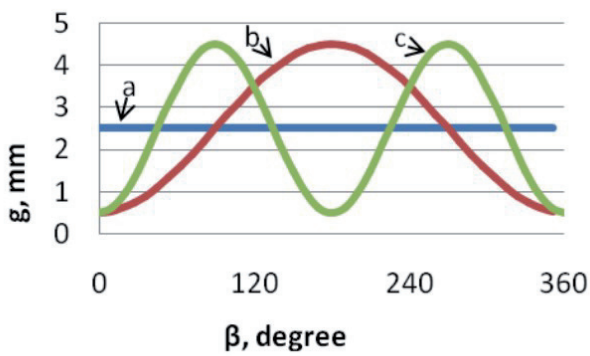

Figure 5.3. Air gap according to the mechanical position, a – healthy, b – static and dynamic, c – elliptic. Note that in the dynamic eccentricity case the position of the maximal and minimal air gap are changing in time as the rotor rotates.

The magnetic flux density in the air gap was calculated analytically in case of different eccentricities and it is shown on Figs. 5.4, 5.5 and 5.6, respectively for the cases of healthy machine, dynamic/static and elliptic eccentricity. In the

case of dynamic eccentricity the waveform of the magnetic flux density is time dependent and it is moving along the angular position. The calculations are based on the assumption that in case of eccentricities, the change of the air gap is 2 mm. From the Fig. 5.4 it can be seen that in case of a healthy machine, the waveform of the magnetic flux density along the angular position is uniform in the whole generator in the sense that the peak value is the same after each pole. In case of eccentricities, the waveform of the magnetic flux density is asymmetrical in the sense that it is modulated by the varying air gap.

In case of the healthy machine, the maximum magnetic flux density is 0.67 T. In the case of both dynamic and static eccentricities of 2 mm, at minimum air gap dimensions the magnetic flux density rises 13.6% and at maximum air gap dimensions the flux density falls 11%. Calculations of elliptic deviations show similar results.

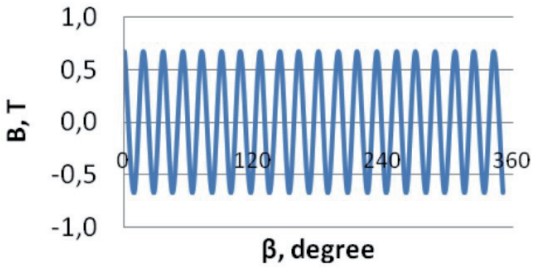

Figure 5.4. Waveform of the magnetic flux density in the healthy machine along the angular position.

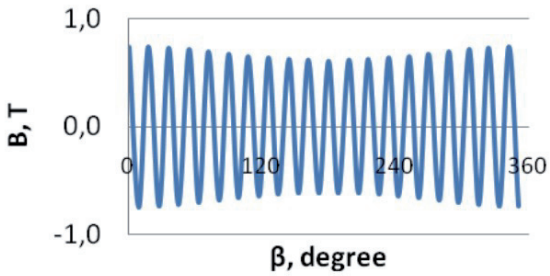

Figure 5.5. Waveform of the magnetic flux density distribution along the angular position under static and dynamic eccentricity. Note that in the case of dynamic eccentricity the modulated waveform is moving along the angular position.

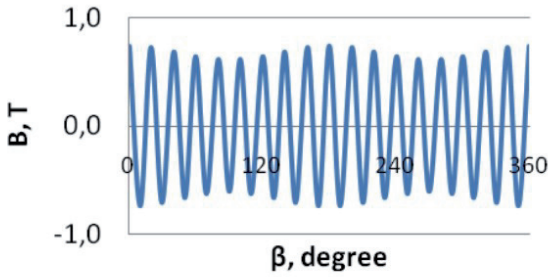

Figure 5.6. Waveform of the magnetic lux density distribution along the angular position under elliptic eccentricity. The modulation is due to the modulated air gape as seen in Fig. 5.3.

The Changes in the maximum values of the magnetic flux density with the eccentricity deviations from rated air gap dimensions were also investigated for different values of eccentricity. The results of such investigations are shown in Fig. 5.7.

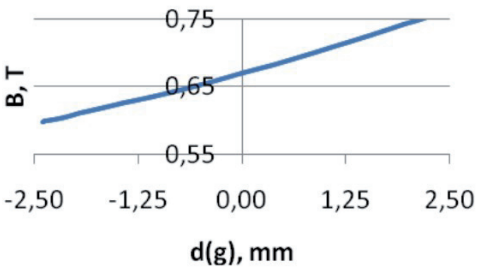

Figure 5.7. Maximum values of the magnetic flux density as function of the eccentricity.

The total force acting on the stator caused by the primary magnetic field has also been investigated. In case of a healthy machine with uniform air gap the magnetic forces are distributed in a homogeneous way across the air gap. This means that the resultant force acting on the mechanical construction between the stator and the rotor is zero. In case of eccentricity, the air gap becomes asymmetrical, and so are the forces, resulting in an unbalanced magnetic pull. Figure 5.8 show the calculated resultant force in the case of static eccentricity as function of the degree of deviation. It can be seen that the force acting on the construction in case of the shifted stator and rotor symmetry points is linear.

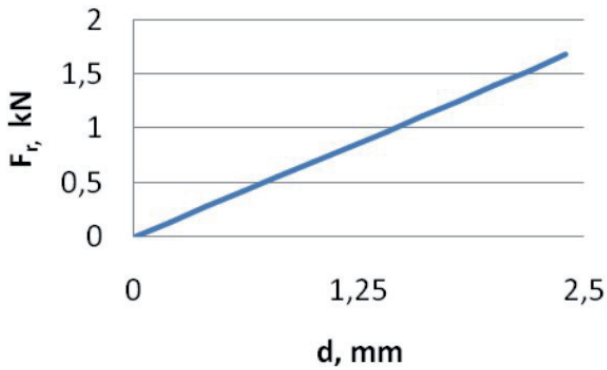

Figure 5.8. Resulting unbalanced magnetic pull as function of the degree of deviation in the case of static eccentricity. The linearity is due to the linearly assumed magnetic circuit.

In the case of elliptic eccentricity, although the deviation of the air gap dimensions is asymmetric in the generator, the resultant forces acting on the construction is zero due to the fact that the air gape deviation and also the magnetic flux density are in radial symmetry.

The next investigated parameter of the generator was the induced EMF. The calculations show that in case of a healthy machine, the induced EMF in every coil has a constant effective value of 32 V. As the air gap becomes asymmetrical due to assumed eccentricity the induced EMF in different coils becomes asymmetric too. Figure 5.9 show the calculated value of induced EMF in one coil as function of the eccentricity deviation of the air gap in case of static eccentricity.

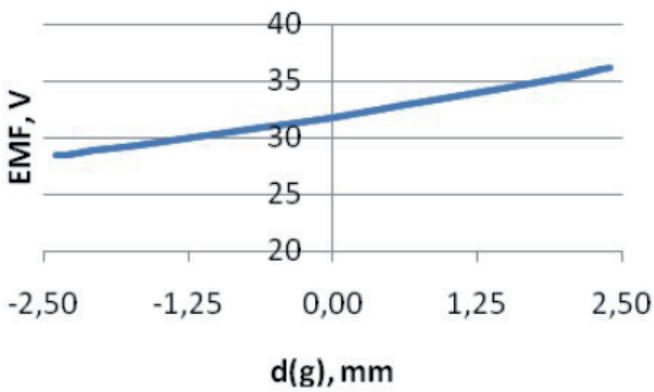

Figure 5.9. EMF of a single coil as function of the air gap change.

The investigated generator has its windings connect in a three-phase system, where the coils are distributed equally in the stator and all the coils corresponding to a given phase are connected in series. In case of eccentricity, the induced EMF in the coils depends on the position of the eccentricity.

Analytically it was found that the highest difference between the phases emerges when the shift vector of the rotor is oriented between two phases, i.e. 7.5 degrees. These calculations have been made for the case of a 2 mm rotor shift and the results are presented in Table 5.*1*. In such case, similar voltages are induces in phases A and C, but the voltage of phase B differs from the two first ones. It can also be seen from Table 5.*1* that when the coils are connected in series, the resultant EMF in all the phases are equal, but the resulting voltages are higher than in the case of a healthy machine. This increase in the voltage is due to the additional motion of the rotor caused by the eccentricity which induces additional voltage in the coils.

Table 5.1. Calculated EMF for static and dynamic eccentricity

	Phase A	Phase B	Phase C
Static and dynamic eccentricity			
Min per coil	28,43	28,64	28,43
Max per coil	36,11	35,78	36,11
Serial connection	256,32	256,32	256,32
Elliptic eccentricity			
Min per coil	29,01	29,72	29,01
Max per coil	35,22	34,24	35,22
Serial connection	255,84	255,84	255,84
Healthy			
EMF per coil	31,82	31,82	31,82
Serial connection	254,56	254,56	254,56

Testing showed that the used analytical methods are sufficient for the calculations of the characteristics of the designed generator. The test results agree well with the calculated values. The verification of the eccentricity results through measurements has not been carried in view of keeping the generator healthy until all validations has been done as the introduction of faults in the prototype might destroy it.

5.1.4 Analyses

In the present investigation of how the eccentricity affects the generator it was found that any kind of eccentricity causes additional stresses to generator construction, which has to be taken into account in the design process of the generator mechanical support.

In case of static eccentricity it was found that even a small deviation of the rotor symmetry from the center point of the stator symmetry causes a significant increase in the unbalanced magnetic pull, which in turn causes the bearings to

wear. It was also found that the force affecting the construction increases linearly with the eccentricity of the air gap. As this force is not changing in time, it does not induce remarkable additional vibrations in the generator. At the same time the induced EMF in the coils causes deviations in the phases voltage values. The Resulting voltage deviations and their presence in the generator system depends on the connection method of the coils. If the coils are connected in parallel, then the different voltage values between the coils induce circulating currents, which in turn in the case of static eccentricity cause additional resistive losses. In addition to these losses, static eccentricity causes the deviation of voltages between phases. On the other hand, when the coils are connected in series, there will be no difference of voltage between the phases, but the phase voltage rises when compared to a healthy machine. Dynamic eccentricity is quite similar to static eccentricity, except for the fact that the shift-vector changes in time. This causes additional vibrations in the generator.

In the case of elliptic eccentricity no additional forces are induced that affect the bearings, but as the forces are distributed un proportionally along the air gap angular position, the forces affecting the construction can cause additional bend and since they are time dependent they will cause vibrations of the stator and rotor. The induced EMF values are similar to the ones of dynamic eccentricity.

5.2 Demagnetization

5.2.1 Method of analysis and case study

The demagnetization of a permanent magnet can happen due to different reasons. One of the main reasons for permanent magnet demagnetization in electrical machines is the armature reaction field that is oriented in opposite direction to the magnet field and is created due to the loading currents. Secondly, the shape of permanent magnet demagnetization curve depends strongly on the temperature of the magnet and at a certain temperature there is the possibility that the load point of the magnet will be beyond the knee of the curve, where the magnet is irreversibly demagnetized. The third reason for the demagnetization is that the Halbach array construction produces a nontraditional path of the magnetic flux density, which can also demagnetize some of the magnets constructing the array.

5.2.2 Demagnetization process

Permanent magnets are usually defined by their demagnetization curve. The magnetization curve of the ferrite magnets used in work is shown in Fig. 5.10. It can be seen from the figure that there is a linear dependency between the magnetic field strength and the magnetic flux density up to a certain value of the magnetic field strength. However, when the magnetic field strength is high enough, the magnetic flux density drops more rapidly. It can also be seen that the demagnetization curve depends on the temperature of the magnet in a rather different way than in rare earth magnets.

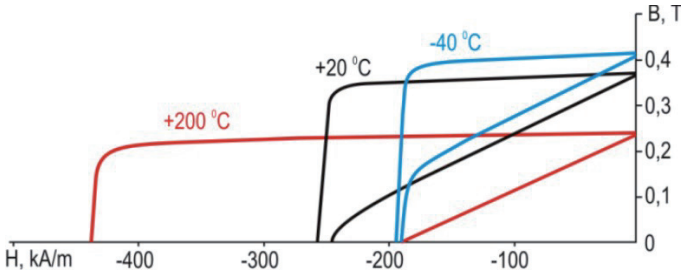

Figure 5.10. Ferrite magnet demagnetization curve. These mag-nets are characterized by low remanence, weak coercivity and also low energy product.

The working point of the magnet is defined by the length of the magnetic path which the magnetic flux has to pass and eventually the value of the current producing opposing flux. In other words, it is defined by the construction of the generator and the armature reaction magnetic flux density that emerges when the generator is loaded. The work or load point of the magnet can be found using Ampere's law:

$$\int Hdl = nI \tag{5.11}$$

where H describes the magnetic field strength, l the length of the magnetic path, I is the current and n number of turns. As the current is missing in no load operation we have to specify magnetic field strength in the magnet, which is non-zero and opposite to the magnetic field strength along the rest of the magnetic path.

The shape of the demagnetization curve for the magnet is defined by the recoil magnetic permeability μ_{rec}, which can be found according to the following equation:

$$\mu_{rec} = \frac{\Delta B}{\Delta H} \tag{5.12}$$

To find the partial demagnetization of permanent magnet, the working point of the magnet has to be defined. While the working point is set on the BH curve in the area where μ_{rec} is constant and with a minimum value, no demagnetization occurs in the magnet. When the working point moves to the area where μ_{rec} is rising, partial demagnetization will start to emerge.

Partial demagnetization means that the demagnetization curve of the permanent magnet drops from its original one (Figure 5.11). As μ_{rec} tries to always keep its minimum value, a new BH curve can be created, knowing the load point between B_m and H_m and using the following formula:

$$B_{rdemag} = B_m - H_m \mu_{rec} \tag{5.13}$$

where B_{rdemag} is the new remanence value of the demagnetization curve of the permanent magnet.

In order to describe how much the magnet has demagnetized the ratio between B_{rdemag} and B_r must be found. This ratio is the demagnetization constant k_{demag}:

$$k_{demag} = \frac{B_{rdemag}}{B_r} \qquad 5.14$$

The fact that the demagnetization curve depends on the temperature of the magnet must be taken into account when using the magnet either in modeling or in constructing the wind generator. Fig. 5.11 shows an example where no demagnetization occurs at the working point of the magnet at 20 °C but as the temperature drops to -40 °C the working point reaches to the demagnetization area of the *BH* curve and the curve starts changing. After demagnetization there are changes of the curve also at 20 °C by the value of k_{demag}. This means that the irreversible demagnetization at -40 °C will persist even if the magnet is heated back to the 20 °C

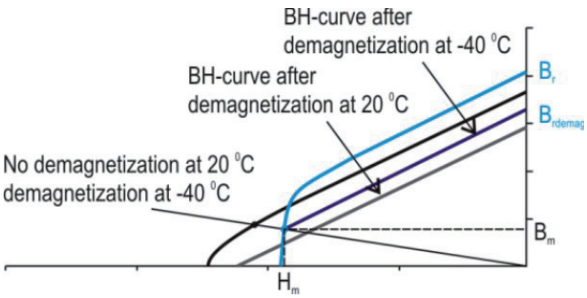

Figure 5.11. Illustration of the demagnetization at -40 °C but not at 20 °C for the same load (working point) of the magnet. If the magnet is first demagnetized at -40 °C it will also stay demagnetized at 20 °C.

5.2.3 Method

To demonstrate the demagnetization phenomenon and compare it with the measurements, a test model was constructed. The test model consisted of three poles and the corresponding iron supports as well as the stator yoke as shown in Fig. 5.12.

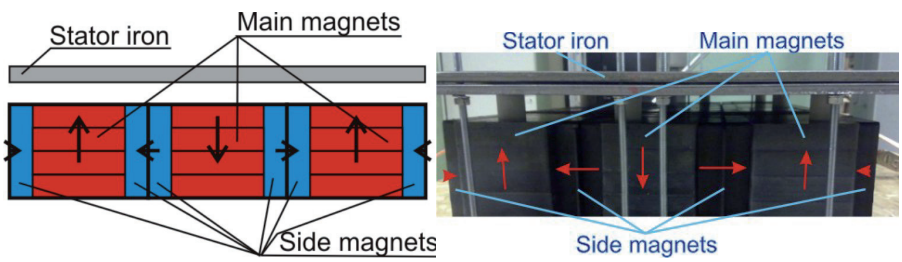

Figure 5.12. Illustration of the constructed Halbach prototype module and a photo of the actual setup. The coils of the stator are represented as air as they do not participate in the modeling or operation of the machine under no-load.

Finite elements analysis is the main tool used in this work. A parameterized model has been constructed in the software FEMM, where the side magnet blocks were divided into 64 subdomains that are observable as small squares in Fig. 5.13. Two different situations were investigated. First, one side magnet was placed next to the main magnet and the resulting field distribution was computed with a static approach. This simulation showed that some parts of the side magnets were demagnetized as explained in the results section below.

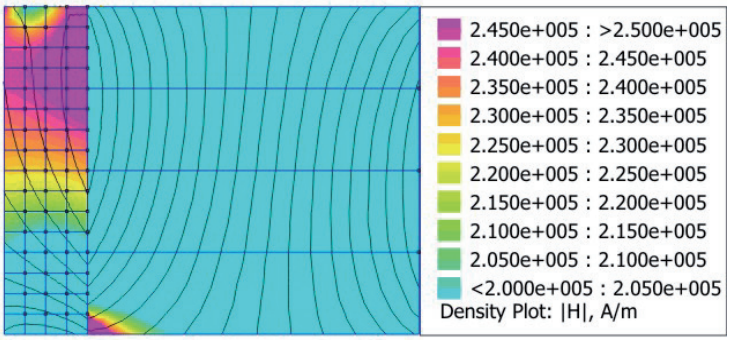

Figure 5.13. Computed distribution of the magnetic field strength for the case where the side magnet is positioned next to the main magnet. Static approach.

The second analysis aimed at finding when the demagnetization started. This was achieved by simulating the process of bringing the side magnet near the main magnet. The side magnet was moved to its final position next to the main magnet from an initial position far enough from this latter one. The motion was made in steps of 5 mm after which a new computation of the magnetic field was carried out. The motion of the side magnet was carried out in a quasi-static manner, i.e. no eddy-currents were considered. This assumption is justified by both the low speed at which the magnet is moved in the actual manufacturing process and the low conductivity of ferrite magnets. A modified demagnetization curve was applied to the demagnetized part of the magnet whenever such a phenomenon occurred during the motion of the side magnet. The methodology for updating the BH-curve for each separate region is illustrated by the flow chart shown in Fig. 5.14. A set of the BH-curves of the magnets in use, which resulted from the simulations are shown in Fig.5.15. The curves in Fig. 5.15are numbered according to the numbers shown in the subdomains of Fig.5.16. Once the dynamically simulated mounting process of the Halbach array was finalized, an additional simulation was needed to account for the iron yoke and also to make it possible to compare the results with measurements made on a prototype module.

Regardless of the fact that we ignored the Eddy currents in this kind of simulations, as justified above, we call this approach a dynamic one as it accounts for the approach of the magnet as well as for the degradation of its local magnetization curve.

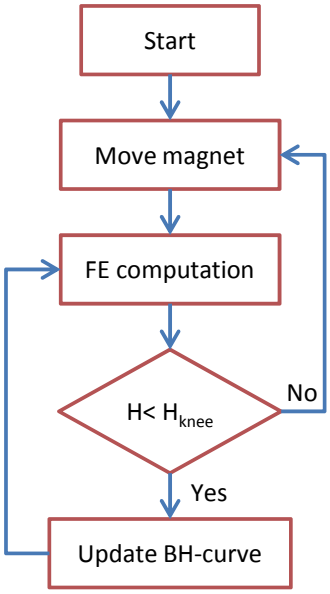

Figure 5.14. Flow chart of the dynamic computation procedure. The computation is stopped when the magnet has reached its final position.

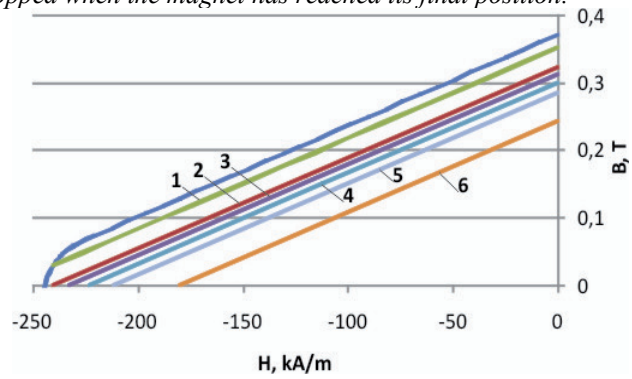

Figure 5.15. Initial and updated BH-curves of the magnets. The curves are the ones used for updating after demagnetization. Numbering corresponds to Fig.5.16.

5.2.4 Computation results

Static Results

The results from a static computation, where the side magnet was at its final position are shown in Fig. 5.13. From this figure it can be seen that 12 domains out of the 64 are fully demagnetized, and the domains next to them are partially demagnetized. The demagnetization of the subdomains is shown by the magnitude of the magnetic field strength in these domains compared with the magnitude of the field at the knee of the demagnetization curve. FE calculations of the magnetic field were carried out on the complete test model without taking into account any demagnetization. The computed solution of the magnetic field is shown in Fig. 5.17where the field lines as well as the magnetic field strength

in the whole construction can be seen. Figure 5.17shows that the side magnets, situated between the main magnets are not demagnetized but these on the outer side are suffering demagnetization.

A second static simulation accounting for the demagnetization was carried out. The side magnet was considered to demagnetize as shown in Fig. 5.13and thus its BH-curve was replaced with new one corresponding to the maximum field strength. Based on the demagnetized magnet blocks a new module was created in the software and considering the partial demagnetization, new FE calculation was performed, the results of which are shown in Fig. 5.18.

Dynamic Results

The Results of the dynamic modeling procedure are shown in Fig. 5.16 where the field is plotted for each position of the side magnet and also for the main magnet at the final position. It can be seen that the demagnetization of the side magnet started when the distance from the main magnet was 20 mm. When the side magnet is brought closer to the main magnet, the demagnetization reaches more and more domains as the magnetization curves of the previously demagnetized ones where updated. This is due to the fact that after partial demagnetization, the demagnetizing field from the middle magnet penetrates the side magnet deeply and thus produces demagnetization inside the side magnet.

A careful look at the field distributions from Fig. 5.13 and Fig. 5.16, at the final position, shows clear differences in terms of demagnetized subdomains and severity of demagnetization. In Fig. 5.13 the demagnetization occurred in a wide region of the side magnet and some of its parts are even fully demagnetized.

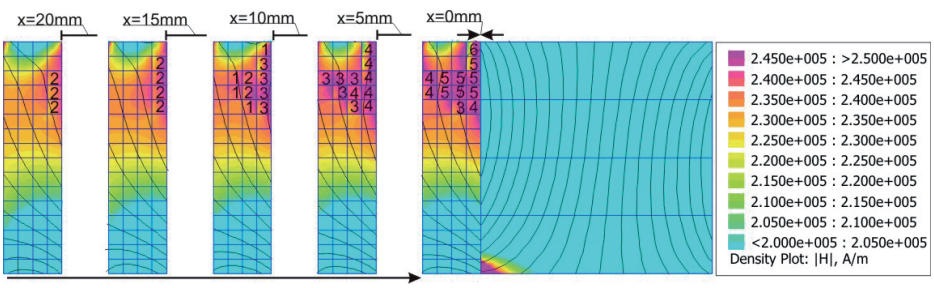

Figure 5.16. Computed magnetic field strength from the dynamic simulation at five different positions of the side magnet during its approach to the main magnet. The numbering of the subdomains corresponds to the updated BH-curves from Fig.5.15.

Fig. 5.16 shows that as the permanent magnet starts to demagnetize at a certain distance from the main magnet, and the magnetization curves are updated, the final demagnetization is not as serious as the one computed with the static approach, where the side magnet is already at its final position. In fact both simulations are different from the one in which all the magnets were at their final position. Results of this computation can be seen in Fig. 5.17, where the iron yoke is also present as a final construction. Such a difference is also seen in the measurements as explained later.

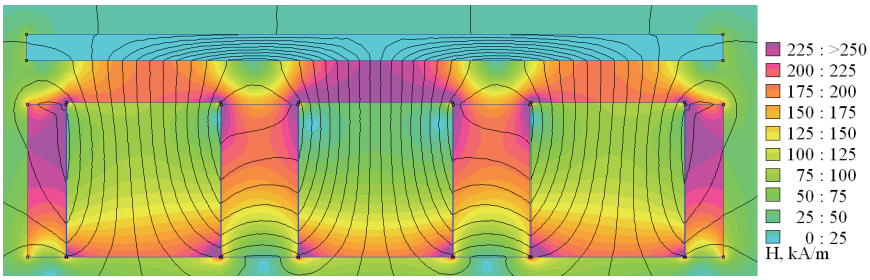

Figure 5.17. Simulation result without accounting for the demagnetization during the assembly process. The field strength is within the limit of demagnetization but not as high as in the cases of static or dynamic simulations.

The dynamic simulation was continued by bringing the second side magnet near the assembly made by the main magnet and one side magnet. As a result from this simulation, the second side magnet also demagnetized in the same way as the first one when it was around 20 mm away from the assembly. However, the demagnetization did not concern only the second side magnet but also the already in place first magnet demagnetized deeper. The simulation result from this mounting process is shown in Fig. 5.19 as the second side magnet has reached its final position. It should be noted that during this simulation the BH-curves of each subdomain was updated according to the process in Fig. 5.14.

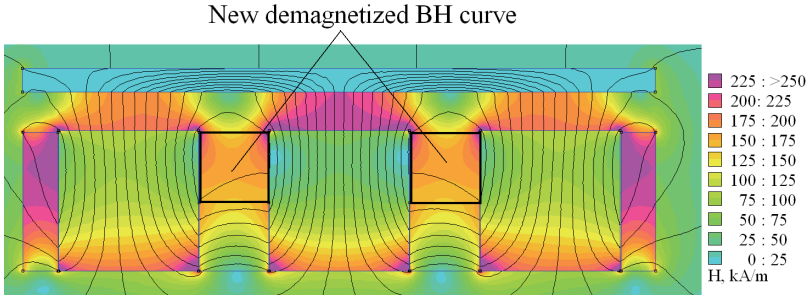

Figure 5.18. Simulation result accounting for the demagnetization only at the final position (static approach). The BH-curve of the demagnetized region has been updated for the purpose of comparison with the measurements presented in Fig. 5.13.

A further dynamic simulation was carried out to model the addition of the third magnet block to the already assembled one. The methodology followed is the same as in the bringing of the side magnets near the main one. The final result of this simulation is shown in Fig. 5.20. Here again, the outer side magnet did not demagnetize any further but the side magnets in the area between the two subassemblies demagnetized deeper and the severity of demagnetization is increased in some subdomains.

The process was continued by adding the next subassembly, with similar results as above. The outer magnet does not demagnetize but the side magnet in the middle demagnetizes deeply and the demagnetization of some subdomains gets more and more severe. The result from this last simulation is shown in Fig. 5.21.

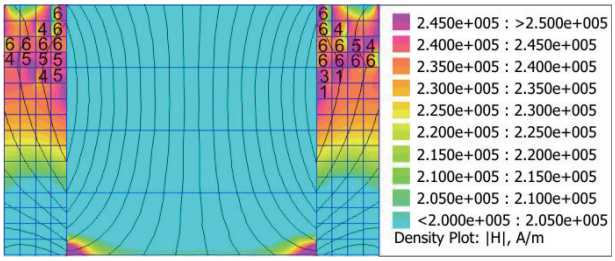

Figure 5.19. Computed magnetic field strength from the dynamic simulation with added two side magnets. The newly added magnet has contributed to further demagnetization of the already positioned one.

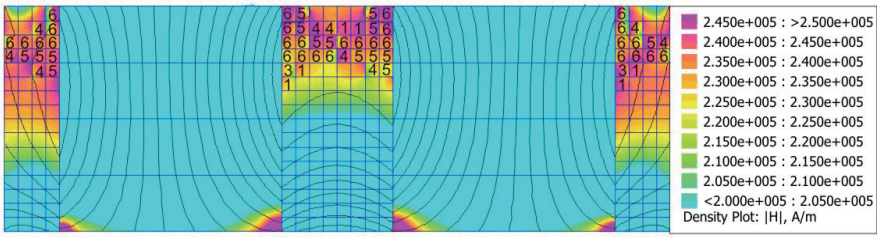

Figure 5.20. Computed magnetic field strength from the dynamic simulation with added two magnet blocks. The middle side magnets are further demagnetized.

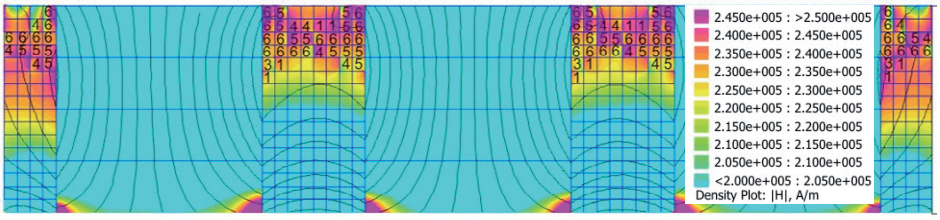

Figure 5.21. Computed magnetic field strength from the dynamic simulation with added three magnet blocks. The middle magnets further demagnetize as the field is penetrating them under the effect of the new ones.

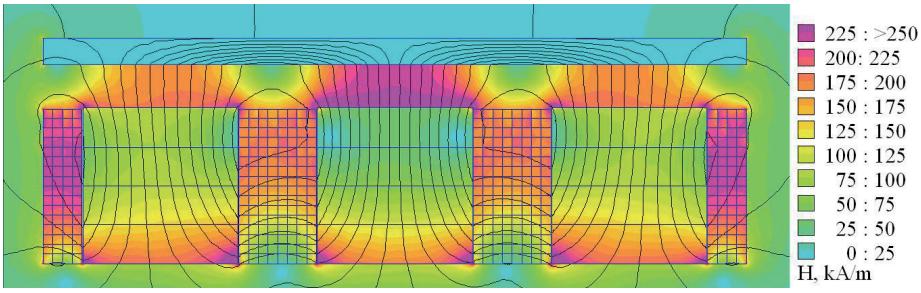

Figure 5.22. Final assembly simulated with the dynamic approach at each step of the assembling process. The iron yoke does not affect the demagnetization.

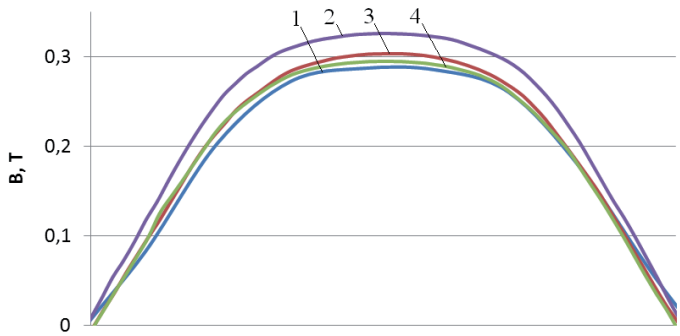

Figure 5.23. Comparison of measured and computed magnetic flux densities in the air gap of the prototype module over the middle pole. 1 – measured, 2 – without demagnetization effect, 3 – demagnetization with static approach, and 4 – demagnetization with dynamic approach.

Once the dynamically simulated mounting process of the Halbach array was finalized, an additional simulation was needed to account for the iron yoke and make it possible to compare the results with measurements. The result of this final simulation is shown in Fig. 5.22 with all the components of the model and with the assembly magnetic state recovered from the series of dynamic simulations described above.

When compared to the results of the static simulation it looks like in the case of the static simulation, the outer side magnets are demagnetized in a similar way as in the dynamic one but the inner side magnet are much more demagnetized when simulated dynamically than in the static approach. This is due to the fact that the process of putting together the different blocks ignites a demagnetization process in the inner side magnets that cannot be caught by the static simulation. Indeed, in the static simulation, an equilibrium is achieved between the field of the inner and outer side magnets, which prevent both of them from demagnetizing deeply.

5.2.5 Testing and measurement

To demonstrate the demagnetization phenomenon and compare it with the measurements, a prototype was constructed. It consisted of three poles and the stator yoke on top of the magnets as shown in Fig. 5.12. Measurements of the magnetic flux density in the air gap region above the central pole next to the yoke were carried out. A flux meter AlphaLab Gaussmeter Model GM-2 with accuracy 1% of DC reading was used. The measuring probe was moved in steps of 20 mm.

The comparison is made on the basis of the results from Fig. 5.17, Fig. 5.18 and Fig.5.22. Only the flux density over the middle pole is compared to reduce the effect of the boundaries on the result and thus provide reasonable comparison. Fig. 5.23 shows such a comparison, where curve 1 corresponds to measured values, curve 2 is calculated without taking into account the demagnetization, curve 3 is calculated with a static simulation accounting for

the demagnetization, and curve 4 is calculated with the dynamic simulation approach.

The computed maximum value of the magnetic flux density in the air gap without taking into account demagnetization was 0.32 T, whereas the measurements showed that value to be 0.29 T, i.e., 10% less than expected. When taking into account the demagnetization in a static approach, the difference between the measured and the computed value was only 3.3 % and with the dynamic approach the difference dropped to 1,7 %. In fact, this latter figure falls within the measurements accuracy.

The Demagnetization due to the temperatures was also investigated through computations. As the remanence magnetic flux density B_r of ferrite magnets rises when the temperature drops and the coercitive magnetic field strength H_c decreases, it can be assumed that the highest demagnetization takes place inside the magnets at low temperatures. FE analysis was conducted in an extreme situation as it was assumed that the temperature of the magnets will drop to -40 °C. To simplify the computations, it was assumed that the demagnetization has not occurred beforehand i.e. at the construction process. The results of the FE computation are shown in Fig. 5.24. It can be seen that the demagnetization arises at the top half of the side magnets. The coordinates of the magnet load point in that area was H_m = -188 kA/m and B_m = 0.06 T. At that value it was found that in the demagnetized part the new B_r value of the magnet was 0.31 T which means 26% of de-magnetization. There would have not been any demagnetization at 20 °C with the same construction, if the magnets would have been assembled correctly. The de-magnetization due to the drop of temperature must be taken into account in the future works at all temperature levels.

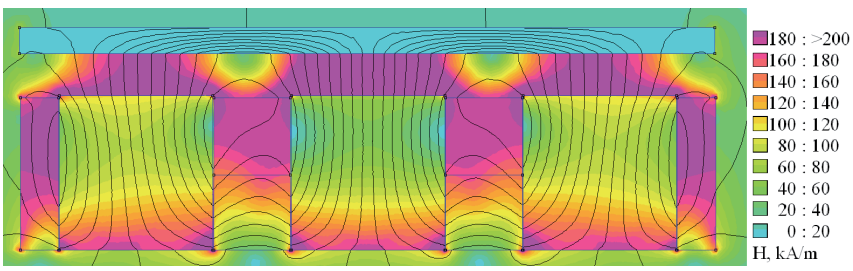

Figure 5.24. Results of the FE analysis at -40 °C

5.2.6 Validation

In this chapter the possibility of using ferrite magnets in electrical machines set up in a Halbach array was investigated. It was found that using Halbach array helps to increase the value of magnetic flux density in the air gap but this benefit has its own risk. Firstly it was found that one of the problems is the low coercitive filed strength of ferrite magnets, due to which there is a high risk of demagnetizing the magnets. The biggest risk involves the side magnets of the Halbach array because their working point is very near the demagnetization point. Demagnetization of the magnets occurs due to a number of reasons. From

these reasons the thesis describes the ones that are relevant in the construction process.

It was found that the construction of magnets plays a big role in further construction process. From our experience we can say that the smallest risk of demagnetization occurs when the rotor is built first with middle magnets. After this is done, the rotor and stator can be put together and only then the side magnets can be put to their place around the middle magnets.

As the demagnetization curve of ferrite magnets depends highly on the temperature, possible problems that can occur in an electrical machine due to temperature were also investigated. It was found that when machine calculations are performed using normal temperature or working temperature, not considering outer magnetic field that occurs due to the load, there is a low risk of demagnetizing the magnets. When it was investigated what happens when the machine is left to freezing temperature, it was found that partial demagnetization of side magnets will appear. This happens due to increasing remanence and falling coercivity of the demagnetization curve of ferrite magnets when the temperature was decreasing. The result of which is that the working point of the side magnets is in the area of strong demagnetization.

Although this chapter describes only one of the possible solutions for Halbach array and only ferrite magnets were investigated, it can be assumed that using a different layout for Halbach array can lead to similar problems. This means that already during the design process of the machine it is necessary to consider not only the behaviour of the machine during exploitation but also investigate the problems that arise during the assembly process and due to environmental issues especially in arctic regions where the temperature can fall to very low values.

6 Conclusion and Future Works

In this study, the first goal has been the development of the design method for preliminary design of slow speed slotless permanent magnet generator for windmills. The design tool demonstrates the generator preliminary parameterization for windmills. Analytic tool is developed to calculate the generator parameters where the developed computation procedure is described. A thermal model for the studied generator is developed and included in the design tool. To validate the low cogging torque on this type of generator calculation are presented.

To verify the design tool and to get manufacturing expertise a prototype machine was constructed. Several measurements were carried out on the prototype machine and compared with the design results. Despite some errors to do manufacturing process in the generator coils causing some distortion in the EMF and the generator line voltage, the measurement results, generally, agree well with the calculation results. Thus the design tool can be considered to be suitable for calculating and predicting the output characteristics of the slow speed slotless permanent magnet generator.

To do the generator coil design future researcher should include further study on the coil misplacement. In the slotless generator design there is possibility to misplace the coils witch result in difference in generator line voltages. There should be carried out more tests to clarify this effect and mathematic model should be developed which could be implemented to the design model.

The generator thermal testing was carried out with passive cooling, but the generator is designed to work with active air cooling. As the generator temperature for active cooling was achieved approximately from testing than in future study the test bench has to upgrade and further measurements have to be carried out.

The further goal was to study the possibility of changing the NdFeB permanent magnets on the generator to the lower grade magnets. The study should that changing to the SmCo magnets there is not needed to make changes in the designed generator stator. Adding the ferrite magnets is more complicated as there is difficult to achieve needed magnetic flux density. To raise the magnetic flux density in the air gap with ferrite magnets there was presented a solution of using the magnets in Halbach array. Future work should include the constructing of the generator rotor with lower grade magnets. This would allow carrying out testing and comparisons between the generators with different type of magnets.

As the studied generator is with large diameter compared to the length of machine the study of possible air gap eccentricities were presented in the work. In the work there were presented the possible eccentricities which can accrue on this type of machine and how to take them into account on the design process. Further study should include the testing the generator with eccentricity.

The study was carried out of the permanent magnet demagnetization in the generator resulting of the manufacturing proses. With the study it was proved

that there is high risk to demagnetize the permanent magnets during the construction of Halbach array. Two calculation method were presented for calculating the demagnetization, the static calculation shows the permanent magnet demagnetization and can be used for preliminary study but it is not accurate as the dynamic demagnetization calculation. The dynamic demagnetization calculation proses were presented and it should good correlation with measured values but it is time consuming compared to the static demagnetization calculation. As the demagnetization was studied on the ferrite permanent magnets the future work should be included the demagnetization study with different type of permanent magnets.

As a conclusion, the slow speed slotless permanent magnet generator is shown to be attractive solution for considering it to be implemented into windmills. From the study it was presented the this type of generator is cogging torque free, it is simpler construction and lighter weight compared to the conventional wind generator which makes the slow speed slotless permanent magnet generator competitive type generator in windmills. The drawback of this type of generator can be considered the amount of permanent magnets needed compared to the conventional generator.

References

[1] K. Toom, „Tuulikute väljundvõimsuste balansseerimise võimalusi“ Ph.D. dissertation, Estonian University of Life Science, 2012.

[2] K. Janson, A. Kallaste, „Energeetika“ Horisont 6, 2012.

[3] „Small Wind World Report 2013“ World Wind Energy Association, 2013.

[4] http://www.tuuleenergia.ee/vaiketuulikud/

[5] L. H. Hansen, L. Helle, F. Blaabjerg, E Ritshie, S. Munk-nielsen, H. Binder, P. Sörensen, B. Bak-Jensen, „Conceptual Survey of Generators and Power Electronics for Wind Turbines“ Publicaion R-1205, Report of Risö National Laboratory, Roskilde, Denmark. 2001.

[6] M. R. Dubois. „Review of Electromechanical Conversion in Wind Turbines“ Report EPP00.R03, Technical University of Delfi. Delfi, 2000.

[7] P. Lampola, „Directly Driven, Low-Speed Permanent-Magnet Generators for Wind Power Application“ Ph.D. Dissertation, Helsinki University of Technology, Laboratory of Electromechanics. Espo. 2000.

[8] A. Kilk, “Paljupooluseline püsimagnetitega sünkroongeneraator tuule-agregaatidel” Ph.D. dissertation, Tallinna Tehnikaülikool, Tallinn, 2008.

[9] D. McMillan, G. W. Ault, “Techno-economic comparison of operational aspects for direct drive and gearbox-driven wind turbines,” IEEE Trans. Energy Convers., vol. 25, no. 1, pp 191-198, Mar. 2010.

[10] H. Polinder, F. F. A. van der Pijl, G. J. de Vilder, P. J. Tavner, “Comparison of direct-drive and geared generator concepts for wind turbines,” IEEE Trans. Energy Convers., vol. 21, no. 3, pp 725-733, Sep. 2006.

[11] D. Yao, R. G. Harley, "Present and future trends in wind turbine generator designs," in IEEE Power Electronics and Machines in Wind Applications, pp. 1-6, 2009.

[12] H. Li, Z. Chen, “Design optimization and evaluation of different wind generator systems,” in Proc. IEEE ICEMS 08 Conf., vol. 2, pp. 2396–2401, Oct. 2008.

[13] M. G Kanabar, S. A. Khaparde, "Evaluation of Rotor Speed Stability Margin of a Constant Speed Wind Turbine Generator," Proceedings of IEEE Power India Conference, pp. 1-6, October 2008.

[14] T. Ackermann, “Wind Power in Power Systems,” John Wiley and Sons Ltd. 2005.

[15] M. R. Dubois, “Review of Electromechanical Conversion in Wind Turbines. Report EPP00.R03”, Technical University of Delfi, pp. 93, 2000.

[16] A. Grauers, “Design of Direct-Driven Permanent-Magnet Generators for Wind Turbines” PhD Dissertation, Technical Report no. 292, Chalmers University of Technology. Göteborg: Chalmers University of Technology, pp. 133, 1996.

[17] M. Henriksen, B. Jensen, "Induction generators for direct-drive wind turbines," in Electric Machines Drives Conference (IEMDC), 2011 IEEE International, pp. 1125 –1130, May 2011.

[18] V. Delli Colli, F. Marignetti, C. Attaianese, "Feasibility of a 10 MW doubly fed induction generator for direct-drive wind turbines," in Proc. IEEE-PES/IAS Conf. Sustainable Alternative Energy, pp. 1–5, 2009.

[19] M. R. J. Dubois, "Optimized Permanent Magnet Generator Topologies for Direct-Drive Wind Turbines." PhD Thesis. Report of the WIND research program. Technical University of Delft, Netherlands. Delft: Technical University of Delft, pp. 235, 2004.

[20] T. F. Chan, L. L. Lai, "An axial-flux permanent magnet synchronous generator for a direct-coupled wind-turbine system," IEEE Trans. Energy Conv., vol. 22, no. 1, pp. 86–94, Jan. 2007.

[21] Y. Chen, P. Pillay, A. Khan, "PM wind generator topologies," IEEE Trans. Industry Appl., vol. 41, no. 6, pp. 1619–1626, Jun. 2005.

[22] A. Parviainen, J. Pyrhönen, and P. Konthanen, "Axial flux permanent magnet generator with concentrated winding for small wind power applications," in Proc. IEEE Int. Conf. Electric Machines Drives, San Antonio, TX, USA, pp. 1187–1191, 2005.

[23] M. A. Khan, P. Pillay, "Design of a PM wind generator, optimised for energy capture over a wide operating range," in Proc. IEMDC, pp. 1501–1506, May 2005.

[24] S.-Y. Jung, H. Jung, S.-C. Hahn, H.-K. Jung, C.-G. Lee, "Optimal design of direct-driven PM wind generator for maximum annual energy production," IEEE Trans.Magn., vol. 44, no. 6, pp. 1062–1065, Jun. 2008.

[25] E. Koutroulis, K. Kalaitzakis, "Design of a maximum power tracking system for wind-energy-conversion applications," IEEE Trans. Ind. Electron., vol. 53, no. 2, pp. 486–494, Apr. 2006.

[26] A. Mirecki, X. Roboam, F. Richardeau, "Comparative study of maximum power strategy in wind turbines," in Proc. IEEE Int. Symp. Ind. Electron., pp. 993–998, 2004.

[27] M. Hsieh, F. Hsu, D. G. Dorrell "Winding Changeover Permanent-Magnet Generators for Renewable Energy Applications" Magnetics, IEEE Transactions on, vol. 48, Issue 11, 2012

[28] J. H. J. Potgieter, M. J. Kamper, "Cogging torque sensitivity in design optimisation of low cost non-overlap winding PM wind generator," in Proc. ICEM, pp. 1–6, 2010.

[29] E. Muljadi, J. Green, "Cogging torque reduction in a permanent magnet wind turbine generator," in Proc. Amer. Soc. Mechanical EngineersWind Energy Symposium, Reno, NV, 2002.

[30] T. Tudorache, L. Melcescu, M. Popescu, "Methods for cogging torque reduction of directly driven PM wind generators," in Proc. Int. Conf.

Optimization of Electric and Electronic Equipment (OPTIM 2010), Moieciu, Romania, 2010.

[31] S. C. Jae, K. Izui, S. Nishiwaki, A. Kawamoto, T. Nomura, “Topology optimization of the stator for minimizing cogging torque of IPM motors,” IEEE Trans. Magn., vol. 47, no. 10, pp. 3024–3027, Oct. 2011.

[32] M. Nagrial, J. Rizk, and A. Hellany, “Design and performance of permanent magnet slotless machines,” in Proc. 18th ICEM, pp. 1–5, Sep. 2008,

[33] A. Looser, T. Baumgartner, J. W. Kolar, C. Zwyssig, "Analysis and Measurement of Three-Dimensional Torque and Forces for Slotless Permanent-Magnet Motors", Industry Applications, IEEE Transactions on, On page(s): 1258 - 1266 Volume: 48, Issue: 4, July-Aug. 2012.

[34] Min-Fu Hsieh, Yu-Han Yeh, “Rotor Eccentricity Effect on Cogging Torque of PM Generators for Small Wind Turbines” Magnetics, IEEE Transactions on, vol. 49, issue 5, pp. 1897 – 1900, 2013.

[35] C. Muller, B. Kalkmann, J. Sontheim, ” A highly innovated transversal flux motor design with integrated inverter” Electric Drives Production Conference (EDPC), 2012 2nd International, pp. 1 – 6, 2012.

[36] E. Spooner, P. Gordon, J.R. Bumby, C. D. French, "Lightweight, Ironless-Stator, PM Generators for Direct-Drive Wind Turbines," IEE Proc. Electr. Power Appl., vol. 152, pp. 17-26, 2005.

[37] Z. Zhang, A. Matveev, R. Nilssen, A. Nysveen, ‘‘Large-Diameter Ironless Permanent Magnet Generator for Offshore Wind Power Application,’’ Proc. of ICEM, France, Sep. 2012.

[38] M. Nagrial, J. Rizk, A. Hellany, "Design and performance of permanent magnet slotless machines", 18th International Conference on Electrical Machines, 2008. ICEM 2008., 6-9 Sept.2008.

[39] A. Tessarolo, F. Luise, P. Raffin, V. Venuti, "Multi-objective design optimization of a surface permanent-magnet slotless alternator for small power wind generation", 2011 International Conference on Clean Electrical Power (ICCEP), pp.371-376, 14-16 June 2011.

[40] P. Kurronen, “Torque Vibration Model of Axial-Flux Surfacemounted Permanent Magnet Synchronous Machine” Ph.D. Dissertation, Lappeenranta University of Technology, 2003.

[41] P. Sekerak, V. Hrabovcova, M. Onufer, L. Kalames, P. Rafajdus, “Synchronous Motors with Different PM Materials” Proceedings of the 9th International Confer-ence – 2012 ELEKTRO, vol. 3, pp. 241-246, 2012.

[42] Material of Magnet Technology Center at Prizztech Ltd.

[43] J. Pyrhönen, J. Nerg, P. Kurronen, J. Puranen, M. Haavisto, “Permanent Magnet Technology in Wind Power Generators.” XIX International Conference on Electrical Machines - ICEM 2010, Rome, pp. 1-6, 2010.

[44] J. Ofori-Tenkorrang, J. H. Lang, "A comparative analysis of torque production in Halbach and conventional surface-mounted permanent-magnet

synchronous motors," in Industry Applications Conference, Thirtieth IAS Annual Meeting, Conference Record of the IEEE, vol.1, pp. 657-663 1995.

[45] Z. Q. Zhu, "Recent Development of Halbach Permanent Magnet Machines and Applications," in Power Conversion Conference, PCC - Nagoya., pp. K-9-K-16, 2007.

[46] Z. Q. Zhu, Z. P. Xia, K. Atallah, G. W. Jewell, and D. Howe, "Novel permanent magnet machines using Halbach cylinders," in Power Electronics and Motion Control Conference Proceedings, IPEMC, The Third International, vol.2, pp. 903-908, 2000.

[47] R. Krishnan, "Permanent Magnets and Machines," in Permanent Magnet Synchronous and Brushless DC Motor Drives, ed: CRC Press, pp. 3-133, 2009.

[48] M. Rosu, J. Saitz, A. Arkkio, “Hysteresis model for finite-element analysis of permanent-magnet demagnetization in a large synchronous motor under a fault condition,” IEEE Trans. Magn., vol. 41, no. 6, pp. 2118–2123, Jun. 2005.

[49] D. Casadei, F. Filippetti, C. Rossi, A. Stefani, "Magnets faults characterization for Permanent Magnet Synchronous Motors," in IEEE International Symposium on Diagnostics for Electric Machines, Power Electronics and Drives, 2009. SDEMPED, pp. 1-6, 2009.

[50] S. Ruoho, J. Kolehmainen, J. Ikaheimo, A. Arkkio, “Interdependence of demagnetization, loading, and temperature rise in a permanent-magnet synchronous motor,” IEEE Trans. Magn., vol. 46, no. 3, pp. 949–953, Mar. 2010.

[51] A. R. Tariq, C. E. Nino-Baron, E. G. Strangas, “Consideration of magnet materials in the design of PMSMs for HEVs application,” in Proc. IEEE Power Energy Society General Meeting, Jul. 24–29, pp. 1–6, 2011.

[52] M. D. Calin, E. Helerea, “Temperature influence on magnetic characteristics on Nd-Fe-B permanent magnets,” in Proc. 7th International Symposium on Advanced Topics in Electrical Engineering (ATEE), Bucharest, Romania, May 12–14, 2011.

[53] O. Winter, C. Kral, E. Schmidt, “Augmented temperature degrading effect of rare earth magnets arranged in segmented Halbach arrays,” in IEEE International Magnetics Conference, (INTERMAG’12), no. 4, May 2012.

[54] T.J Kim, S.M Hwang, W.B Jung, C.U Kim, “Comparison of Dynamic Responses For IPM and SPM Motors by Considering Mechanical and Magnetic Coupling” Magnetics, IEEE, Volume 37, NO. 4., pp. 2818-2820, July 2001.

[55] A. Belahcen, A. Arkkio , “Computation of additional losses due to rotor eccentricity in electrical machines” IET Electric Power Applications, Volume. 4, NO 4, pp. 259-266, 2010.

[56] G. Dorrell, M.-F. Hsieh, Y. Guo, “Unbalanced magnet pull in large brushless rare-earth permanent magnet motors with rotor eccentricity,” IEEE Trans. Magn., vol. 45, no. 10, pp. 4586–4589, Oct. 2009

[57] Y.K. Chin, P. Kanninen, P. Maki-Ontto, R. Sakki, H. Lendenmann, “Phenomenon of Magnetic Force in Permanent Magnet Wind Turbine Generarors” Electrical Machines and Systems, 2009. ICEMS 2009.

[58] B.M. Ebrahimi, J. Faiz and M.J. Roshtkhari, “Static-, Dynamic-, and Mixed-Eccentricity Fault Diagnoses in Permanent-Magnet Synchronous Motors” Industrial Electronics, IEEE proceedings, Volume 56, NO.11. November, 2009.

[59] M, Hajiaghajani, Lei Hao, S.M. Madani, H.A. Toliyat, “A method for detection of eccentricity in permanent magnet machines“ Industry Applications Conference, 2003. 38th IAS Annual Meeting, volume 3, pp. 1833-1838, 2003.

[60] W. le Roux, R.G. Harley,T.G. Habetler, “Detecting Rotor Faults in Low Power Permanent Magnet Synchronous Machines” Power Electronics, IEEE Transactions on, volume 22, issue 1, pp. 322-328, 2007.

[61] D. Bang, H. Polinder, G. Shrestha, J.A. Ferreira, “Promising Direct-Drive Generator System for Large Wind Turbine”, Wind Power to the Grid - EPE Wind Energy Chapter 1st Seminar, 2008. EPE-WECS, pp. 1-10, 2008.

[62] M. Florence, “Permanent-Magnet Synchronous Machines with Non-Overlapping Concentrated Windings for Low-Speed Direct-Drive Applications” Ph.D. Dissertation, KTH, Sweden 2008.

[63] A. Rosin, H. Hõimoja, T. Möller, M. Lehtla, ; , "Residential electricity consumption and loads pattern analysis," Electric Power Quality and Supply Reliability Conference (PQ), 2010 , vol., no. , pp.III-116, 16-18, June 2010.

[64] A. Auvaart, A. Rosin, N. Belonogova, D. Lebedev, "NordPoolSpot price pattern analysis for households energy management," 7th International Conference-Workshop Compatibility and Power Electronics, 2011 , pp. l03-106, June 01 - 03, 2011.

[65] Energy Yearly Statistics 2006, Eurostat statistical books, Luxembourg, 2008.

[66] M. Sathyajith, “ Wind Energy Fundamentals, Resource Analysis and Economics” Springer, Netherland, 2006.

[67] http://www.mathworks.se/help/physmod/powersys/ref/windturbine.html

[68] http://www.sma.de/en/products/wind-energy-inverters.html

[69] http://www.power-one.com/renewable-energy/products/wind/aurora-wind

[70] J. A. Baroudi,V.Dinavahi, A.M.Knight, “Areviewof power converter topologies for wind generators,” in Proc. IEEE Electr. Mach. Drives Int. Conf., vol. 1, pp. 458–465, May 2005.

[71] M. Chinchilla, S. Arnaltes, J. Burgos, “Control of permanent-magnet generators applied to variable-speed wind-energy systems connected to the grid,” IEEE Trans. Energy Convers., vol. 21, no. 1, pp. 130–135, Mar. 2006.

[72] F. Blaabjerg, M. Liserre, and K. Ma, “Power electronics converters for wind turbine system,” in Proc. IEEE ECCE, pp. 281–290, Sep. 2011.

[73] S. Muller, M. Deicke, R. W. DeDoncker, “Doubly fed induction generator systems for wind turbines” IEEE Industry Application Magazine, vol. 8 no. 3, pp. 26-33, May-June 2002.

[74] N. Bianchi, A. Lorenzoni. “Permanent magnet generators for wind power industry: an overall comparison woth traditional generators” International Conference on Oppertunities and Advances in International Electric Power Generation, Durham, pp.49-54, 18-20 March 1996.

[75] A. Kallaste, J. Järvik, A. Kilk, “Permanent magnet axialflux generator with toroidal winding.” In: 5th International Conference "Electric power quality and supply reliability" : conference proceedings : August 23-26, 2006, Viimsi, Estonia: Tallinn: Tallinn University of Technology, 167 - 171, 2006.

[76] J. Pyrhönen, J. Nerg, P. Kurronen, J. Puranen, M. Haavisto, “Permanent Magnet Technology in Wind Power Generators”, XIX International Conference on Electrical Machines - ICEM 2010, Rome, pp. 1-6, 2010.

[77] J. Pyrhonen, T. Jokinen, V. Hrabovcova, “Design of Rotating Electrical Machines” Wiley, 2008.

[78] H. Mõlder, “Vedelmetalli juhitava segamisvõimaluse uurimine alalisvoolu kaarleekahjus” doktoritöö väitekiri, Tallinna Tehnikaülikool, Tallinn, 2012.

[79] N. Chayopitak, D. Taylor, “Performance assessment of air-core linear permanent-magnet synchronous motors”, IEEE Trans. Magn, 44, pp. 2310–2316, 2008.

[80] A. Mohammadpour, A. Gandhi, L. Parsa, “Winding factor calculation for analysis of back EMF waveform in air-core permanent magnet linear synchronous motors” Electric Power Applications, IET, Volume: 6 , Issue: 5, 2012.

[81] J.R. Bumby, E. Spooner, M. Jagiela, “Equivalent Circuit Analysis of Solid-rotor Induction Machines with Reference to Turbocharger Accelerator Applications,” IEE Proceedings Electric Power Applications, vol. 153, issue 1, pp. 31–39, 1 Jan. 2006.

[82] http://www.femm.info/wiki/HomePage

[83] F. Magnussen, C. Sadarangani, “Winding factor on Joule losses of permanent magnet machines with concentrated windings,” in Proc. Electric Machines Drives Conference IEMDC 2003, vol. 1, pp. 333–339, Jun. 2003.

[84] A. Mohammadpour, A. Gandhi, L. Parsa, “Winding factor calculation for analysis of back EMF waveform in air-core permanent magnet linear synchronous motors” Electric Power Applications, IET. Volume: 6 , Issue: 5., pp. 253 – 259, 2012.

[85] Y. Chin “A permanent magnet synchronous motor for an electric vehicle - design analysis” Ph.D. Dissertation, Royal Institute of Technology, Sweden 2004.

[86] T. Li, G. Slemon, “Reduction of Cogging Torque in Permanent Magnet Motors.“ IEEE Transactions on Magnetics, Volume: 24 Issue: 6, pp. 2901 – 2903, Nov. 1988.

[87] A. Parviainen, “Design of axial-flux permanent-magnet low-speed machines and performance comparison between radial-flux and axial-flux machines” Ph.D. Dissertation, Lappeenranta University of Technology, Lappeenranta, Finland, 2005.

[88] F.P. Incropera, D.P. DeWitt, “Fundamentals of Heat and Mass Transfer.” New York: John Wiley&Sons, pp. 886, 1996.

Acknowledgements

I would like to express my appreciation to my supervisors Prof. Anouar Belahcen and Prof. Kuno Janson for their helpfulness and encouragement during the years of my research.

Secondly I would like to express my gratitude to Prof. Ed Spooner for the idea of the thesis topic and advises.

Also I would like to thank my colleagues Toomas Vaimann and Lauri Kütt for giving me relevant and substantial advices regarding to scientific work. Also I am thankful for them for revising and editing the English in my thesis.

Special thanks to the companies My!Wind and Goliath Wind for the support building the prototype generator and for the help in my study.

Also, I would like to express my sincere thanks to all other colleagues from Tallinn University of Technology, Department of Electrical Engineering for their versatile help and support during the years of research.

My sincere thanks go to my family and my friends for their care and motivation, because it was thanks to them that this thesis became possible.

Ants Kallaste

Abstract

Low Speed Permanent Magnet Slotless Generator Development and Implementation for Windmills

Wind generation industry is one of the most rapidly developing industries in the world, which also puts large pressure on the generators used in the windmills. There are a large number of different generator types, because the generators used in wind applications must fulfil a number of design requirements and due to this fact it is difficult to find a universally acceptable and adaptable solution. In recent years permanent magnet machines have found their way into the wind industrial applications and are gaining popularity due to their high power density and higher efficiency compared to traditional machines. In the thesis there is taken under investigation one possible permanent magnet generator solution which would fulfil the requirements for the windmill

This thesis is devoted to design and development of new type of low speed permanent magnet slotless generator for windmills. Emphasis has been placed on determining the design parameters from the windmill for the generator. The model developed in the thesis incorporated the preliminary parameterization of the generator, the generator electromagnetic design and the thermal design of the generator.

A prototype machine with rated 5 kW output power at 230 rpm has been designed and constructed to verify the results obtained from the developed model. The testing was concentrated on validating the generator output characteristics as well as the generator thermal behaviour.

Study has been made with possibility of changing the NdFeB permanent magnets on the generator to the lower grade magnets. Two types of lower grades magnets are presented SmCo and Ferrite. With ferrite magnets it is proposed to use the magnets in a Halbach array to achieve higher flux density in the air gap.

The slotless low-speed permanent magnet wind generator design has been investigated with different types of eccentricity taken into account. The causes for different types of air gap eccentricities have been analysed including static, dynamic, elliptic and mixed eccentricities. Analytical equations for calculating the dimensions of the air gap eccentricities have been developed and analysis of the consequences of the eccentricities on the operation of the machine have been presented.

The study is carried out for the permanent magnet demagnetization in the generator resulting from the manufacturing process too. This study was made based on the magnets used in Halbach array as they present the highest risk to demagnetize the magnets. The study presents the demagnetization calculation methods with static and dynamic approach.

Kokkuvõte

Aeglasekäigulise uurdevaba püsimagnetgeneraatori väljatöötamine ja rakendamine tuulikutes

Tuuleenergeetikatööstus on üks kiiremini arenevaid tööstusharusid maailmas. See tekitab nõudluse tuulikutes kasutatavate generaatorite järele. Sobiva generaatori valimine on tulenevalt tuuliku eripärast keerukas. Seetõttu on ka tuulikutes kasutatavate generaatoritüüpide arv suur. Üha enam populaarsust on viimastel aastatel kogunud püsimagnetgeneraatorite kasutamine. Võrreldes traditsiooniliste generaatoritega pakuvad seda tüüpi generaatorid suuremat energiatihedust ja kasutegurit. Käesolevas töös ongi võetud uurimise alla püsimagnetitega tuulegeneraatorid.

Doktoritöö üheks peamiseks eesmärgiks oli uut tüüpi aeglasekäigulise uurdevaba püsimagnetgeneraatori väljatöötamine. Lähtuti sellest, et generaator peab olema traditsioonilistest generaatoritest kergem ja kleepumismomendivaba. On tehtud generaatori tüübi valik vastavalt püstitatud eesmärgile ja välja töötatud arvutusmetoodika seda tüüpi generaatorite jaoks. Arvutusmetoodikas käsitletakse nii generaatori elektromagnetilist arvutust kui ka soojuslike parameetrite määramist. Töös on pakutud ka meetodid generaatori projekteerimise lähteparameetrite määramiseks vastavalt valitud tuuleturbiinile ning etteantud generaatori väljundpingele.

Arvutusmetoodika paikapidavuse kontrollimiseks projekteeriti ning ehitati valmis 5 kW võimsusega katsegeneraator, mille nimipöörlemiskiirus on 230 p/min. Sellel katsemasinal viidi läbi mitmeid erinevaid katsetusi. Peamiselt keskenduti generaatori väljundparameetrite määramisele ning generaatori soojuslike protsesside uurimisele.

Töös käsitletud generaatoril kasutati NdFeB püsimagneteid. Lisaks neile magnetitele uuriti ka madalama energiatihedusega magnetite kasutamise võimalust selles generaatoris. Uurimise alla võeti kaks erinevat püsimagnetmaterjali – SmCo magnetid ja ferriitmagnetid. SmCo magnetid on võrreldes NdFeB magnetitega ainult veidi väiksema energiatihedusega ning nende rakendamisel kasutati samasugust magnetite paigutust kui NdFeB magnetite puhul. Ferriitmagnetite energiatihedus on aga oluliselt väiksem kui NdFeB magnetitel. Nende juures kasutati Halbach'i jadapaigutust. Töös leiti, et see lahendus võimaldab ferriitmagnetite abil saada piisava väärtusega magnetvootiheduse õhupilus. Sellise lahenduse korral on ka ferriitmagnetite rakendamine generaatoris otstarbekas.

Töös on uuritud ka õhupilu ebaühtluse mõju uurdevabale aeglasekäigulisele püsimagnet-tuulegeneraatorile. On kirjeldatud õhupilu ebaühtluse võimalikke tekkepõhjusi, milleks on kas staatiline, elliptiline või dünaamiline ekstsentrilisus või ka kombinatsioon nendest ekstsentrilisustest. On näidatud, kuidas õhupilu ebaühtlust leida analüütiliselt. On läbi viidud ka ekstsentrilisusega kaasneda võivate probleemide analüüs.

Töös uuriti ka püsimagnetite demagneetumist generaatoris. Demagneetumine võib olla tingitud muu hulgas ka vigadest generaatori konstrueerimisel.

Peamiselt uuriti püsimagnetite demagneetumist magnetite Halbach'i jadapaigutuse korral. Töös pakutakse välja kaks erinevat moodust demagneetumise uurimiseks. Esiteks staatiline arvutus, mis on oma olemuselt püsimagnetite demagneetumise uurimise traditsiooniline viis. Teiseks pakutakse välja dünaamiline arvutusmudel, mis annab võrreldes staatilise arvutusega täpsema tulemuse. Sel juhul on arvutusprotsess aga oluliselt aeganõudvam.

Author's publications

[A1] Tuttelberg, K.; Vaimann, T.; **Kallaste, A**. (2013). Analysis of a slow-speed slotless permanent magnet synchronous generator. In: Proceedings of the 4th International Youth Conference on Energy: IYCE2013, 6-8 June, Siofok, Hungary. IEEE, 2013, ID - 71.

[A2] **Kallaste, A**.; Vaimann, T.; Janson, K.; Bolgov, V. (2013). Components selection of local power supply system for sparsely populated areas. In: Proceedings of the 14th International Scientific Conference Electric Power Engineering 2013: EPE 2013, May 28-30, 2013, Kouty nad Desnou, Czech Republic. (Toim.) Rusek, S.; Goňo, R. IEEE, 2013, 181 - 186.

[A3] Vaimann, T.; Janson, K.; Bolgov, V.; **Kallaste, A**. (2013). Analysis of off-grid hybrid power supply for sparsely populated areas. In: Proceedings of the 14th International Scientific Conference Electric Power Engineering 2013: EPE 2013, May 28-30, 2013, Kouty nad Desnou, Czech Republic. (Toim.) Rusek, S.; Goňo, R.. IEEE, 2013, 175 - 179.

[A4] Janson, K.; **Kallaste, A**.; Bolgov, V. (2013). Energeetika otsapidi üksnes taastuvenergia küljes. Horisont, 2, 31 - 36.

[A5] Lindh, P.; Vaimann, T.; **Kallaste, A**.; Pyrhönen, J.; Vinnikov, D.; Naumanen, V. (2013). Influence of slot wedge material on permanent magnet losses in a traction motor with tooth coil windings. International Journal of Applied Electromagnetics and Mechanics, 42(2), 227 - 236.

[A6] Vaimann, T.; **Kallaste, A**.; Kilk, A. (2012). Pöörlevate elektrimasinate diagnostika staatorisignaalide analüüsi meetodil. In: TEUK XIV: Taastuvate energiaallikate uurimine ja kasutamine - neljateistkümnenda konverentsi kogumik: TEUK XIV: Taastuvate energiaallikate uurimine ja kasutamine, Tartu, 8. november 2012. Tartu: Eesti Maaülikool, 2012, 78 - 87.

[A7] **Kallaste, A**.; Vaimann, T.; Pabut, O. (2012). Aeglasekäiguline otsetoimeline püsimagnetgeneraator tuuleagregaatidele. In: TEUK XIV: Taastuvate energiaallikate uurimine ja kasutamine - neljateistkümnenda konverentsi kogumik: TEUK XIV: Taastuvate energiaallikate uurimine ja kasutamine, Tartu, 8. november 2012. Tartu: Eesti Maaülikool, 2012, 68 - 77.

[A8] Shklovski, J.; Janson, K.; **Kallaste, A**. (2012). Load-resonant converter with changing resonant tank topology for welding applications. In: IECON 2012 : 38th Annual Conference of the IEEE Industrial Electronics Society, 25–28 October 2012, Montreal, Canada : conference proceedings: IEEE, 2012, 518 - 524.

[A9] **Kallaste, A**.; Belachen, A.; Kilk, A.; Vaimann, T. (2012). Analysis of the Eccentricity in a Low-Speed Slotless Permanent-Magnet Wind Generator. In: Proceedings of 8th International Conference 2012 Electric Power Quality and Supply Reliability: 2012 Electric Power Quality and Supply Reliability, Tartu, June 11 - 13, 2012. (Toim.) Sakkos, T.. IEEE, 2012, 47 - 52.

[A10] **Kallaste, A**.; Kilk, A.; Belahcen, A.; Vaimann, T.; Janson, K. (2012). Demagnetization in Permanent Magnet Slotless Generator Using Halbach Array. In: Proceedings of the 13th International Scientific Conference Electric Power Engineering 2012: EPE 2012, May 23-25, 2012, Brno, Czech Republic. Brno: IEEE, 2012, 1053 - 1057.

[A11] Niitsoo, J.; Taklaja, P.; Kütt, L.; Niilo, H.; **Kallaste, A**.; Mõlder, H.; Vaimann, T. (2012). Keskkonnamõjust hoolimata on põlevkivielekter möödapääsmatu.

[A12] Vaimann, T.; **Kallaste, A**.; Kilk, A. (2012). Using Clarke vector approach for stator current and voltage analysis on induction motors with broken rotor bars. Electronics and Electrical Engineering, 123(7), 17 - 20.

[A13] Vaimann, T.; **Kallaste, A**. (2012). Condition Monitoring of Electrical Machines. In: 11th International Symposium "Topical Problems in the Field of Electrical and Power Engineering" and "Doctoral School of Energy and Geotechnology II": (Toim.) Zakis, J.. Tallinn: Elektriajam, 2012, 209 - 212.

[A14] **Kallaste, A**.; Vaimann, T.; Pabut, O. (2012). Slow-Speed Ring-Shaped Permanent Magnet Generator for Wind Applications. In: 11th International Symposium "Topical Problems in the Field of Electrical and Power Engineering" and "Doctoral School of Energy and Geotechnology II": (Toim.) Zakis, J.. Tallinn: Elektriajam, 2012, 66 - 69.

[A15] Vaimann, T.; **Kallaste, A**.; Kilk, A. (2011). Sensorless Detection of Induction Motor Rotor Faults Using the Clarke Vector Approach. Scientific Journal of Riga Technical University. Power and Electrical Engineering, 29, 43 - 48.

[A16] Vaimann, T.; **Kallaste, A**.; Kilk, A. (2011). Overview of Sensorless Diagnostic Possibilities of Induction Motors with Broken Rotor Bars. In: Proceedings of the 12th International Scientific Conference Electric Power Engineering 2011, Kouty nad Desnou, Czech Republic, May 17-19, 2011: IEEE, 2011, 183 - 186.

[A17] Vaimann, T; **Kallaste, A**; Kilk, A. (2011). Using analysis of stator current for squirrel-cage induction motor rotor faults diagnostics. In: Proceedings of the 6th International Conference on Electrical and Control Technologies ECT-2011, May 5-6, 2011, Kaunas, Lithuania:

(Toim.) Navickas, A; Sauhats, A; Virbalis, A; Ažubalis, M; Galvanauskas, V; Brazauskas, K; Jonaitis, A. Kaunas: Kaunas Technologija, 2011, 245 - 251.

[A18] Vaimann, T.; **Kallaste, A**. (2011). Detection of broken rotor bars in three-phase squirrel-cage induction motor using fast Fourier transform. In: 10th International Symposium "Topical Problems in the Field of Electrical and Power Engineering" and "Doctoral School of Energy and Geotechnology II", Pärnu, Estonia, January 10 - 15, 2011: (Toim.) Lahtmets, R.. Tallinn: Eesti Moritz Hermann Jacobi Selts, 2011, 52 - 56.

[A19] Lehtla, M.; Kõivastik, I.; Möller, T.; **Kallaste, A**.; Rosin, A. (2010). Design of Renewable Micro Generation Monitoring and Control Application. In: PQ2010: 7th International Conference 2010 Electric Power Quality and Supply Reliability, Conference Proceedings: 7th International Conference 2010 Electric Power Quality and Supply Reliability, Kuressaare, Estonia, June 16-18, 2010. Tallinn: IEEE, 2010, 105 - 110.

[A20] Kilk, A; **Kallaste, A** (2008). Multipole Surface-Mounted Permanent Magnet Synchronous Generators for Wind Application. In: PQ 2008. The 6th International Conference "2008 Power Quality and Supply Reliability". Conference Proceedings: The 6th International Conference "2008 Power Quality and Supply Reliability" (PQ 2008). Pärnu, 27-29 August 2008. Tallinn: Tallinn University of Technology, 2008, 235 - 240.

[A21] **Kallaste, A**.; Kütt, L.; Bolgov, V.; Janson, K. (2008). Reactive Power Compensation for Spot Welding Machine Using Thyristor Switched Capacitor. In: PQ 2008. The 6th International Conference "2008 Power Quality and Supply Reliability". Conference Proceedings: The 6th International Conference "2008 Power Quality and Supply Reliability" (PQ 2008). Pärnu, 27-29 August 2008. Tallinn: Tallinn University of Technology, 2008, 241 - 245.

[A22] Janson, K.; Bolgov, V.; Kütt, L.; **Kallaste, A**.; Mõlder, H. (2008). Passive Shaping of Line Current Waveform by Converter with Alternating of Parallel and Series Resonance in AC-DC Switch Mode Power Supplies. In: ICECS 2008. The 15th IEEE International Conference On Electronics, Circuits and Systems. Conference Guide.: The 15th IEEE International Conference On Electronics, Circuits and Systems (ICECS 2008), The Westin Dragonara Resort, Malta. (Toim.) IEEE CAS Society. IEEE, 2008, 77 - 80.

[A23] Janson, K.; Bolgov, V.; Kütt, L.; **Kallaste, A**.; Mõlder, H. (2008). New Practical Approach to Input Current Shaping in AC-DC Power Converters. In: Proceedings of 13th International Power Electronics and Motion Control Conference EPE-PEMC 2008: 13th International Power

Electronics and Motion Control Conference EPE-PEMC 2008, 1-3 September, 2008, Poznan, Poland. Poland: IEEE, 2008, 154 - 158.

[A24] **Kallaste, A**.; Kilk, A. (2007). Permanent magnet axial-flux generator with toroidal winding. In: 4th International Symposium "Topical problems of education in the field of electrical and power engineering". Doctoral school of energy and geotechnology. [Proceedings volume 1] : Kuressaare, Estonia, January 15-20, 2007: 4th International Symposium "Topical problems of education in the field of electrical and power engineering". 15.-20.01.2007, Kuressaare. Tallinn: Tallinn University of Technology, Faculty of Power Engineering; Elektriajam, 2007, 186 - 189.

[A25] **Kallaste, A**.; Järvik, J.; Kilk, A. (2006). Permanent magnet axialflux generator with toroidal winding. In: 5th International Conference "Electric power quality and supply reliability" : conference proceedings : August 23-26, 2006, Viimsi, Estonia: Tallinn: Tallinn University of Technology, 2006, 167 - 171.

[A26] Järvik, J.; **Kallaste, A**.; Kilk, A. (2005). Permanent magnet wind generator with toroidal winding. In: Proc. of the III International Scientific Symposium Elektroenergetika 2005, Stara Lesna, Slovak Republic: III International Scientific Symposium Elektroenergetika 2005. 21.-23. september 2005, Stara Lesna (Slovak Republik). 2005, 11.

Curriculum Vitae

1. Personal data

   Name: Ants Kallaste
   Date and place of birth: 06.11.1980
   E-mail address: ants.kallaste@ttu.ee

2. Education

Educational institution	Graduation year	Education (field of study/degree)
Tallinn University of Technology	2006	Electrical Drives and Power Electronics, Master of Science
Tallinn University of Technology	2004	Electrical Drives and Power Electronics, Bachelor of Science
Pärnu Koidula Gymnasium	1999	Secondary education
Are Elementary School	1996	Basic education

3. Language competence/skills (fluent, average, basic skills)

Language	Level
Estonian	Fluent
English	Fluent
Russian	basic

4. Special courses

Period	Educational or other organisation
2006-2013	Tallinn University of Technology, Estonia
2012	Aalto University, Finland
2011	Lappeenranta University of Technology, Finland
2010	Lappeenranta University of Technology, Finland

5. Professional employment

Period	Organisation	Position
2011 - 2012	Goliath Wind OÜ	Electrical engineer
2007 - …	Tallinn University of Technology	Researcher
2007 - 2011	OÜ Energiatehnika	Engineer
2006 - 2007	Tallinn University of Technology	Assistant to Director
2004 - 2006	Tallinn University of Technology	Engineer
2001 - 2002	Metro Ehituskonsultandid OÜ	Draughtsman
2000 - 2001	Suike Pärivere tõuhobuse kasvatus OÜ	Computer administrator

6. Scientific work

- Design and Optimization Methodology for Electrical Motor-Drives
- Design of permanent magnet synchronous generators
- Development of equipment for specific purpose
- Energy saving and sustainable electrical power engineering
- Generator
- Minimization of the non-active power in converters using a virtual time-variable matching transformer, loss free resistor or loss free gyrator
- New Smart Grid Technology and its Applications in Estonian Power System
- Optimization of the functioning of the Energy System to balance changeable loads
- Permanent magnets for sustainable energy application (MagMat).
- Power compensator for spot welding machine
- Research and adjustment of a drive
- Synthesis of the power electronic converters with improved power quality

- Welding apparatus with alternating resonant converter
- Member of the organizing committee of an international scientific conference PQ2006, PQ2008, PQ2010 and PQ2012

7. Supervisions

- Maanus Roosmann „Püsimagnetite mõõtmismetoodikate uurimine“ master of science thesis, Tallinn University of Technology, 2013
- Kaur Tutelberg „Aeglasekäigulise püsimagnetergutusega sünkroon-generaatori elektriliste parameetrite analüüs katsete ja matemaatilise modelleerimise alusel“ bachelor of science thesis, Tallinn University of Technology, 2012
- Kristiina Vilsaar „Generaator velotrenažöörile schwinn spinner comp“ master of science thesis, Tallinn University of Technology, 2009

Elulookirjeldus

8. Isikuandmed

Ees- ja perekonnanimi: Ants Kallaste
Sünniaeg ja -koht: 06.11.1980, Pärnu
Kodakondsus: Eesti
E-posti aadress: ants.kallaste@ttu.ee

9. Hariduskäik

Õppeasutus (nimetus lõpetamise ajal)	Lõpetamise aeg	Haridus (eriala/kraad)
Tallinna Tehnikaülikool	2006	Elektriajamid ja jõuelektroonika, Tehnikateaduste magistri kraad
Tallinna Tehnikaülikool	2004	Elektriajamid ja jõuelektroonika, Tehnikateaduste bakalaureuse kraad
Koidula Gümnaasium	1999	Keskharidus
Are Põhikool	1996	Põhiharidus

10. Keelteoskus (alg-, kesk- või kõrgtase)

Keel	Tase
Eesti keel	Kõrgtase
Inglise keel	Kõrgtase
Vene keel	Algtase

11. Täiendusõpe

Õppimise aeg	Täiendusõppe korraldaja nimetus
2006-2013	Tallinna Tehnikaülikool, Eesti
2012	Aalto ülikool, Soome
2011	Lappeenranta ülikool, Soome
2010	Lappeenranta ülikool, Soome

12. Teenistuskäik

Töötamise aeg	Tööandja nimetus	Ametikoht
2011 - 2012	Goliath Wind OÜ	Elektriinsener
2007 - …	Tallinna Tehnikaülikool	Teadur
2007 - 2011	OÜ Energiatehnika	Insener
2006 - 2007	Tallinna Tehnikaülikool	Direktori abi
2004 - 2006	Tallinna Tehnikaülikool	Insener
2001 - 2002	Metro Ehituskonsultandid OÜ	Joonestaja
2000 - 2001	Suike Pärivere tõuhobuse kasvatus OÜ	Administraator

13. Teadustegevus

- Ajami uuring ja seadistamine
- Elektrimootorajamite projekteerimis- ja optimeerimismetodoloogia
- Energiasüsteemi talitluse optimeerimine muutuvkoormuste tasakaalustamiseks Eriotstarbeliste seadeldiste väljatöötamine
- Muundurite mitteaktiivvõimsuse minimeerimine muutuvate pingenivoode vahelise virtuaaltrafo, kaovaba resistori või kaovaba güraatori realisatsiooni abil
- Nutikate elektrivõrkude (smart grid) uus tehnoloogia ja võimalikud rakendused Eesti elektrisüsteemis
- Parendatud energiakvaliteedi ning kasuteguriga võimsuselektroon-muundurite süntees harmooniliste vahelise energiavahetuse optimeeri-mise ja mitmefunktsionaalsete korrektsioonielementide kasutamisega
- Permanent magnets for sustainable energy application (MagMat).
- Punktkeevitusaparaadi reaktiivvõimsuse kompensaator
- Püsimagnetgeneraatori arvutusliku mudeli analüüs ja täiustamine
- Püsimagnetitega sünkroongeneraatorite väljatöötamine
- Säästev ja jätkusuutlik elektroenergeetika
- Vahelduvresonantsmuunduriga keevitusaparaat
- Korralduskomitee liige konverentsidel PQ2006, PQ2008, PQ2010 ja PQ2012

14. Juhendamised

- Maanus Roosmann „Püsimagnetite mõõtmismetoodikate uurimine“ magistritöö, Tallinna Tehnikaülikool, 2013
- Kaur Tutelberg „Aeglasekäigulise püsimagnetergutusega sünkroon-generaatori elektriliste parameetrite analüüs katsete ja matemaatilise modelleerimise alusel“ bakalaureusetöö, Tallinna Tehnikaülikool, 2012
- Kristiina Vilsaar „Generaator velotrenažöörile schwinn spinner comp“ magistritöö, Tallinna Tehnikaülikool, 2009

DISSERTATIONS DEFENDED AT TALLINN UNIVERSITY OF TECHNOLOGY ON *POWER ENGINEERING, ELECTRICAL ENGINEERING, MINING ENGINEERING*

1. **Jaan Tehver**. Boiling on Porous Surface. 1992.
2. Salastatud.
3. **Endel Risthein.** Electricity Supply of Industrial Plants. 1993.
4. **Tõnu Trump**. Some New Aspects of Digital Filtering. 1993.
5. **Vello Sarv.** Synthesis and Design of Power Converters with Reduced Distortions Using Optimal Energy Exchange Control. 1994.
6. **Ivan Klevtsov**. Strained Condition Diagnosis and Fatigue Life Prediction for Metals under Cyclic Temperature Oscillations. 1994.
7. **Ants Meister**. Some Phase-Sensitive and Spectral Methods in Biomedical Engineering. 1994.
8. **Mati Meldorf**. Steady-State Monitoring of Power System. 1995.
9. **Jüri-Rivaldo Pastarus**. Large Cavern Stability in the Maardu Granite Deposit. 1996.
10. **Enn Velmre**. Modeling and Simulation of Bipolar Semiconductor Devices. 1996.
11. **Kalju Meigas**. Coherent Photodetection with a Laser. 1997.
12. **Andres Udal**. Development of Numerical Semiconductor Device Models and Their Application in Device Theory and Design. 1998.
13. **Kuno Janson**. Paralleel- ja järjestikresonantsi parameetrilise vaheldumisega võrgusageduslik resonantsmuundur ja tema rakendamine. 2001.
14. **Jüri Joller**. Research and Development of Energy Saving Traction Drives for Trams. 2001.
15. **Ingo Valgma**. Geographical Information System for Oil Shale Mining – MGIS. 2002.
16. **Raik Jansikene**. Research, Design and Application of Magnetohydrodynamical (MHD) Devices for Automation of Casting Industry. 2003.
17. **Oleg Nikitin**. Optimization of the Room-and-Pillar Mining Technology for Oil-Shale Mines. 2003.
18. **Viktor Bolgov**. Load Current Stabilization and Suppression of Flicker in AC Arc Furnace Power Supply by Series-Connected Saturable Reactor. 2004.
19. **Raine Pajo**. Power System Stability Monitoring – an Approach of Electrical Load Modelling. 2004.
20. **Jelena Shuvalova**. Optimal Approximation of Input-Output Characteristics of Power Units and Plants. 2004.
21. **Nikolai Dorovatovski**. Thermographic Diagnostics of Electrical Equipment of Eesti Energia Ltd. 2004.

22. **Katrin Erg**. Groundwater Sulphate Content Changes in Estonian Underground Oil Shale Mines. 2005.
23. **Argo Rosin**. Control, Supervision and Operation Diagnostics of Light Rail Electric Transport. 2005.
24. **Dmitri Vinnikov**. Research, Design and Implementation of Auxiliary Power Supplies for the Light Rail Vehicles. 2005.
25. **Madis Lehtla**. Microprocessor Control Systems of Light Rail Vehicle Traction Drives. 2006.
26. **Jevgeni Šklovski**. LC Circuit with Parallel and Series Resonance Alternation in Switch-Mode Converters. 2007.
27. **Sten Suuroja**. Comparative Morphological Analysis of the Early Paleozoic Marine Impact Structures Kärdla and Neugrund, Estonia. 2007.
28. **Sergei Sabanov**. Risk Assessment Methods in Estonian Oil Shale Mining Industry. 2008.
29. **Vitali Boiko**. Development and Research of the Traction Asynchronous Multimotor Drive. 2008.
30. **Tauno Tammeoja**. Economic Model of Oil Shale Flows and Cost. 2008.
31. **Jelena Armas**. Quality Criterion of road Lighting Measurement and Exploring. 2008.
32. **Olavi Tammemäe**. Basics for Geotechnical Engineering Explorations Considering Needed Legal Changes. 2008.
33. **Mart Landsberg**. Long-Term Capacity Planning and Feasibility of Nuclear Power in Estonia under Certain Conditions. 2008.
34. **Hardi Torn**. Engineering-Geological Modelling of the Sillamäe Radioactive Tailings Pond Area. 2008.
35. **Aleksander Kilk**. Paljupooluseline püsimagnetitega sünkroongeneraator tuuleagregaatidele. 2008.
36. **Olga Ruban**. Analysis and Development of the PLC Control System with the Distributed I/Os. 2008.
37. **Jako Kilter**. Monitoring of Electrical Distribution Network Operation. 2009.
38. **Ivo Palu**. Impact of Wind Parks on Power System Containing Thermal Power Plants. 2009.
39. **Hannes Agabus**. Large-Scale Integration of Wind Energy into the Power System Considering the Uncertainty Information. 2009.
40. **Kalle Kilk**. Variations of Power Demand and Wind Power Generation and Their Influence to the Operation of Power Systems. 2009.
41. **Indrek Roasto**. Research and Development of Digital Control Systems and Algorithms for High Power, High Voltage Isolated DC/DC Converters. 2009.
42. **Hardi Hõimoja**. Energiatõhususe hindamise ja energiasalvestite arvutuse metoodika linna elektertranspordile. 2009.
43. **Tanel Jalakas**. Research and Development of High-Power High-Voltage DC/DC Converters. 2010.

44. **Helena Lind**. Groundwater Flow Model of the Western Part of the Estonian Oil Shale Deposit. 2010.
45. **Arvi Hamburg**. Analysis of Energy Development Perspectives. 2010.
46. **Mall Orru**. Dependence of Estonian Peat Deposit Properties on Landscape Types and Feeding Conditions. 2010.
47. **Erik Väli**. Best Available Technology for the Environmentally Friendly Mining with Surface Miner. 2011.
48. **Tarmo Tohver**. Utilization of Waste Rock from Oil Shale Mining. 2011.
49. **Mikhail Egorov**. Research and Development of Control Methods for Low-Loss IGBT Inverter-Fed Induction Motor Drives. 2011.
50. **Toomas Vinnal**. Eesti ettevõtete elektritarbimise uurimine ja soovituste väljatöötamine tarbimise optimeerimiseks. 2011.
51. **Veiko Karu**. Potential Usage of Underground Mined Areas in Estonian Oil Shale Deposit. 2012.
52. **Zoja Raud**. Research and Development of an Active Learning Technology for University-Level Education in the Field of Electronics and Power Electronics. 2012.
53. **Andrei Blinov**. Research of Switching Properties and Performance Improvement Methods of High-Voltage IGBT based DC/DC Converters. 2012.
54. **Paul Taklaja**. 110 kV õhuliinide isolatsiooni töökindluse analüüs ja töökindluse tõstmise meetodid. 2012.
55. **Lauri Kütt**. Analysis and Development of Inductive Current Sensor for Power Line On-Line Measurements of Fast Transients. 2012.
56. **Heigo Mõlder**. Vedelmetalli juhitava segamisvõimaluse uurimine alalisvoolu kaarleekahjus. 2012.
57. **Reeli Kuhi-Thalfeldt**. Distributed Electricity Generation and its Possibilities for Meeting the Targets of Energy and Climate Policies. 2012.
58. **Irena Milaševski**. Research and Development of Electronic Ballasts for Smart Lighting Systems with Light Emitting Diodes. 2012.
59. **Anna Andrijanovitš**. New Converter Topologies for Integration of Hydrogen Based Long-Term Energy Storages to Renewable Energy Systems. 2013.
60. **Viktor Beldjajev**. Research and Development of the New Topologies for the Isolation Stage of the Power Electronic Transformer. 2013.
61. **Eduard Brindfeldt**. Visually Structured Methods and Tools for Industry Automation. 2013.
62. **Marek Mägi.** Development and Control of Energy Exchange Processes Between Electric Vehicle and Utility Network. 2013